Czech Technical University in Prague

Faculty of Electrical Engineering
Department of Electromagnetic Field

# *OPTICAL PACKET SWITCHING TECHNIQUES BASED ON NONLINEAR OPTICS*

## Doctoral Thesis

### *Ing. Matěj Komanec*

Prague, August 2013

Ph.D. Programme: Electrical Engineering and Information Technology
Branch of study: Radioelectronics

**Supervisor: *doc. Ing. Stanislav Zvánovec, Ph.D.***

# Acknowledgements

# Abstract

The dissertation thesis was focused on optical packet switching based on nonlinear optics. To fulfill the aim of the thesis, an analysis of various optical packet switching state-of-art aspects was carried out with the decision for a fiber-based optical packet switch. State-of-art technological aspects of nonlinear fibers were summarized with the emphasis on various approaches of achieving higher nonlinear coefficient.

A single-mode arsenic-selenide fiber with cut-off at 1300nm and nonlinear coefficient over $1000W^{-1}km^{-1}$ was connectorized and a component with 26m length was developed. Attenuation lower than 0.6dB/m was obtained with connection losses under 1dB, thus presenting enhancement of current state-of-art parameters. Ge-doped suspended-core fiber was evaluated as a representative of microstructured fibers, with nonlinear coefficient of $21W^{-1}km^{-1}$. Splicing technology was developed and a 100m component was produced with approximately 6dB insertion loss. Technology of the connectorization process is currently being patented.

Afterwards the development of the switching methodology was presented. First an opto-electronic controller was developed for label processing, achieving less than 5ns switching time. Then conversion efficiencies were measured for all utilized fibers, where the best results were obtained for HNLF at -15dB. Conversion efficiency for the $As_2Se_3$ fiber was below -40dB due to high component insertion loss. Ge-SCF showed almost no nonlinear response.

Based on the results a frequency plan was proposed employing HNLF. Modulation format transparent switching, sixteen channels flat conversion efficiency profile and polarization insensitive operation in the final proposed switching methodology configuration was achieved. BER and OSNR values verified operation at 10Gbps NRZ, where for 40Gbps DPSK and 100Gbps DP-QPSK the verification was carried out in simulations.


**Keywords:** Optical packet switching, four-wave mixing, chalcogenide fiber, suspended-core fiber, highly-nonlinear fiber, fiber connectorization, conversion efficiency, polarization insensitivity, modulation format transparency.

# List of abbreviations

| Abbreviation | Meaning |
| --- | --- |
| AAWG | Athermal arrayed-waveguide grating |
| AM | Amplitude modulation |
| ASE | Amplified spontanneous emittion |
| AWG | Arrayed-waveguide grating |
| BER | Bit-error rate |
| BERT | Bit-error rate tester |
| CIRC | Circulator |
| CW | Continuous wave |
| CWDM | Coarse wavelength-division multiplexing |
| DEMUX | Demultiplexer |
| DFB | Distributed-feedback |
| DP-QPSK | Dual-polarization quadrature phase-shift keying |
| DQPSK | Differential quadrature phase-shift keying |
| DS-HNLF | Dispersion-shifted highly-nonlinear fiber |
| DWDM | Dense wavelength-division multiplexing |
| EDFA | Erbium-doped fiber amplifier |
| FBG | Fiber Bragg grating |
| FOPA | Fiber optic parametric amplifier |
| FPGA | Field-programmable gateway array |
| FSO | Free-space optics |
| FUT | Fiber under test |
| FWHM | Full-width-at-half-maximum |
| FWM | Four-wave mixing |
| HCF | Hollow-core fiber |
| HNLF | Highly-nonlinear fiber |
| IPM | Iterative polar modulation |
| ITC | Isolated thermal chamber |
| KEOPS | Keys to optical switching (project) |
| LBG | Lead-bismuth-gallate |
| MEMS | Micro-electrical mechanical system |
| MOD | Modulator |
| MOF | Microstructured optical fiber |

| Abbreviation | Meaning |
| --- | --- |
| MUX | Multiplexer |
| NLSE | Nonlinear Schrödinger equation |
| NOLM | Nonlinear optical loop mirror |
| NRZ | Non-return-to-zero |
| OCDMA | Optical code-division multiple access |
| OCSS | Optical carrier supression and separation |
| OEC | Opto-electronic controller |
| OFDM | Orthogonal frequency-division multiplexing |
| OOK | On-off keying |
| OPS | Optical packet switch |
| OSA | Optical spectrum analyzer |
| OSNR | Optical signal-to-noise ratio |
| OTDM | Optical time-division multiplexing |
| PBG | Photonic bandgap |
| PBGF | Photonic bandgap fiber |
| PBS | Polarization beam splitter |
| PCF | Photonic crystal fiber |
| PCS | Polymer-clad silica |
| PDM | Polarization-divison multiplexing |
| PLZT | Perovskite Lead Lanthanum Zirconate Titanate |
| PRBS | Pseudo-random binary sequence |
| QAM | Quadrature amplitude modulation |
| RZ | Return-to-zero |
| SBS | Stimulated Brillouin scattering |
| SCF | Suspended core fiber |
| SEM | Scanning electron microscope |
| SFP | Small form-factor pluggable |
| SOA | Semiconductor optical amplifier |
| SPM | Self-phase modulation |
| SRS | Stimulated Raman scaterring |
| SSFM | Split-step Fourier method |
| TIR | Total internal refraction |
| WDM | Wavelength-division multiplexing |
| XGM | Cross-gain modulation |
| XPM | Cross-phase modulation |
| ZDWL | Zero-dispersion wavelength |

# Contents

# Chapter 1

# Introduction

Data transmission via a single optical fiber has recently exceeded 100 Tbps [1]. The growth of data traffic naturally imposes demands for all-optical network solutions, such as optical burst switching or optical packet switching. The reason lies in fundamental electronic processing limits (at approximately 100Gbps). High-capacity optical network devices will therefore have to be remade into an all-optical solution as current wavelength division multiplexing (WDM) networks will be limited in scalability of the network routers and switching fabrics. All-optical switching, more specifically optical packet switching (OPS) provides an opportunity to switch data traffic in an all-optical manner excluding all or most of opto-electronic conversions. Ultrafast data communication, including 3D multimedia data streams, full-HD videos and real-time data transfers will form the data payload of optical packets.

Another reason for all-optical solutions ensues from newly applied spectrally efficient modulation formats in optical communication, e.g. differential phase-shift keying (DPSK) [2] , differential quadrature phase-shift keying (DQPSK) [3], multiple-quadrature amplitude modulation (m-QAM) [4] and novel multiplexing methods, e.g. orthogonal frequency division-multiplexing (OFDM) [5] and polarization division-multiplexing (PDM) [6]. In these cases opto-electronic modulation processing is significantly more complicated than preserving the signal in an optical form. Modulation insensitive switching processes with very fast relaxation time of the fabric, i.e. switching speed, accompanied by polarization insensitivity, minimal insertion losses and ability to route the signal independently of its bitrate, will be required.

Highly-nonlinear materials (e.g. chalcogenide glass and photonic crystals) propose a viable solution for various switching schemes exploiting nonlinear phenomena, such as cross-phase modulation and four-wave mixing. They provide intrinsic material response of several femtoseconds. Among their advantages are extremely high nonlinearities, dispersion properties, short waveguide lengths and utilization in mid-infrared region.

The dissertation thesis focuses on the proposal of a new methodology for optical packet switching and on a novel technological development of enhanced nonlinearity fibers for optical packet switching. Highly nonlinear fiber will be theoretically and experimentally evaluated and confronted to novel soft-glass nonlinear fibers and microstructured fibers developed in the framework of this thesis and co-running projects. Thermal study

1

of chalcogenide fibers will be carried out. Switching methodology exploiting these enhanced nonlinearity fibers will be discussed, based on measurements and analyses and final optical packet switch configuration will be proposed. Conversion efficiency, polarization sensitivity, modulation format and bitrate insensitivity will be taken into account.

In Chapter 2 major aspects of optical packet switching, label processing and modulation formats are discussed. State-of-art methods are presented for various switching techniques, labelling methods and switching setups. Nonlinear phenomena suitable for switching purposes are discussed in Chapter 3, with focus on self-phase modulation (SPM) cross-phase modulation (XPM) and four-wave mixing (FWM) in optical fibers. Limiting effects such as stimulated Brillouin scattering (SBS) and stimulated Raman scattering (SRS) will be briefly mentioned, as their impact on discussed nonlinear phenomena cannot be discarded. Afterwards optical switches based on XPM and FWM are examined and a comparison is carried out for the purpose of employment in the thesis. Chapter 4 provides a comparison of various nonlinear optical fibers, starting from conventional highly-nonlinear fiber (HNLF) to microstructured optical fibers (MOF) and soft-glass fibers with fiber tapering as a different approach of aquiring increased nonlinearities. The chapter is concluded with a summary of state-of-art nonlinear fibers. Resulting from previous chapters, the main thesis objectives are presented in Chapter 5. The objectives represent novel research ideas and thesis outputs with respect to current state-of-art research level. Chapter 6 is focused on technological development of nonlinear fibers, their properties and characterization for optical packet switching. Chosen fibers are improved and tested for application in OPS. In Chapter 7 the whole OPS setup with optical and electronic part is described and discussed. A new switching methodology exploiting novel specialty optical fibers is proposed, measured and optimized. Chapter 8 concludes the dissertation thesis by discussing the achieved results and providing further enhancement possibilities.

# Chapter 2

# Optical packet switching

This chapter briefly discusses the main aspects of an optical packet switch, whereas detailed information could be found in the references. General description of OPS considers an optical packet composed of a label and data payload at the OPS input as depicted in Fig. 2.1. The label is separated from the payload and processed. For label filtering a wavelength-division demultiplexer (DEMUX), an arrayed-waveguide grating (AWG) or a spectrally-narrow fiber Bragg grating (FBG) accompanied by a circulator could be employed. For label processing two basic concepts are represented by an all-optical setup or a electro-optic hybrid setup. Hybrid OPS converts the label into an electronical representation and processes it in a CPU - generally a digital signal processor (DSP) or a field-programmable gateway array (FPGA) - and then a routing signal is generated, according to the label content. Hybrid solution sustains the advantages of electronic processing and preserves the optical data payload format and bitrate. All-optical solutions have been proposed recently [7], with increasing label content and processing capabilities. According to label processing time, the payload is buffered for an appropriate time period. Afterwards the payload is switched to the proper output, a new label is attached to the data payload, thus forming a new optical packet for further optical network transmission.
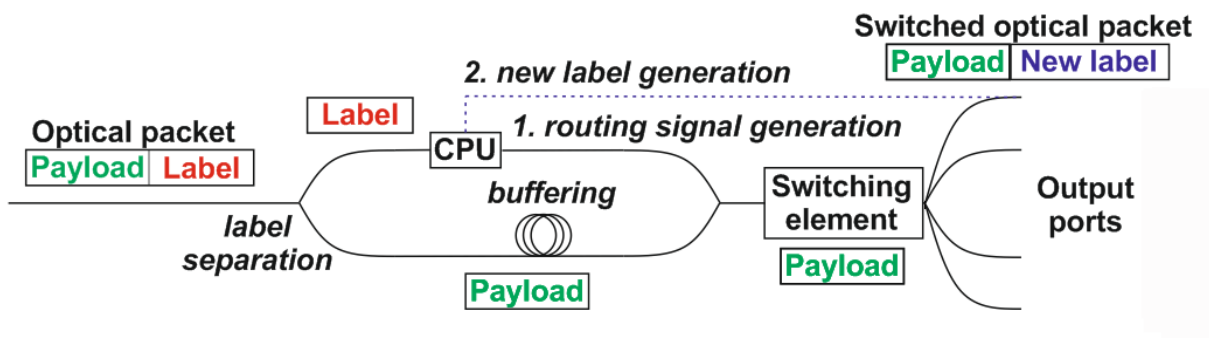


Figure 2.1: Generalized setup of a hybrid OPS introducing main function blocs.

This chapter at first focuses on conventional and novel state-of-art modulation formats employed in optical data communication, as they place additional requirements on proposed OPS. Major labelling techniques are then discussed with respect to spectral efficiency and multiplexing possibilites. Afterwards up-to-date switching fabrics are presented altogether with basic switching schemes. References to recent research achievements are included. The chapter is concluded with a summary providing comparison of state-of-art switching techniques and methods.

## 2.1 Modulation formats and multiplexing

For a long time the abundant modulation format in optical data communication used to be represented by the amplitude modulation (AM), more specifically by on-off keying (OOK) with receiver employing direct detection. Recently coherent data transmission has become feasible [8] and new modulation formats have appeared in optical communication, e.g. phase-shift keying (PSK) modulations [3] and QAMs with increasing symbol count [5, 4, 9]. As a midstep between coherent and direct detection DPSK must be mentioned [2] , whereas detection is provided by an interferometric 1-bit delay.

Multiplexing in optical communication can be solved by several approaches. Among the well-known are coarse wavelength-division multiplexing with (CWDM) or dense wavelength-division multiplexing (DWDM) channel grid, optical time-division multiplexing (OTDM) and scarcely optical code-division multiplexing (oCDMA). Orthogonal frequency-division multiplexing [6] and polarization-division multiplexing have attracted attention recently [4] as coherent detection became viable.

Most of the following state-of-art data transmissions combine multiplexing and novel modulation formats for higher spectral efficiency and data throughput, such as DWDM-PDM m-QAM transmissions [10] and PDM-QPSK transmissions [3]. Figure 2.2 depicts how the data formats employing high-level modulation and multiplexing are reaching close to the Shannon theorem, with ever increasing bit efficiencies.
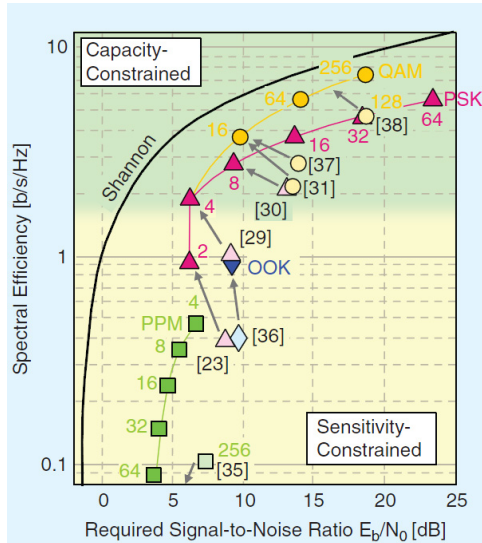
Figure 2.2: Optical modulations and their spectral efficiencies [11].

### 2.1.1 Amplitude modulation

Amplitude modulation, represented in optical communication by OOK, stands for the most widespread modulation format. As data speeds have increased to 40 and 100Gbps, amplitude modulation encountered problems with significant dispersive effects for long-haul transmissions. In OOK modulations one bit is represented by one amplitude symbols.

OOK coding is speed-limited by rise/fall time of the transmitter - a laser diode or an external modulator (current commercially available Mach-Zehnder modulators provide 40Gbps modulation speeds). Two major OOK variants are represented by non-return zero (NRZ) and return zero (RZ). 10Gbps NRZ has became more widespread than RZ and is exploited in most 10Gbps optical networks.

For nonlinear optics RZ format provides the possibility of pulse energy compression, where for a defined modulation speed, signal pulse occupies only a small portion of the bit slot duration. Therefore average signal power is compressed in the time domain and peak pulse power exceeding 1W can be easily obtained.

### 2.1.2 Phase modulation

From PSK modulation formats, differential phase-shift keying is the only format not utilizing coherent detection, whereas interferometric detection is sufficient. 40Gbps DPSK is nowadays frequently employed in high-speed optical networks [2] . For DPSK one bit is represented by one phase symbol (phase difference) and for QPSK [2] two bits are represented by one phase symbol. Even higher symbol count was achieved by employing 8PSK modulation [2], where three bits are represented by one phase symbol. When QPSK is combined with PDM a data format of 100Gbps PDM-QPSK is formed.

### 2.1.3 Quadrature amplitude modulation

Quadrature amplitude modulation combines both coding in amplitude and phase domain, thus forming a multisymbol data format. Utilization of $n$ bits form $2^n$ phase/amplitude symbols. 256-QAM has been presented [4], where for coherent transmission PDM was employed achieving 4GSymbol/s data throughput and having optical signal-to-noise ratio (OSNR) of 28.6dB. Maximum modulation of 1024-QAM was recently achieved in [9] by utilizing both PDM and OFDM methods. Signal was propagated through 160km of large-mode area fibers with hybrid Erbium-doped fiber amplifier (EDFA) and Raman amplification.
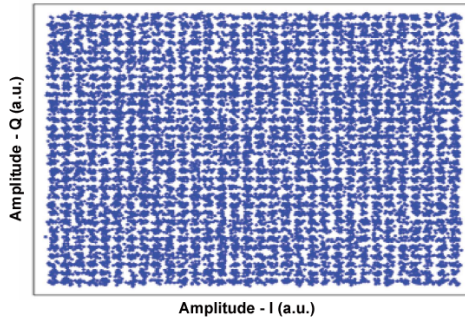


Figure 2.3: 1024-QAM constelation diagram [9]

### 2.1.4 Iterative polar modulation

In order approach closer to the Shannon limit, a novel modulation format, i.e. constellation diagram was developed, the iterative polar modulation (IPM). Constellation shaping was utilized and iterative polar quantization [12] was exploited. 256-IPM subcarrier multiplexing was presented in [6], occupying only 20.75GHz bandwidth. Together with PDM and OFDM spectral efficiency of 11.15 b/s/Hz was achieved.
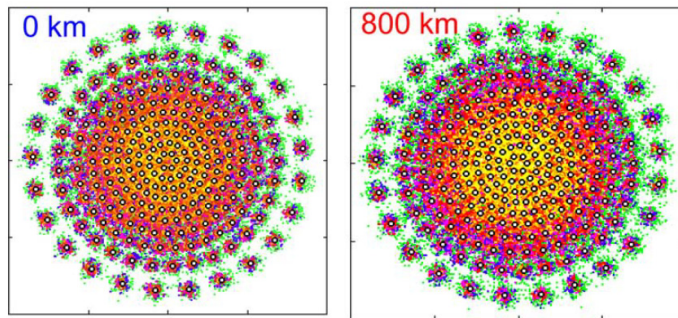


Figure 2.4: 256-IPM constellation diagrams before (left) and after 800km transmission (right) [6]

## 2.2 Labelling techniques

In the following subsections various packet labelling techniques will be introduced. At the end of each subsection particular advantages and disadvantages will be briefly summarized. Serial labelling represented by OTDM is the first method discussed. WDM labelling methods involve optical carrier supression and separation (OCSS), out-band and in-band labelling. Other labelling techniques are mentioned at the end of the section.

### 2.2.1 Serial labelling

The serial labelling method exploits the OTDM scheme, where the label preceeds the data payload by a specific time (guard time). The label consists of a specified bit sequence identifying its front (typically a predefined stream of binary zeros and ones) and the destination address. Precise synchronization is required to detect the label properly. The payload is either delayed until the label is processed or if the guard time is longer than label processing time, no delay for the payload is necessary. Fig. 2.5 illustrates the form of the serial labelled optical packet. In [13] a serial label was employed, where the payload was separated from the label by a defined 150ns guard time; the label had a duration of 700ns and the packet duration varied from 2 to $3\mu$s. Label was modulated by 10Gbps and payload was 160Gbps OTDM. In [14] a 64ns optical packet consisting of 128 bit NRZ label at 10Gbps and 40Gbps data payload was presented, guard time of 43.2ns was utilized.
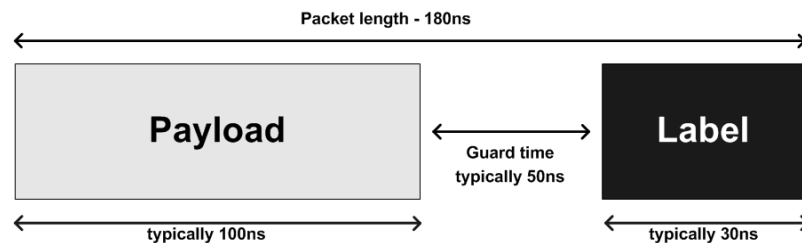


Figure 2.5: Serial labelling technique.

**Advantages:**

- A simple OTDM labelling technique

**Disadvantages:**

- Synchronization requirement
- Guard time increases packet duration, thus decreasing data throughput

## 2.2.2 Optical carrier suppression and separation

Optical carrier suppression and separation technique utilizes exact wavelength span between optical packet payload and label. When processing the label, payload is filtered out and only the label is received and detected. For instance, data payload was modulated at 10Gbps DPSK, while the label was encoded in OOK at 2.5Gbps [15] employing the OCSS labelling method. The main principle can be observed in Fig. 2.6, where a predefined frequency shift $f_0$ between the central frequency and the label/payload is preserved. This was achieved by modulating a CW signal in an amplitude Lithium-Niobate modulator (LN-MOD) by two sinusoidal clock signals having the same frequency, but one being inverse to another. Original CW signal is suppressed and two new signals are created, having a frequency span of exactly $2f_0$. Then the payload is modulated on one signal and label is modulated to the other signal. By an optical coupler both signals are coupled together at the output.

**Advantages:**

- Defined wavelength span for payload and label generation

**Disadvantages:**

- Complicated generation setup
- Clock recovery requirement
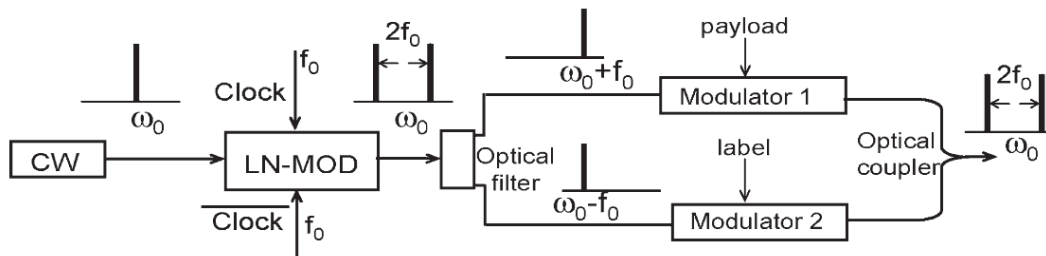


Figure 2.6: Optical carrier separation and supression generation scheme [15].

### 2.2.3 Out-band labelling

Out-band label is represented by a label encoded on a different wavelength than the data payload. If multiple data wavelengths are utilized, the labels have to be placed out of the payload spectrum. Employing out-band labelling ensures a facile approach for achieving label detection without distortion of the data spectrum. This method is similar to the OCSS technique, however the wavelength separation is not defined so strictly. In Fig. 2.7 the wavelength allocation of the payload and the label is demonstrated. Out-band labelling was utilized in a multi-wavelength OPS setup [16], with FBG label filtering, where the label was represented by 25Mbps NRZ and the payload was formed by 5x 40Gbps NRZ data signal. Length of the label was 120ns and the payload occupied a 300ns time slot.

**Advantages:**

- Simple label allocation and separation

**Disadvantages:**

- Spectrally inefficient
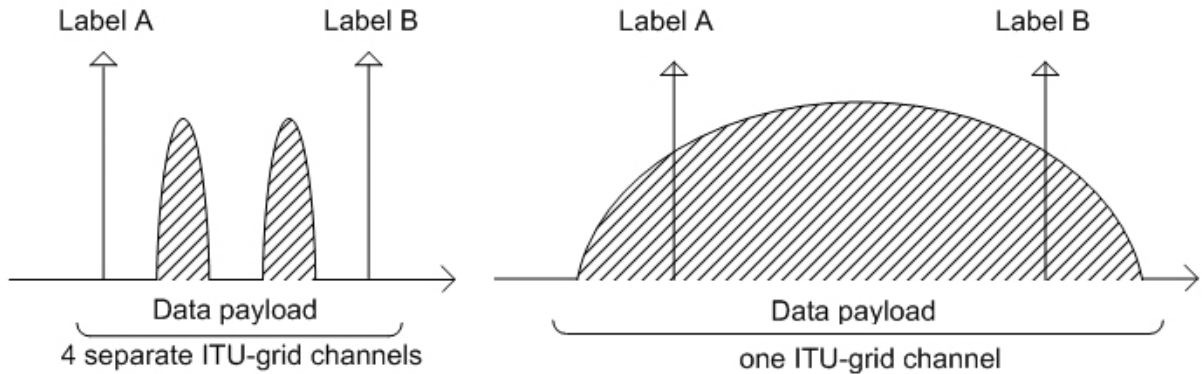


Figure 2.7: Out-band (left) and in-band labelling scheme (right).

### 2.2.4 In-band labelling

Recently in-band labelling has become one of frequently exploited labelling techniques. Its main advantage is in including labels within the data spectrum and then separating them with a very narrow filter. The label separation is usually carried out by a narrow fiber Bragg grating, which allows filtering in orders of 0.1nm or even less. Labels are represented by a continuous binary zeros or binary ones, thus enabling $2^n$ addresses. Fig. 2.8 describes the optical packet spectrum, where the labels are placed directly in the payload spectrum. Insertion of multiple in-band labels was presented in [7], where also all-optical label recognition and processing was proposed. Recently enhanced in-band RF-tone labelling was achieved [17], which provided $2^{n*m}$ addresses carried in one label-wavelength.

Error-free (BER $<10^{-9}$) operation was verified for 40 and 160Gbps transmissions.

**Advantages:**

- Spectrally efficient

**Disadvantages:**

- Ultra-narrow label lasers linewidth requirement ($\sim$kHz)
- Ultra-narrow filter for label separation requirement ($\sim$0.03nm)
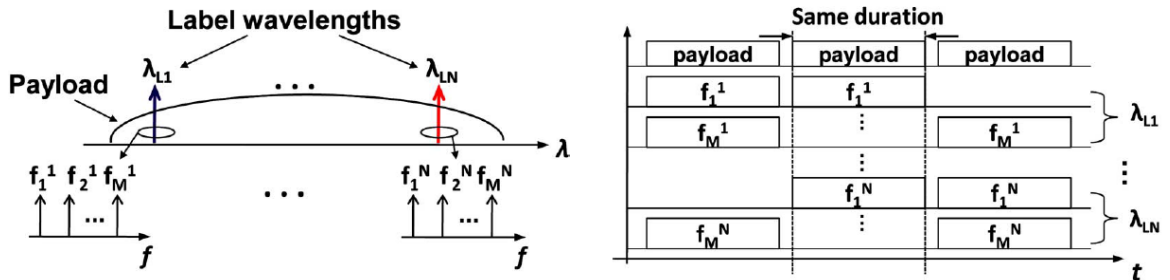


Figure 2.8: In-band labelling scheme with RF-tones utilization, frequency spectrum (left), time domain (right) [17].

## 2.2.5  Other labelling techniques

Subcarrier multiplexed (SCM), i.e modulation diversity [18] labelled optical packet consists of the data payload, which is represented by a high speed signal in order of Gbps (OOK, DPSK, DQPSK, etc.) and the label, which is amplitude modulated with a slowly varying envelope. Label is then detected together with the payload, but with a slow photodiode, thus obtaining only the slow amplitude variations. Major disadvantage of this method is unavoidable interference between payload and label. Another approach is space-diversity labelling, which was utilized in [19], where the packet label was derived from amplifier noise and modulated in a reflective semiconductor optical amplifier. The label and payload were transmitted on two separate optical fibers. Tunable multiple optical orthogonal codes sequence based optical label was presented in [20] with 1.25 to 5.0 Gbps payloads. In-band label allocation was exploited with employment of FBGs for label insertion and separation.

## 2.2.6  Label recognition techniques

Opto-electronic conversion and direct detection can be employed for label recognition only when the label is represented by OOK or DPSK. With the advent of novel modulation formats, higher bitrates and spectrally efficient data transfers, all-optical label processing became essential.

Label recognition based on XPM in a Sagnac loop was proposed already in 2003 [21], where a semiconductor laser amplifier in a loop mirror configuration (SLALOM) was utilized. The main advantage was that this method did not require clock recovery. On the other hand, SLALOM worked only for a specific types of label format (Manchester coding was required, otherwise label could not be distinguished from the data payload). In basic principle SLALOM introduced a two pulse correlation method, where the payload was suppressed and the label received at the output.

Recognition of DPSK labels was presented in [22], employing a serial-to-parallel convertor with phase operation for 10Gbps DPSK signals. One-bit preamble with a phase of $\pi/2$ is added to each packet, where 2-bit labels were succesfully detected with additional improvement by employing an IQ modulator. The detection process is depicted in Fig. 2.9 utilizing Mach-Zehnder delay interferometers (DIs) and balanced photodetectors. For processing an $N$-bit label, input signal is split into $N$ branches, and each label bit is injected to the receiver with a delay length of $k$-bit ($k$=1, 2, .., $N$), and $N$-bit label is thus converted to $N$ parallel label bits.
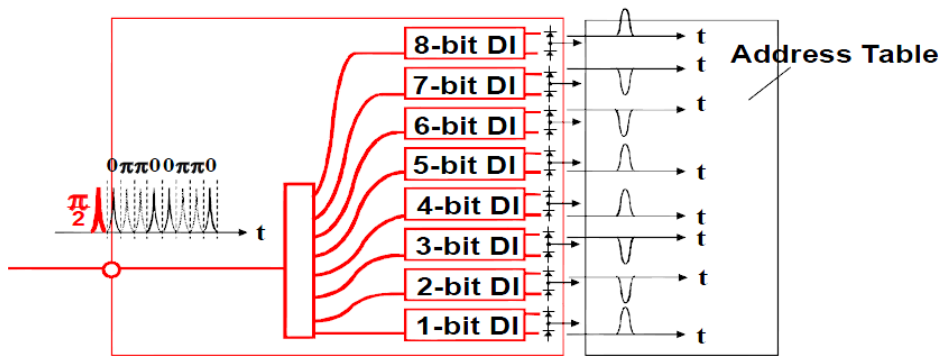


Figure 2.9: Serial-to-parallel DPSK label recognition [22].

Orthogonal label generation and recognition [23] provided reduction in code cross-correlation requirements. The label processing was based on FBG encoder/decoder and SOA, employing multiple two dimensional optical orthogonal codes, which meant encoding the label in both the time and frequency domain. For emerging QPSK and dual polarization QPSK (DP-QPSK) modulation formats, two label recognition schemes were already proposed. In [24] a free-space approach with time-to-space conversion was exploited. A setup including cylindrical lenses enabled 16 label detection with 1.8 contrast ratio for QPSK signal and almost 2.5 for binary PSK (BPSK) signal, where two-symbol labes were distinguished. The free-space approach may not be suitable for non-laboratory application as it requires precise adjustment of the setup. In [25] a cascaded multi-stage integrated optical circuit scheme was theoretically studied, providing 1.47 contrast ratio for 256 label detection. Label recognition utilizing an identifying pulse in interference with QPSK encoded pulses was employed. One stage of the proposed setup is depicted in Fig. 2.10.
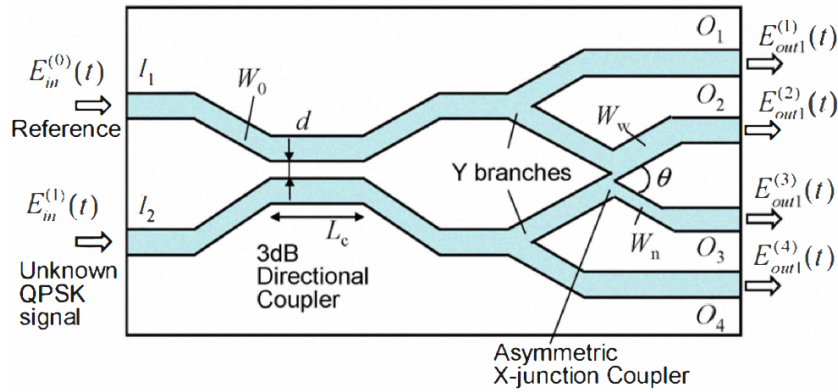
Figure 2.10: QPSK label recognition scheme [25].

## 2.3 Switching schemes

There are three major switching schemes; the broadcast-and-select switching technique, the space-switch and the wavelength routing scheme. Each of them will be discussed in detail in the following subsections.

### 2.3.1 Broadcast-and-select

In the broadcast-and-select switching technique (Fig. 2.11) an optical packet is multicast to all outputs and according to label content a proper output gate is selected and opened. Other gates remain closed for the signal. Two representatives of the broadcast-and-select switching technique are presented, a broadcast-and-select switch with a recirculation buffer [26] and the European ACTS Keys to Optical Switching (KEOPS) project [27].
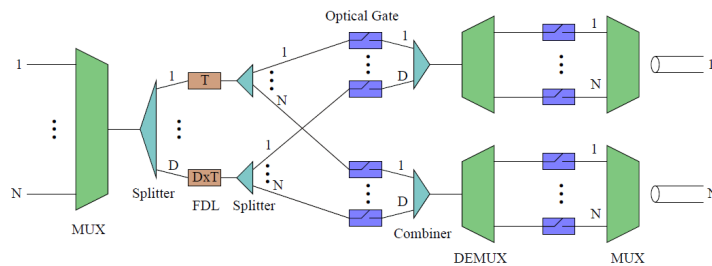


Figure 2.11: Broadcast and select switch architecture [26], FDL - fiber delay line

For KEOPS switch each input and output fiber carries only one wavelength, which nevertheless may change depending on each packet. The input part is composed of fixed wavelength converters (FWC) and a multiplexer. The buffering block employs $n$ optical delay lines (ODLs). Splitters, optical gates and combiners then form the space-switching stage. At the output a wavelength selector block is utilized.

The broadcast-and-select switch with recirculation buffer architecture is similar to the KEOPS switch in having one wavelength at input and output ports, varying with each packet. The difference can be found in combining $n$ input wavelengths by a coupler and distribution of the combined signal to $n$ tunable optical filters (TOFs) and $m$ fixed optical filters (FOFs). The switch is slotted and controlled by a CPU. For each time slot, the CPU determines the output ports for the incoming packets and from the one time slot delay-line. According to the output port destinations, tunable wavelength converters (TWCs), TOFs and optical gates are controlled. Packets not passing out are recirculated and occupy the next time slot for the switch processing.
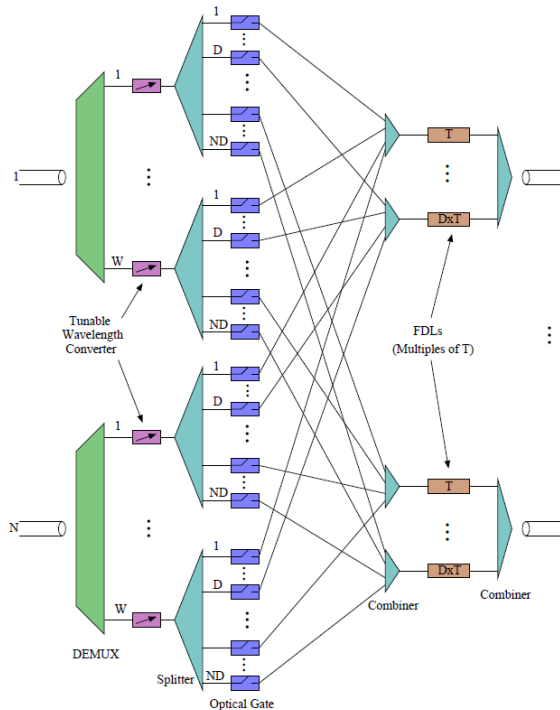


Figure 2.12: Space switch architecture [26]

## 2.3.2 Space switching

A space switch fabric architecture is shown in Fig. 2.12. The switch consists of $n$ incoming and $n$ outgoing fiber links, each carrying $n$ wavelengths. Each incoming optical packet is demultiplexed (e.g. by an AWG) and fed into a different TWC which converts the wavelength of the optical packet to a wavelength of the destination optical output. Then, through the space-switch fabric, the optical packet can be switched to any of the $n$ outputs. The optical packet is forwarded to an ODL by appropriately keeping one optical gate open while the remaining are closed. An experimental setup employing a space switch is illustrated in Fig. 2.13 (demonstrated in [28] as a part of an all-optical packet switch). A semiconductor optical amplifier in a Mach-Zehnder interferometer (SOA-MZI) served as an optical gate.
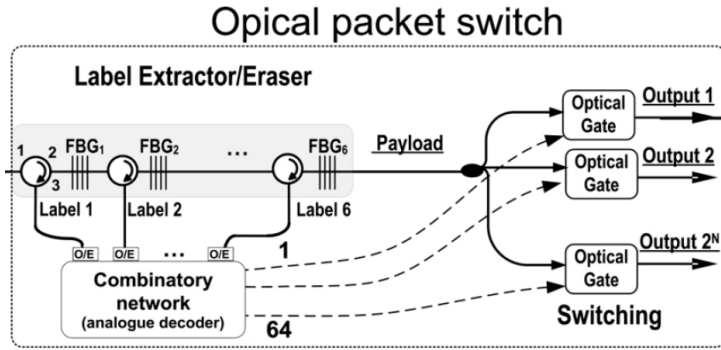
Figure 2.13: Space switch [28].

### 2.3.3 Wavelength routing

Wavelength routing represents a method, where an optical packet of a defined wavelength arrives at the input of OPS and is fed into TWC. In TWC the wavelength of the packet is modified according to the label content. The wavelength conversion is based either on four-wave mixing (FWM), cross-phase modulation (XPM) or cross-gain modulation (XGM) effect. The TWC fabric is mostly represented by a SOA wavelength converter. A wavelength routing switch is typically composed of AWG and a set of TWCs. A typical setup is illustrated in Fig. 2.14, having multiple inputs each connected to TWC [29] . After the wavelength conversion, optical packets are sent into AWG and to the desired output port. AWGs are utilized especially for their great advantage in monolithical integration, low losses ($\sim$3dB per channel) and scalability.
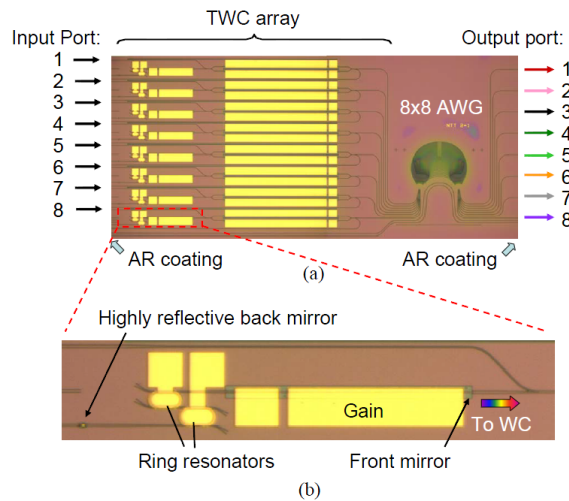


Figure 2.14: Wavelength routing scheme utilizing AWGs [29]

## 2.4    Switching fabrics

The switching process is closely related to the utilized switching fabric. Planar switching fabrics are represented either by a monolithically integrated switch based on Indium Phosphide (InP) [14, 30], a switch based on Perovskite Lead Lanthanum Zirconate Titanate (PLZT) [31] or a switch formed by micro-electro-mechanical systems (MEMS) [32]. Another approach is to utilize nonlinearities of the second or third order, such as XPM, XGM or FWM in SOAs or optical fibers.

In this section a brief summary will follow with the main technologies and works related. To the first subclass belong monolithically integrated switches (PLZT, InP and SOA-MZI switches). MEMS switches form second subclass. Third subclass represented by nonlinear optical fiber based switches will be discussed in detail in Chapter 3.

### 2.4.1    InP switches

Integrated optical switches developed on InP planar chips provide very promising results thanks to their scalability, low insertion losses in respect to size (∼1dB/cm), possibilities of large scale integration and switching times in orders of nanoseconds. They are usually fabricated using epitaxial structure p-i-n InP-InGaAsP. Active (lasers, amplifiers) and passive (waveguides, splitters, WDMs) elements are integrated together on the chip enabling numerous applications. A setup of such an application is illustrated in Fig. 2.15, where 24 arrayed phase shifters enable switching to 16 outputs on one chip [30] . Each of the phase-shifters enables full control of the transmitted signal. The phased-array switch is a monolithic single-stage interferometric device that routes the optical beam to one point at the output plane if linear phase distribution in the array plane is preserved. The deflection point is controlled by the bias voltages of the phase-shifters, which leads to switching with a single-stage control independent of the number of ports. The phased-array switches are bit rate transparent and modulation format insensitive.

40 Gbps signal was successfully switched and buffered in a photonic integrated circuit based on [14]. 1x16 monolithic InP chip was presented in [30], where the signal suffered only a 0.7dB power penalty. The switch was capable of switching 160Gbit/s optical data signal.
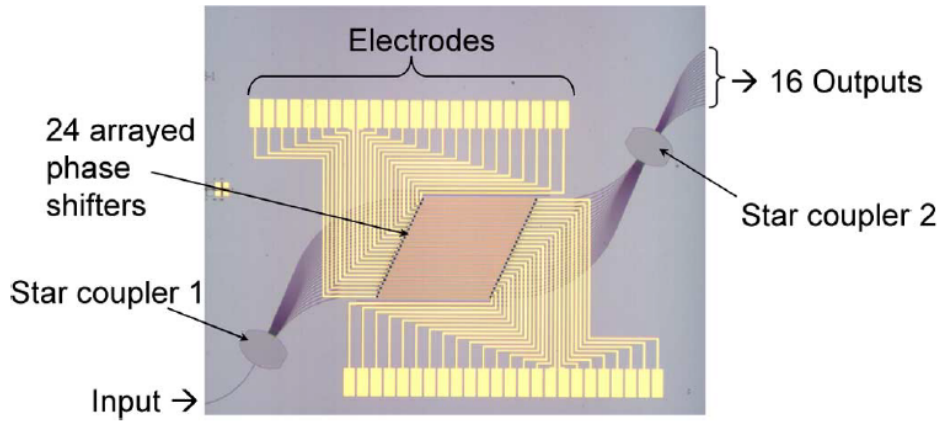
Figure 2.15: Planar InP switch with high level of active and passive element integration [30]

### 2.4.2  PLZT switches

PLZT switch is made of an efficient electro-optic material (PLZT), which could be deposited on a semiconductor, thus enabling miniaturization and integration. Typical operating voltages are thanks to the large electro-optic coefficients lowered by a significant amount (PLZT has more than 5 times higher EO coefficient than $LiNbO_3$). PLZT switches offer switching speeds in order of ns, they are wavelength independent in the whole C-band and they are polarization and modulation format insensitive. Detailed study of a PLZT switch can be found in [33]. In [31] were utilized PLZT switches to demonstrate switching of 1.28Tbps NRZ-DQPSK optical packets, together with other data formats such as OOK or DPSK. 200Gbit/s multi-wavelength optical packet switch with switching time of 2ns was presented in [16].

### 2.4.3  MEMS switches

Micro electro-mechanical systems can be utilized for many electro-optical applications. MEMS are miniature structures fabricated by using a process of micro-machining. The structures are in a range from a few hundred microns to a few millimetres, mostly fabricated on silicon substrates. Their advantage is in the possibility of creating large scale NxN optical switches by cascading numerous MEMS. The basic operation principle is based on free-space optical cross-connects. The most common setup is the 3D MEMS switch, which is composed of micromirrors and collimators to achieve blocking-free interconnections as illustrated in Fig. 2.16, where also the switching principle is demonstrated. Large scale MEMS optical switches were reported [32, 34] , but also 2x2 switches were presented [34]. The switching times are in the order of milliseconds. The fastest MEMS reported 0.2ms switching time, which is insufficient for current optical network bit rates, but on the other hand no other switching fabric can provide as many inputs and outputs as the MEMS switch.
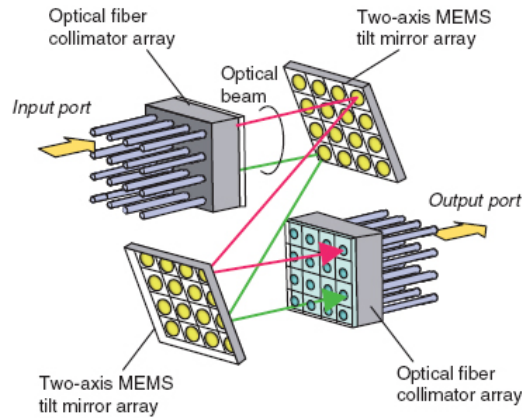
Figure 2.16: MEMS switch architecture [34]

## 2.4.4 SOA-based switches

The SOA-MZI switch acts as an interferometric optical gate, where the control signal is driven into the SOA-MZI, thus opening the gate for a defined time period, which can be as long as the optical packet time interval. The basic function principle of the optically controlled gating is illustrated in Fig. 2.17. In case no control signal is present, incoming data packets are switched only to output port 2. If a control signal is sent into SOA, data packets are routed via nonlinear effects and their phase is modulated, thus affecting the constructive and destructive interference. Selected optical packets are gated to output 1, while the rest is switched to output 2. Payload is switched according to the label, which is extracted from the incoming optical packet and processed by the CPU, generating control signal and a new label. The gate is opened not only for the payload but also for the new label, thus securing identical duration of both the packet and the new label. SOA-MZI is utilized in a space optical switch configuration, employing the broadcast-and-select method. Latency under 400ps was achieved in [7], where four SOA-MZI optical gates were utilized.
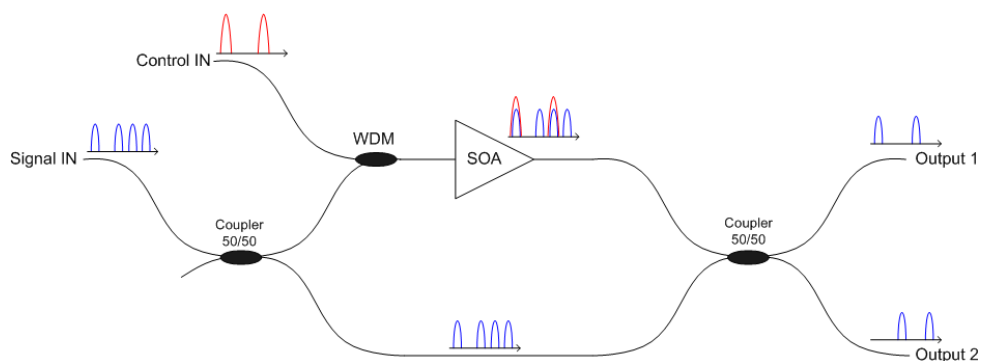


Figure 2.17: SOA-MZI switch

## 2.5 Conclusion

In this chapter a state-of-art overview of particular OPS aspects was carried out. In table 2.1 a summary of state-of-art modulations and multiplexing is presented. Channel spectral efficiency over 10bit/s/Hz was achieved in [6, 9, 4]. As can be observed, for future applications high-level of modulation and multiplexing is expected.

Table 2.1: Modulation format comparison

| Modulation | bit/s/Hz | Tbit/s | Channels | Multiplex | Ref. |
|---|---|---|---|---|---|
| RZ DQPSK | 3.2 | 25.6 | 160 | WDM+PDM | [3] |
| 256-QAM | 11.8 | 0.064 | 1 | PDM | [4] |
| RZ 8-QAM | - | 32.0 | 320 | WDM+PDM | [35] |
| 16-QAM | 4.1 | 0.336 | 3 | WDM+PDM | [10] |
| 256-IPM | 11.5 | 0.231 | 1 | OFDM+PDM | [6] |
| 32-QAM | 7.0 | 0.650 | 8 | OFDM+WDM+PDM | [5] |
| 1024-QAM | 11.7 | 0.050 | 1 | OFDM+PDM | [9] |

Labelling techniques were discussed with emphasis on the requirement for proper balance among label content, spectral efficiency and facile label generation/processing. Table 2.2 could be utilized for the purpose of labelling techniques comparison.

Table 2.2: Modulation format comparison

| | Label multiplex | Spectral eff. | Filtering | Main disadvantage |
|---|---|---|---|---|
| Serial | OTDM | High | No | Synchronization |
| OCSS | WDM | Low | Yes | Spectral efficiency |
| Out-band | WDM | Low | Yes | Spectral efficiency |
| In-band | WDM | High | Yes | Narrow filter requirement |
| SCM | Modulation | High | No | Intersymbol interference |
| Orthogonal | OFDM | High | No | Coherent |
| Space-diversity | Space | None | No | Multiple fibers |

Label recognition techniques were briefly mentioned focusing on novel modulations and $n$-bit labels. Switching schemes and switching fabrics were summarized, with consideration of planar, MEMS and SOA-based approaches. In the following chapter fiber-based switches will be discussed.

# Chapter 3

# Nonlinear fiber based switches

## 3.1 Nonlinear phenomena in optical fibers

In optical fibers major nonlinearities result from the Kerr effect, which can be described as a dependence of the refractive index on optical intensity. When an optical signal with intensity $I$ is launched into a fiber, the refractive index $n$ is modified, affecting all other co-propagating signals. The equation describing the Kerr effect can be written as:

$$n(\omega, I) = n(\omega) + n_2 I, \tag{3.1}$$

where $n_2$ is the nonlinear refractive index of the fiber and $\omega$ represents wavelength. Generally the nonlinear refractive index is defined as:

$$n_2 = \frac{3}{8n} Re(\chi_{\chi\chi\chi}^{(3)}), \tag{3.2}$$

where $\chi_{\chi\chi\chi}^{(3)}$ is the third rank susceptibility tensor of the total nonlinear polarization $\mathbf{P}$:

$$\mathbf{P} = \varepsilon_0(\chi^{(1)} \cdot \mathbf{E} + \chi^{(2)} \cdot \mathbf{EE} + \chi^{(3)} \colon \mathbf{EEE} + \cdots \tag{3.3}$$

Nonlinear refractive index $n_2$ is expressed in $[\text{cm}^2\text{W}^{-1}]$, which is related to the Kerr coefficient as:

$$n_2 = n_0(\sqrt{\frac{\varepsilon_0}{\mu_0}} N_2), \tag{3.4}$$

For nonlinear propagation in optical fibers the approximation of a slowly varying envelope is commonly utilized. Then the pulse propagation can be simplified to a solution by the split-step Fourier method (SSFM) of the Nonlinear Schrödinger equation (NLSE), which can be written as [36] :

$$\frac{\partial A}{\partial z} = (\hat{D} + \hat{N})A, \tag{3.5}$$

where $\hat{D}$ represents the dispersive part and $\hat{N}$ the nonlinear part, defined as:

$$\hat{D} = -\frac{i\beta_2}{2}\frac{\partial^2}{\partial T^2} + \frac{\beta_3}{6}\frac{\partial^3}{\partial T^3} - \frac{\alpha}{2} \qquad (3.6)$$

$$\hat{N} = i\gamma(\mid A \mid^2 + \frac{i}{\omega_0}\frac{1}{A}\frac{\partial}{\partial T}(\mid A \mid^2 A) - T\frac{\partial\mid A \mid^2}{\partial T}), \qquad (3.7)$$

where $\beta_2$ and $\beta_3$ are the fiber dispersion parameters, $\alpha$ stands for fiber attenuation, $\gamma$ is the fiber nonlinear coefficient, $T$ represents time, $\omega_0$ is the carrier angular frequency and $A$ is the amplitude of the optical signal. SSFM provides an approximate solution by assuming propagation of the optical signal along a small distance $z$, where in the first step only dispersion is evaluated and in the second step only nonlinearity acts alone.

It is useful to define the nonlinear fibre length $L_{NL}$, the dispersive length $L_D$ and the effective fibre length $L_{eff}$. By comparing these lengths, in some cases the dispersive part $\hat{D}$ or the nonlinear part $\hat{N}$ of NLSE can be neglected.

$$L_{NL} = (\gamma P_0)^{-1} \qquad (3.8)$$

$$L_{eff} = \frac{[1 - exp(-\alpha L)]}{\alpha} \qquad (3.9)$$

$$L_D = \frac{T_0^2}{\mid \beta_2 \mid}, \qquad (3.10)$$

where $P_0$ is the input power in Watts, $L$ represents length in kilometers and $T_0$ stands for pulse full-width at half-maximum (FWHM) in picoseconds.

A so called soliton number factor $N$ is introduced to describe the relative ratio between $L_D$ and $L_{NL}$.

$$N = \frac{L_D}{L_{NL}} = \frac{\gamma P_0 T_0^2}{\mid \beta_2 \mid}, \qquad (3.11)$$

If $N \gg 1$, then dispersive effects can be neglected. If $N \ll 1$, then nonlinear effects can be neglected. If $N \cong 1$, then both dispersive and nonlinear effects must be considered.

Important effect on the outcome of the nonlinear processes represents the sign of dispersion parameter $D$, which is defined as:

$$D = -\frac{2\pi c}{\lambda^2}\beta_2 \qquad (3.12)$$

When $\beta_2$ is negative, $D$ is positive and the dispersion is considered normal. In case of positive $\beta_2$, inducing $D$ negative, the dispersion is considered anomalous.

When the signal is tuned close to zero dispersion wavelength (ZDWL), i.e. $\beta_2 \sim 0$, the higher order dispersion terms $\beta_3$ and $\beta_4$ must be taken into account:

$$\beta_3 = \frac{S * \lambda_0^4}{(2\pi c)^2} \tag{3.13}$$

$$\beta_4 = -\frac{\lambda_0^4}{(2\pi c)^3} \left( 6D + \lambda \left( \frac{\partial D}{\partial \lambda} \right) + \lambda^2 \left( \frac{\partial^2 D}{\partial \lambda^2} \right) \right), \tag{3.14}$$

where $\lambda_0$ stands for ZDWL and $S$ represents the dispersion slope. The dispersion slope parameter in $ps/nm^2/km$ is significant for nonlinear effects which require the phase-matching condition.

For optical packet switching cross-phase modulation and four-wave mixing will be evaluated. Self-phase modulation (SPM) will be also briefly discussed as it always accompanies XPM and FWM.

### 3.1.1 Self-phase modulation

This phenomenon is a manifestation of the intensity dependence of the refractive index in a nonlinear optical media. High optical intensity causes a nonlinear phase delay, which has the same temporal shape as the optical intensity.

When an optical pulse propagates through a fiber, the Kerr effect causes time-dependent phase shift according to the time-dependent intensity. The initial unchirped optical pulse acquires a so-called chirp, which means a time-varying of instantaneous frequency. The maximum nonlinear phase shift is defined as:

$$\triangle\phi_{SPM} = 2\gamma P L_{eff}, \tag{3.15}$$

This equation is valid only for unchirped signals, with pulse FWHM > 100ps and $P_0 > 1W$, thus dispersion effects can be neglected and the solution is significantly simplified. The SPM-induced optical frequency chirp causes broadening or narrowing of the optical pulse spectrum and results in new frequency components. This phenomenon is widely employed for supercontinuum generation [37] and pulse compression [38].

Examples of SPM induced pulse broadening and frequency chirp are presented in Fig. 3.1. The initial pulse FWHM was set to 2ps, the pulse was unchirped at the input, pulse peak power $P$ was set to 1W and as the simulation fiber a conventional highly-nonlinear fiber (HNLF) with $\gamma$ of 11.35 $W^{-1}km^{-1}$, 0.88dB/km attenuation and 500m length was selected (these values correspond to a measured fiber discussed later in the thesis).
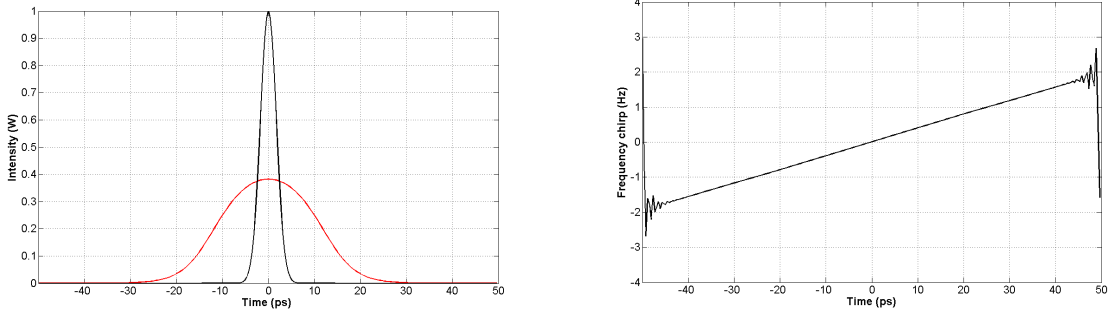
Figure 3.1: SPM induced pulse broadening (left) and frequency chirp (right).

## 3.1.2 Cross-phase modulation

Cross-phase modulation takes place only when two or more signals co-propagate simultaneously in the optical fiber. The higher energy pulse at one wavelength influences the refractive index of the fiber, thus modulating phases of all other co-propagating signals. In contrast to four-wave mixing and stimulated scattering phenomana, XPM takes effect without any energy transfer between co-propagating signals. Cross-phase modulation is always accompanied by SPM. In its simplest form (considering pulses with FWHM $\gg$ 1ps and slowly varying envelope) with signals of linearly co-polarized waves, XPM can be derived by introducing the nonliner polarization, which can be expressed as [36] :

$$\mathbf{P}_{NL}(\mathbf{r}, t) = \frac{1}{2}\hat{\chi}(P_{NL}(\omega_1)exp(-i\omega_1 t), \tag{3.16}$$

$$+P_{NL}(\omega_2)exp(-i\omega_2 t)), \tag{3.17}$$

$$+P_{NL}(2\omega_1 - \omega_2)exp(-i(2\omega_1 - \omega_2)t)), \tag{3.18}$$

$$+P_{NL}(2\omega_2 - \omega_1)exp(-i(2\omega_2 - \omega_1)t)) + c.c., \tag{3.19}$$

where $c.c.$ stands for the complex conjugated terms. The dependence of the terms $E_1$ and $E_2$ is as follows:

$$P_{NL}(\omega_1) = \chi_{eff}\left(\mid E_1 \mid^2 +2\mid E_2 \mid^2\right)E_1, \tag{3.20}$$

$$P_{NL}(\omega_2) = \chi_{eff}\left(\mid E_2 \mid^2 +2\mid E_1 \mid^2\right)E_2, \tag{3.21}$$

$$P_{NL}(2\omega_1 - \omega_2) = \chi_{eff}E_1^2 E_2^*, \tag{3.22}$$

22

$$P_{NL}\left(2\omega_2 - \omega_1\right) = \chi_{eff}E_2^2 E_1^* \tag{3.23}$$

$\chi_{eff}$ is the effective nonlinear parameter, which can be expressed as:

$$\chi_{eff} = \frac{3\varepsilon_0}{4}\left(\chi_{xxxx}^{(3)}\right) \tag{3.24}$$

The last two terms are the result of the FWM phenomenon and can be neglected in the case of XPM, when the phase-matching condition required for significant rise of the FWM components is not met. The induced nonlinear phase-shift can be in a simplified form defined as:

$$\triangle\phi_{XPM} = 2\gamma P_2 L_{eff}, \tag{3.25}$$

where $P_2$ is the power of the second signal co-propagating. The factor of 2 represents that the effect of XPM is double the SPM. XPM is suitable for all-optical switching, because of the XPM capability of achieving high conversion efficiencies as a result [39].

### 3.1.3   Four-wave mixing

The origin of the non-degenerate four-wave mixing results from the nonlinear coupling of four optical waves (through the Kerr effect). When two signals (often denoted as pumps) at $\omega_1$ and $\omega_2$ co-propagate, they beat together and result into new signals, at difference frequencies. The new signals can interact not only with other products but also with the pumps, thus creating secondary FWM products. When there is only one pump at angular frequency $\omega_p$ and one signal with angular frequency $\omega_s$, the so-called degenerate FWM occurs. The newly created signal at angular frequency $\omega_i$ is called the idler. The process represents in fact a transfer of two photons from the pump, one to the signal and the other to the idler. Amplitudes of the pump, signal and idler can be defined as $A_p(z)$, $A_s(z)$, $A_i(z)$ respectively. When inserted in NLSE, the following three coupled equations can be derived:

$$\frac{\partial A_p}{\partial z} = i\gamma\left[\left(\mid A_p \mid^2 + 2\left(\mid A_p \mid^2 + \mid A_i \mid^2\right)\right)A_p + 2A_s A_i A_p^* exp\left(i\triangle\beta z\right)\right], \tag{3.26}$$

$$\frac{\partial A_s}{\partial z} = i\gamma\left[\left(\mid A_s \mid^2 + 2\left(\mid A_p \mid^2 + \mid A_i \mid^2\right)\right)A_s + A_i^* A_p^{2*} exp\left(-i\triangle\beta z\right)\right], \tag{3.27}$$

$$\frac{\partial A_i}{\partial z} = i\gamma\left[\left(\mid A_i \mid^2 + 2\left(\mid A_p \mid^2 + \mid A_s \mid^2\right)\right)A_i + 2A_s A_i A_p^{2*} exp\left(-i\triangle\beta z\right)\right], \tag{3.28}$$

where the propagation mismatch $\Delta\beta$ is:

$$\triangle\beta = 2\beta_p - \beta_s - \beta_i \tag{3.29}$$

If we consider a strong pump $P_p(0) = \mid A_p(0) \mid^2$ and a significantly weaker signal $P_s(0) = \mid A_s(0) \mid^2$, the previous equations are simplified to the form of:

$$\frac{\partial A_p}{\partial z} = i\gamma \mid A_p \mid^2 A_p, \tag{3.30}$$

$$\frac{\partial A_s}{\partial z} = i\gamma 2 \mid A_p \mid^2 A_s + i\gamma \mid A_p \mid^2 A_i^* exp\left(-i\triangle\beta z\right), \tag{3.31}$$

$$\frac{\partial A_s}{\partial z} = i\gamma 2 \mid A_p \mid^2 A_i + i\gamma \mid A_p \mid^2 A_s^* exp\left(-i\triangle\beta z\right), \tag{3.32}$$

For all FWM processes the FWM gain is the significant parameter, which can be defined as:

$$g^2 = \left(\gamma P_p\right)^2 - \left(\kappa/2\right)^2, \tag{3.33}$$

where the net phase mismatch $\kappa$ is:

$$\kappa \approx 2\gamma P_p - \Delta\beta, \tag{3.34}$$

Two major applications of FWM include parametric amplification and wavelength routing. Fiber optic parametric amplifier (FOPA) is focused on maximal signal gain $G_s$, i.e. maximal increase of $P_s$, whereas for wavelength routing conversion efficiency $\eta$ is the key factor.

$$G_s = \frac{P_s(L)}{P_s(0)} = 1 + \left[\frac{\gamma P_p}{g} sinh(gL)\right]^2, \tag{3.35}$$

$$\eta = \frac{P_i(L)}{P_s(0)} = \left[\frac{\gamma P_p}{g} sinh(gL)\right]^2, \tag{3.36}$$

FWM processes are influenced by the zero-dispersion wavelength (ZDWL) parameter, which is significant, whereas the FWM gain and conversion efficiency strongly depends

on the pump placement in respect to ZDWL. For signal wavelengths close to ZDWL the signal gain is simplified to:

$$G_s \approx (\gamma P_p L)^2 \tag{3.37}$$
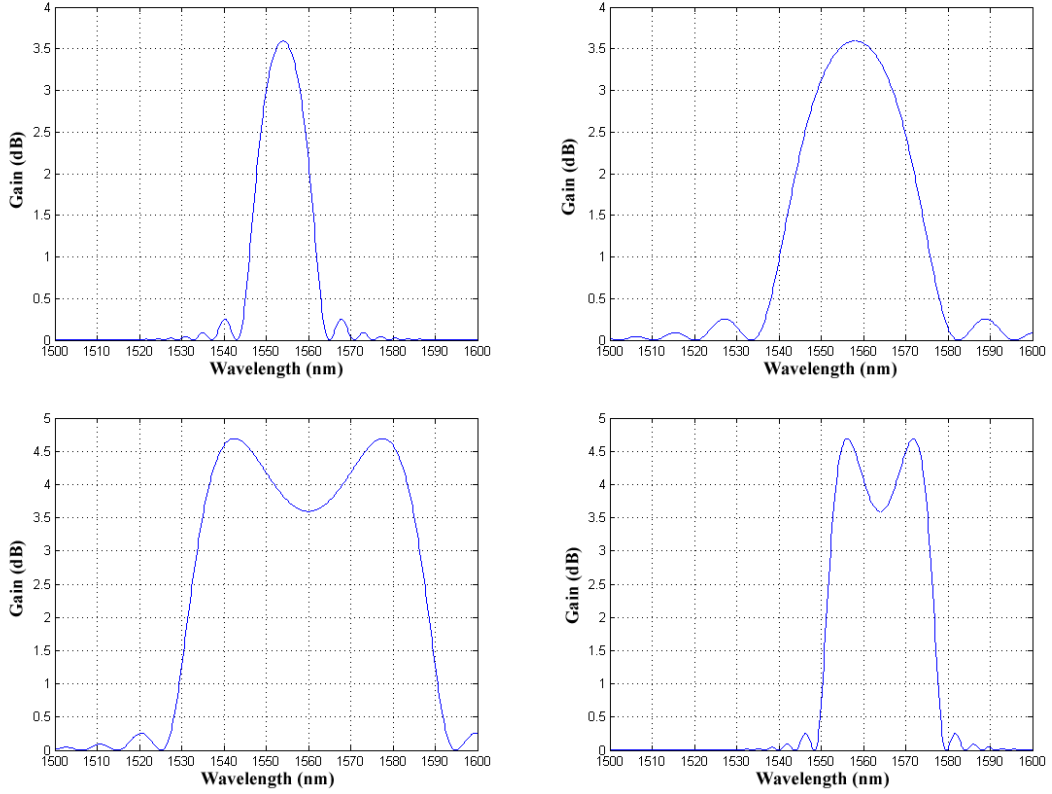


Figure 3.2: Parametric gain curve with pump allocation at 1554nm (a), 1558nm (b), 1560nm (c) and 1564nm (d)

Graphs depicting pump wavelength detuning from the ZDWL by $\pm 1$nm and $\pm 5$nm are summarized in Fig. 3.2. It can be observed that for pump allocation below ZDWL, the gain profile narrows and signal gain is also lower than for pump allocation above ZDWL. This can be connected to the fact stemming from Eq. 3.34, where $\gamma$ and $P_p$ are always positive, $\triangle\beta$ must be also positive. This can be achieved by operating the pump in the anomalous dispersion regime. Nonlinear fiber considered for this simulation is identical with the SPM chirp analysis, i.e. highly-nonlinear fiber (HNLF) 500m, $\gamma$ of 11.35 W$^{-1}$km$^{-1}$, 0.88dB/km attenuation, ZDWL at 1559nm. Pump was set to 20dBm peak power.

### 3.1.4 Limiting effects

Discussed nonlinear processes exploit intensity dependence of the refractive index and demonstrate themselves with greater effect, when intensity is maximized (typically peak powers higher than 1W are desired). Unfortunately some significant undesired nonlinear effects limit optical fiber nonlinear performance. Two major limiting processes are represented by the stimulated Raman scattering (SRS) and the stimulated Brillouin scattering (SBS).

**Stimulated Raman scattering**

Stimulated Raman scattering is a nonlinear process, where due to the interaction of phonons and photons two new spectral components arise (the Stokes and Anti-Stokes wave). It has been known since the year 1928 [40] and is very often used for Raman amplifiers [41] and lasers [42]. The SRS needs to reach a required power threshold to take effect. Basically in any medium a spontaneous Raman scattering can transfer a very small portion (in order of $10^{-6}$) of the optical power from one optical field to another. When stimulated, the amount of transferred power rises and becomes more significant. The power is transferred into a frequency downshifted region (typical shift is 13THz). In optical networks it stands for an undesired phenomenon, where in multichannel systems it is responsible for energy transfer among transmitted channels.

**Stimulated Brillouin scattering**

Stimulated Brillouin scattering is the nonlinear phenomenon of diffraction on the acoustic wave. SBS is based on electrostriction and is a different kind of nonlinearity compared to the Kerr effect. It is a nonlinear phenomenon that occurs at much lower input optical powers than SRS and manifests through the generation of a backward-propagating Stokes wave, which is frequency downshifted (for silica fibers typically 10-14GHz at 1550nm, threshold powers of $\sim$mWs). The threshold power depends mainly on the spectral width of the source, i.e. the pump signal (Fig. 3.3). The threshold can be approximately calculated as [43] :

$$P_{th} = 21kA_{eff}/g_b L_{eff}(\frac{\triangle\nu_B + \triangle\nu_p}{\triangle\nu_B}), \tag{3.38}$$

where $g_b$ is the Brillouin gain coefficient, $\triangle\nu_p$ the spectral width of the pump, $\triangle\nu_B$ stands for the Brillouin line-width and $k$ stands for the polarization factor, where for unvarying polarization along the fiber $k$=1 and for varying polarization $k$=2.

There are several methods to suppress SBS. The often employed one exploits broadening of the pump laser line-width. The pump signal is phase modulated (PM) to widen the pump spectrum to such an extent, that it does not impede the performance of the

system. The most common setting uses a phase modulator driven by three different radio-frequency generators, with their frequencies always being 3.1~3.5 times the preceeding modulation frequency [43]. The SBS threshold can also be increased by combining several fibres with different Brillouin frequency shifts [44]. The Brillouin frequency shift can be influenced, for instance, by concentration of fiber dopants [45]. Induced strain along the fibre represents another possibility of SBS suppression [46].
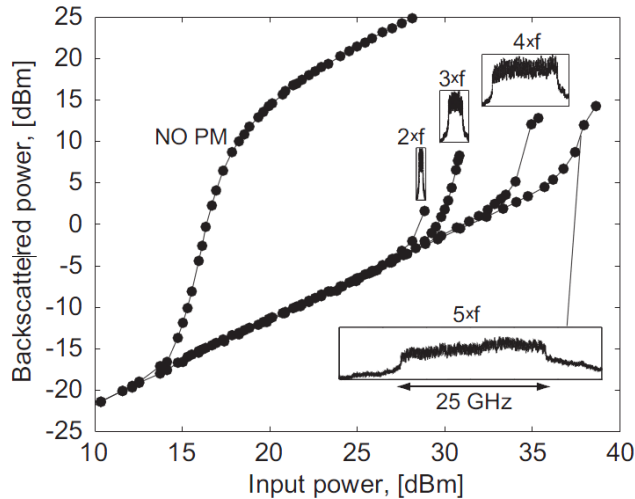


Figure 3.3: SBS threshold increase by phase modulation of the pump [43].

## 3.2 Nonlinear fiber-based switches

Optical fibers provide material response in order of femtoseconds, which enables switching independent of the data bit rate. This section discusses basic approaches and state-of-art achievements in wavelength conversion based on XPM and FWM. Afterwards a summary of major advantages of both approaches, their disadvantages and possible countermeasures is presented. Application of presented switching schemes for proposed OPS is then discussed and the most suitable nonlinear phenomenon is selected for proposed optical packet switching methodology.

### 3.2.1 XPM-based switches

Switching based on XPM can be divided into several major application areas, as XPM can be exploited either in a nonlinear optical loop mirror (NOLM) configuration [47], or XPM can broaden the payload spectrum [48] and desired wavelength can be then filtered out and also XPM can be utilized in optical switches employing fiber gratings [49].

NOLM setup for XPM-based wavelength switching is depicted in Fig. 3.4. A continuous wave (CW) signal is sent into the fiber loop, which in absence of the data signal acts as a perfect mirror. When the data signal is launched into the loop, via the XPM

effect the phase of the CW signal is modulated (in presence of data signal log1) and at the loop output via interference the phase modulation is converted into amplitude modulated signal. The switched signal is an exact copy of the data signal, whereas having the wavelength of the CW signal. Possible wavelength shift achieved by NOLM XPM switching is dependent on the walk-off length. By employing high nonlinearity fibers, shorter lengths could be utilized and the wavelength shift increases. In 2001 over 26nm wavelength shift was presented [50] by utilizing nonlinear fibers. In 2004 160Gbps XPM conversion was published employing a dispersion shifted fiber [47]. Recently XPM in NOLM configuration has been utilized mostly for modulation format conversion [51].
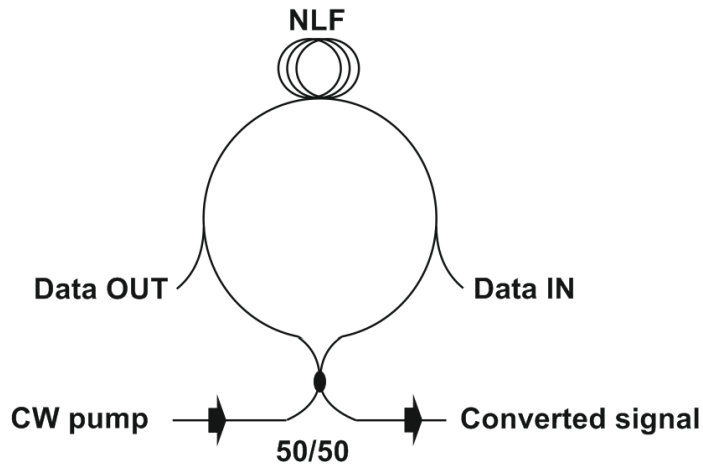


Figure 3.4: Basic operation principle of a NOLM-based switch, NLF - nonlinear fiber.

Apart from the NOLM configuration a XPM-based switch can also employ spectral broadening induced by XPM. In Fig. 3.5 a setup describing this situation is presented. A CW pump signal (probe light) is sent together with the data signal (pump light). In this case the data act as a pump and affect the phase and spectrum of the CW signal. By appropritiate filter setting (while maintaing sufficient bandwidth not to distort the signal) a data signal replica can be obtained at a new wavelength. 40Gbps signal was shifted by several nanometers in a 10km long fiber [48].
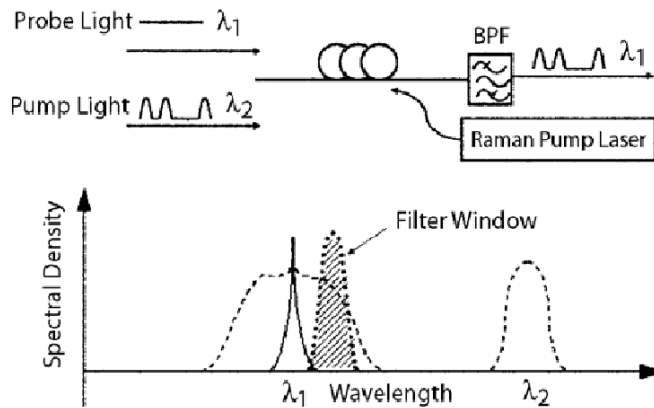
Figure 3.5: Basic operation principle of a XPM-based switch employing spectral broadening [36].

Fiber Bragg gratings could be utilized in various XPM-switching configurations. Latest results include a XPM-based switch with FBG providing PM/AM conversion with 6dB better conversion efficiency than NOLM and operation up to 40Gbps [49]. The setup is depicted in Fig. 3.6, where CWL stands for continuous wave laser. A signal data pattern is phase modulated on the CW laser signal and in the FBG the phase modulation is converted into amplitude modulation. In this case, only RZ modulations could be processed. Another approach employed bismuth fibers with imprinted gratings [52], where high nonlinearity of the bismuth glass was exploited ($\gamma$ over 1000 W$^{-1}$km$^{-1}$). Pump powers of 50W were required to achieve 6.5dB on-off extinction ratio.
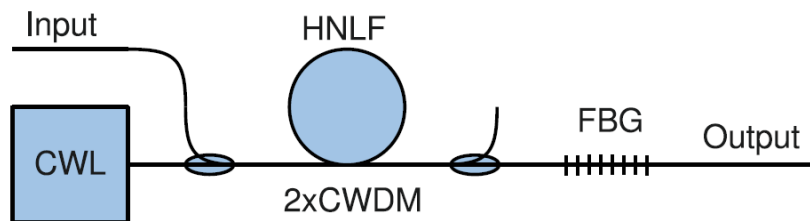


Figure 3.6: XPM-based switch utilizing FBG and PM/AM conversion [49].

## 3.2.2 FWM-based switches

The basic switch is formed by a FWM-based wavelength convertor, its scheme is depicted in Fig. 3.7. CW pump signal is co-propagated with the signal in a nonlinear fiber, where the idler is generated. Signal and pump are then filtered out and only the idler passes through the optical filter. Wavelength convertors based on FWM have been studied since 1992, when the first experiment was presented [53] , providing wavelength conversion range of 8nm in a 10km long dispersion-shifted fiber. Significant improvement of FWM-based wavelength convertor came with the onset of highly-nonlinear fibers with nonlinearities

from 10 to 30 $W^{-1}km^{-1}$. In 1998 a 720m-long HNLF was employed and 40nm conversion range was achieved [54]. In this experiment conversion efficiency of 28dB was presented with 600mW pumps. Recently more than 68nm conversion range was presented in [55] exploiting tellurite fibers.
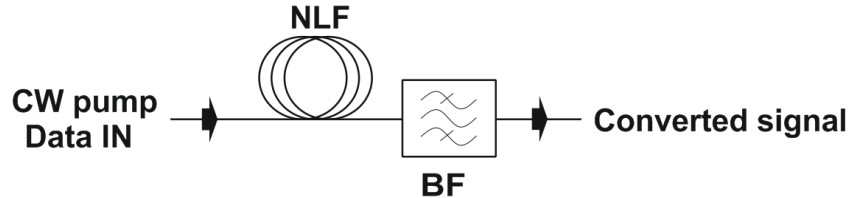


Figure 3.7: Basic operation principle of a FWM-based wavelength convertor, NLF - non-linear fiber, BF - bandpass filter.

Dual-pump FWM-based wavelength convertor architecture was first presented in 1993 [56]. Major advantages are broadband flat gain profile and polarization-independent function, in case the pumps are orthogonally polarized. Requirement is placed on the pumps in respect to their phase, where the same phase must be achieved, not to induce phase modulation on the generated idler. The polarization-independency is a significant advantage over one-pump FWM-based wavelength convertor architectures, but provides lower conversion efficiencies than in case of co-polarized pumps. Conversion efficiencies and polarization sensitivity for a dual-pump FWM-based wavelength convertor is presented in Fig. 3.8. Polarization sensitivity lower than 3dB was obtained in a wide wavelength span [57].
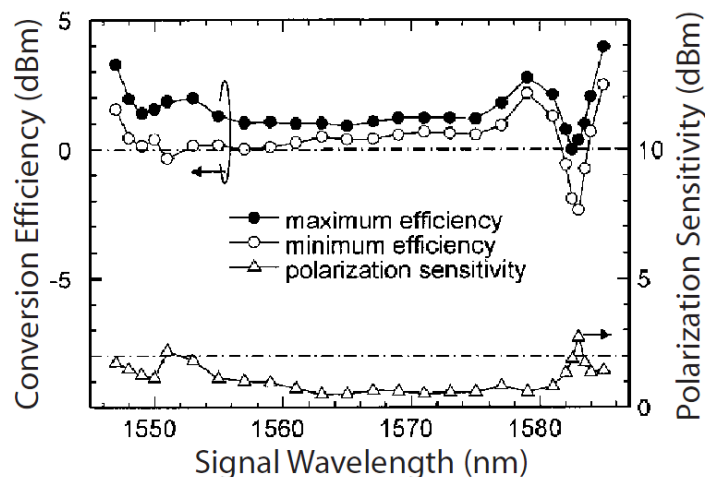


Figure 3.8: Polarization sensitivity and conversion efficiency [57]

Multicasting in FWM-based wavelength convertor was demonstrated in the year 2000 [58], where 26 channels in the L-band were switched with conversion efficiencies lower than -19dB. This low efficiencies were caused by SBS saturation of the pump at 23dBm.

Multicasting with the assistence of the Raman amplification (often also denoted as RA-FOPA - Raman-assisted fiber optic parametric amplifier) was presented in [59], whereas achieving 3x6 multicasting with less than a 2dB penalty at BER $10^{-9}$.

One of the FWM-based wavelength convertor disadvantages are the SBS limitations, as discussed in the previous section, which take stronger effect for long fibers (e.g. for 1km conventional silica fiber, SBS limits the pump power to 50mW). To achieve high conversion efficiencies, either short fibers must be employed or other countermeasures must be taken. The pump phase modulation technique mentioned in previous section is commonly employed.

Another significant drawback of 1-pump FWM-based wavelength convertor is polarization sensitivity, whereas with inproper adjustment no FWM may occur and the optical packet will not be switched. Several solutions for polarization insensitive wavelength conversion have been proposed. First was published as early as 2003 [60] , where FBG and a Faraday rotator mirror ensured pump propagation in both polarization axes through the same nonlinear medium as depicted in Fig 3.9. This setup tunability was limited by the FBG fixed wavelength.
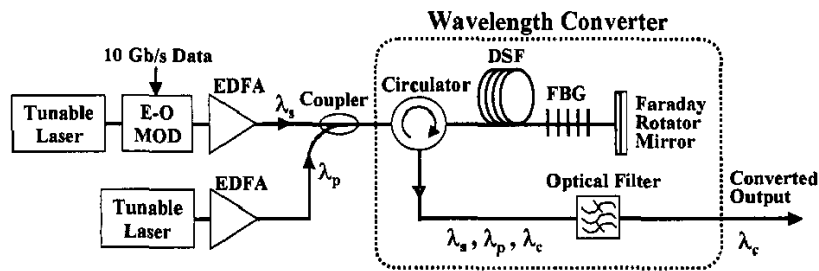


Figure 3.9: FWM-based wavelength convertor polarization insensitive setup utilizing Faraday rotator mirror [60].

Second approach illustrated in Fig. 3.10 utilized a piece of polarization-maintaining fiber to achieve pump distribution between both polarization axes [61] with polarization sensitivity less than 0.5dB, but with the requirement on the signal pulsewidth, which must be half of the bit duration, otherwise slow and fast axis components overlap. This fact requires utilization of RZ modulation format, which is not employed in conventional optical networks.

31
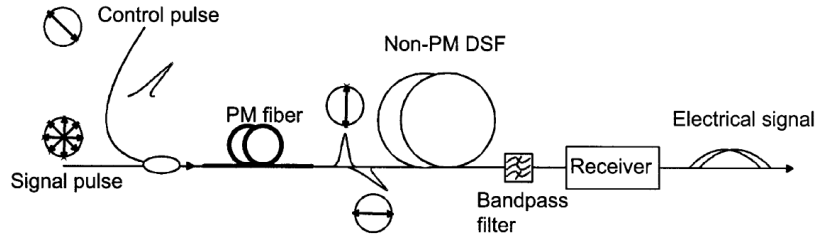
Figure 3.10: FWM-based wavelength convertor polarization insensitive setup utilizing a piece of polarization-maintaining (PM) fiber [61], DSF - dispersion-shifted fiber.

Third possibility of polarization insensitive setup was proposed in [62, 63] for HNLF and photonic crystal fiber (PCF) respectively (Fig. 3.11), where a polarization beam splitter (PBS) was employed to divide the signal and the pump into both polarization axes and then they co-propagated in a loop configuration, clockwise and counter-clockwise. The only requirement was that the pump is polarized 45° along the principal axis, so that the pump power is distributed evenly among both polarization axes. Polarization sensitivity of only 0.2dB was achieved in [62].
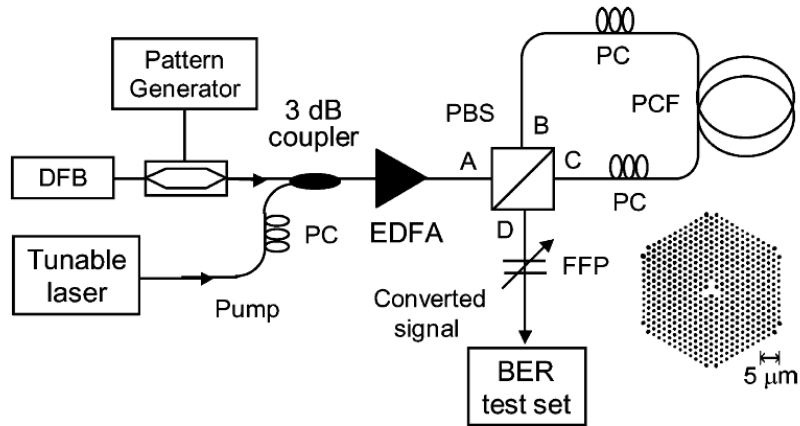


Figure 3.11: FWM-WC polarization insensitive setup utilizing PBS in a nonlinear loop [62, 63], DFB - distributed-feedback laser diode, EDFA - Erbium-doped fiber amplifier, PC - polarization controller, FFP - Fabry-Perot filter.

## 3.3 Conclusion

This chapter summarized major nonlinear phenomena in optical fibers. Nonlinearity, dispersion and effective length were presented as comparative parameters for nonlinear optical fibers, which will be further exploited in nonlinear fiber design for optical packet switching. SPM effects on pulse spectra were discussed, whereas measurements will be presented later on. Basic theoretical aspects of XPM and FWM were summarized. Limiting effects were presented. As Raman threshold is typically higher than 0.5W, it is insignificant for the switching purposes of this thesis. Experimental evaluation of SBS will be carried out for utilized nonlinear fibers in Chapter 7.

Fiber-based wavelength routing techniques exploiting the XPM and FWM phenomena were discussed. Both XPM and FWM are polarization sensitive and require phase-matching to achieve efficient conversion. Among the advantages of FWM over XPM are theoretically >0dB conversion efficiency (conversion gain, i.e. parametric gain) and multicasting possibility. The main advantage of FWM is doubtlessly the modulation format transparency, as FWM can convert any signal, phase or amplitude modulated. Therefore FWM was preffered to XPM for the proposed optical packet switching methodology. The polarization sensitivity can be dealt with by adjusting the switching setup or in the 2-pump setup having two orthogonal pumps.

# Chapter 4

# Optical fibers with enhanced nonlinearity

For comparison of nonlinear fibers the nonlinear coefficient $\gamma$ is utilized, defined as:

$$\gamma = \frac{2\pi n_2}{\lambda A_{\mathit{eff}}},$$

(4.1)

where $A_{\mathit{eff}}$ is the effective mode area, $\lambda$ is wavelength and $n_2$ stands for the nonlinear refractive index of the fiber. Typical SMF-28e provides nonlinear coefficient $\gamma$=2W$^{-1}$km$^{-1}$, whereas having a nonlinear refractive index of $n_2$=1.3·10$^{-20}$cm$^2$W$^{-1}$. $A_{\mathit{eff}}$ can be obtained by solving:

$$A_{\mathit{eff}} = \frac{(\iint\limits_{-\infty} \mid F(x,y) \mid^2 \ \mathrm{d}x\mathrm{d}y)^2}{\iint\limits_{-\infty} \mid F(x,y) \mid^4 \ \mathrm{d}x\mathrm{d}y)},$$

(4.2)

where the function $F(x,y)$ represents the optical field distribution. For a Gaussian distribution of $F(x,y) \approx exp[-(x^2+y^2)/w^2]$ the effective mode area $A_{\mathit{eff}} = \pi w^2$, where $w$ is the fiber core width.

Considering fixed wavelength (typically C-band wavelengths for optical communication) it is possible to achieve higher $\gamma$ by reducing $A_{\mathit{eff}}$. This approach implies increased coupling losses and is limited by the employed wavelength. When the wavelength is close to or lower than the core diameter, light is no further guided by the total internal refraction. To increase $n_2$ it is necessary to change the glass composition as is summarized in Fig. 4.1. For this dissertation thesis chalcogenide glasses will be employed, with the selection of selenide-glass fibers and microstructured fibers with emphasis on suspended core fibers. Both will be analyzed in comparison to conventional silica-based nonlinear fibers.
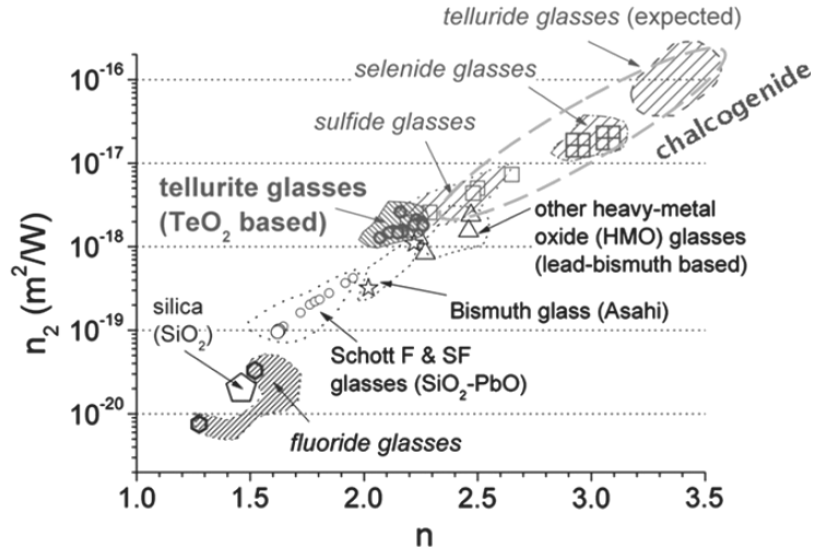
Figure 4.1: Dependence of the nonlinear refractive index on the refractive index for different glass materials [64].

## 4.1 Conventional fibers

### 4.1.1 Silica-based nonlinear fibers

Highly-nonlinear fiber with doped core is the most widespread representative of nonlinear fibers, where HNLF composition varies from conventional silica fibers in the core doping, e.g. with $GeO_2$ and simultaneously by lowering $A_{eff}$ (typically $10\mu m^2$). The coefficient $\gamma$ for conventional HNLF is approximately $11W^{-1}km^{-1}$.

Dispersion-shifted highly nonlinear optical fiber (DS-HNLF) is a special type of HNLF, with ZDWL in the vicinity of 1550nm. DS-HNLF can be manufactured employing doping both in the fiber core and cladding, therefore producing a specific refractive index profile as depicted in Fig 4.2. First published paper appeared in 2002 [65], where $\gamma$ of $20.4W^{-1}km^{-1}$ was achieved. Later $\gamma$ of $30.0W^{-1}km^{-1}$ was reported [66] in 2006 with further reduction of $A_{eff}$ to $8.5\mu m^2$.
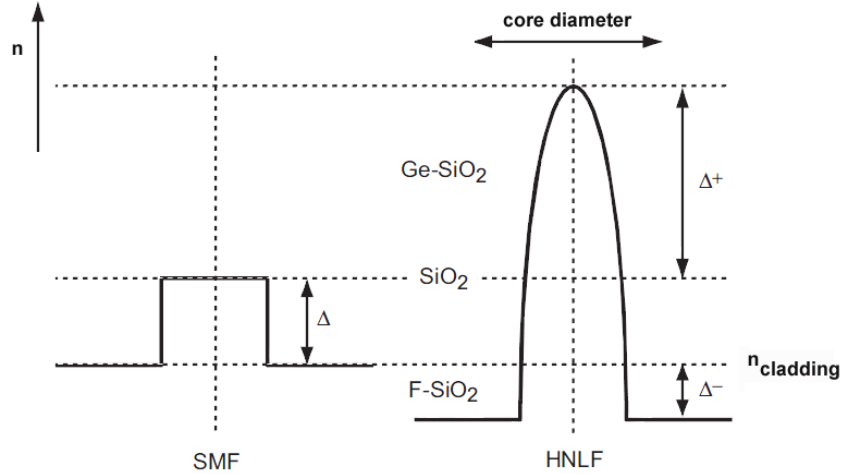
Figure 4.2: Refractive inxex profile comparison of conventional silica fiber to a DS-HNLF fiber [43].

## 4.1.2 Soft-glass nonlinear fibers

Soft-glass fibers based on chalcogenide, bismuth-silicate and lead-silicate provide not only higher nonlinear coefficient ($\gamma$ in orders of 100,1000x higher than silica), but also different IR transparencies (in NIR and MIR), attenuation, refractive indices (e.g. 2.8 for arsenic-selenides) and chemical and mechanical properties.

**Chalcogenide fibers**

Chalcogenide glasses represent an IR-transparent material for state-of-art photonic applications. They are formed by Group-IV chalcogen elements: sulfur (S), selenium (Se) and tellurium (Te). Various other elements may be included to form the lattice or be co-doped to modify their thermal, chemical, mechanical or optical properties, such as silicon (Si), arsenic (As), phosphorus (P), indium (In), germanium (Ge), gallium (Ga) and rare-earths (Er, Yb, Pr, Tm). Chalcogenide glasses are unique for their wide application range in the wavelength region between $1\mu$m $- 10\mu$m, with particular utilization dependent on chemical composition and fabrication process.

Chalcogenide fibers have been fabricated since 1990s, when multimode operation in the telecommunication bands was achieved [67]. Later on single-mode regime was obtained with cut-off wavelength of approximately $2.7\mu$m [68]. After year 2000, fabrication process was further perfected to enable chalcogenide photonic crystal fiber production [69].

Chalcogenide glass fibers (planar waveguides) provide extremely large nonlinearities ($n_2$ is 100 $\sim$ 1000 times greater than in silica) and high refractive indices (e.g. approximately 2.4 and 2.8 for arsenide-sulfide and arsenide-selenide respectively), which leads to suitable employment in high-power delivery for CO or $CO_2$ lasers [70], supercontinuum generation [71], utilization in all-optical devices [72] , for extremely efficient four-wave mixing [73] and slow-light applications [74]. Typical values of the nonlinear coefficient for

36

chalcogenide fibers are over 1000 $W^{-1}km^{-1}$ for arsenic-sulfide and close to 2000 $W^{-1}km^{-1}$ for arsenic-selenide fibers.

Some of the main chalcogenide representatives are presented in Fig. 4.3 in comparison with conventional silica fibers and ZBLAN fibers.
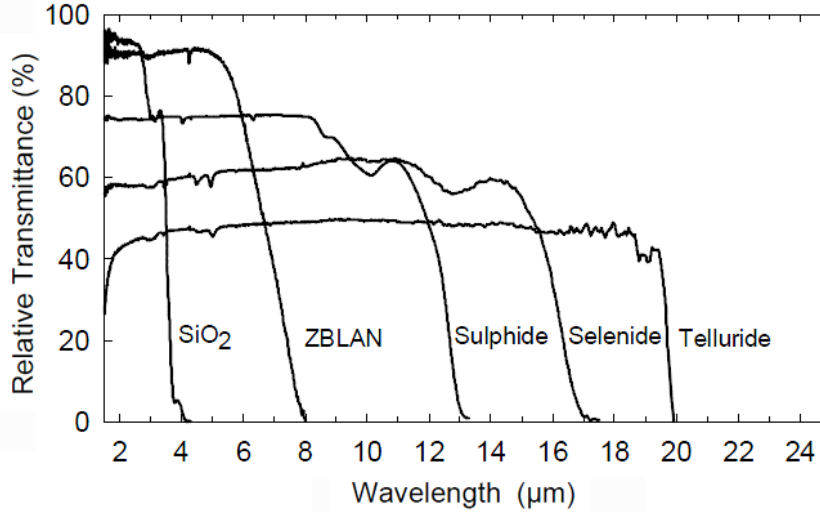


Figure 4.3: IR-transparency comparison of soft-glass nonlinear fibers, ZBLAN and conventional silica [75]

ZBLAN fibers are flouride-based optical fibers with transmission window to approximately 7$\mu$m, with their losses are under 1dB/m, which surpasses conventional silica fibers in terms of MIR applications. ZBLAN fibers can be doped by rare-earth elements for fiber amplification, but their nonlinear properties are insignificant for this thesis and therefore ZBLAN fibers will not be consider further.

**Bismuth-silicate fibers**

Bismuth-oxide based glasses have attracted attention in the last two decades. Their main advantage over chalcogenide glasses is in their non-toxicity and chemical stability. They can be employed thanks to their luminiscence in fiber amplifiers and fiber lasers [76]. Due to their nonlinear properties, they have been also exploited for all-optical processing and supercontinuum generation [77, 78], where nonlinear coefficient $\gamma$ over 1000$W^{-1}km^{-1}$ was reported.

## 4.2 Microstructured fibers

At the end of the twentieth century nonlinear fiber optics experienced a significant scientific interest and a great effort was focused on increasing fiber nonlinearity. Whereas further reduction of the core size was impossible, greater field confinement was achieved by large refractive index contrast of core and cladding, where in the cladding multiple air holes were included. The first microstructured fiber was presented in [79], where

the core and cladding were composed of pure silica with no added dopants. Thus the original microstructured optical fibers were developed (sometimes also denoted as holey fibers). There are some disputations over the terminology considering MOFs, but generally photonic-crystal fibers (PCFs) and MOFs are considered the same, whereas photonic crystal fiber is the more utilized term for fibers with large number of air holes (>10).

During the following years microstructured fibers have evolved and may be divided into two major subcategories as:

- photonic-bandgap fibers (PBGFs), which can be also denoted as hollow-core fibers (HCFs).
- suspended core microstructured optical fibers (SC-MOFs or SCFs), which represent MOF with only a small number of large air holes (typically 3 air-holes) surrounding a very small solid core (one to several microns).

With additional differentiation to large-mode area microstructured optical fibers (LMA-MOFs), endlessly single-mode microstructured optical fibers (ESM-MOFs), multi-core fibers and many others. A summary of different PCF types is depicted in Fig. 4.4 (not counting fiber 5b, the rule of PCF denomination only for MOFs with large number of air holes applies). The black regions are hollow, the white regions are pure glass, and the grey regions are doped glass. An ESM solid-core PCF is presented (a), a nanoweb fiber (b), which is not a PCF. All-solid glass PCF (c) with raised-index doped glass strands in the cladding, SC-PCF (d) with high air-filling fraction and small core, a dual-core PCF (e), a Kagome hollow-core PCF (f), a seven-cell hollow-core PCF (g), a birefringent PCF (h), a carbon-ring structure for PBG guidance (i) and a double-clad PCF (j) are presented.
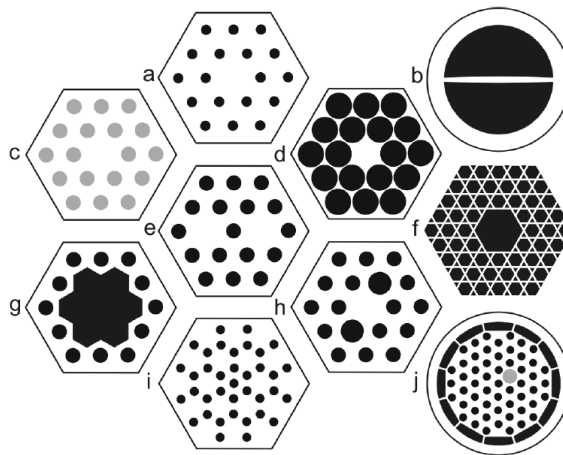


Figure 4.4: Representative sketches of different types of PCF [80].

### 4.2.1 Silica-based microstructured fibers

**Photonic bandgap fibers**

Microstructured fibers exploiting the stopband effect in periodic structures [81], which can be extended to prevent propagation in all directions but the propagation axis are the photonic bandgap fibers. The light propagates in a hollow air-filled core from which the denomination hollow-core microstructured fibers comes. The main advantage is the elimination of the total internal refraction (TIR) requirement. Number of air holes depends on particular fiber properties and parameters, but typically is in orders of 10s or 100s.

From the point of linear and nonlinear properties PBGFs provide losses considerably higher than standard silica fibers (orders of dB/m), but are acceptable for lengths in order of meters. A special low-loss hollow-core PCF design is depicted in Fig. 4.5 with a core diameter of 20.4$\mu$m, and the attenuation in the best cases approaching 1 dB/km at 1550nm.

Nonlinear coefficient $\gamma$ for PBGFs is given as:

$$\gamma = \frac{2\pi n_2}{\lambda A_{eff}}[\Gamma n_{2air} + (1 - \Gamma)n_{2silica}], \tag{4.3}$$

where $\Gamma$ stands for the mode confinement. The nonlinear coefficient is influenced both by air and silica, as the mode propagates in both media. Given that for air $n_2$=2.9$\cdot$10$^{-23}$m$^2$W$^{-1}$ and for silica $n_2$=2.6$\cdot$10$^{-20}$m$^2$W$^{-1}$ it is clear, that the nonlinear coefficient will be almost three orders lower, when most of the mode propagates in air. Values of 0.023$\cdot$10$^{-20}$W$^{-1}$km$^{-1}$ were obtained [82]. Therefore air-filled PBGFs are not considered for the purpose of this thesis.

Fluid-filled PBGs on the other hand provide much larger nonlinearities in contrast to air-filled PBGs. They can be filled either by an appropritiate gas or liquid accroding to desired properties. Theoretical prediction indicates, that with a proper design $\gamma$ of 2400W$^{-1}$km$^{-1}$ can be reached, when PBG is filled with carbon disulfide and nitrobenzene [83].
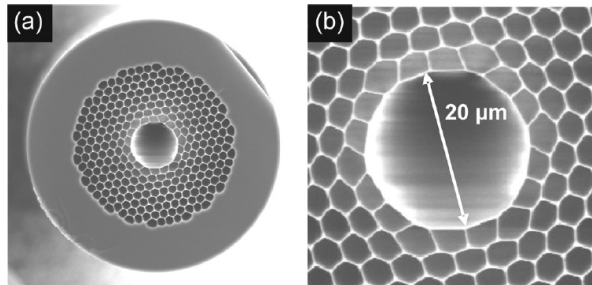


Figure 4.5: Example of a low-loss hollow-core PCF, the whole fiber (left) and detail of the core area (right) [80].

**Suspended core fibers**

Microstuctured fibers with only a few ($<10$) air holes are suspended core fibers. Unlike PBGFs air holes are significantly larger, the core area is solid and can reach diameters under one micron. First report of a silica SCF dates back to the year 1973 [84].

In 2008 silica SCFs were presented [85], with increased nonlinearity achieved by extreme reduction of the core size was reported. As in conventional HNLF, also for SCFs doping of the silica core can be utilized to enhance nonlinear properties, i.e. increase mode confinement. Still considering silica with $n_2$=2.6·$10^{-20}$m$^2$W$^{-1}$ , $\gamma$ of 60W$^{-1}$km$^{-1}$ for $A_{eff}$ of 1.75 $\mu$m$^2$ was acquired. Results of the work are presented in Fig. 4.6. , where SCF1 had no germanium in the core, SCF2 had a germanium doped center of $\sim$60 $\mu$m core radius and graded refractive index with NA=0.275 and SCF3 had a germanium-doped center similar to SCF2. Close-up of SCF1 is essentially the same as SCF2, whereas a global view is used to show the whole fiber structure.
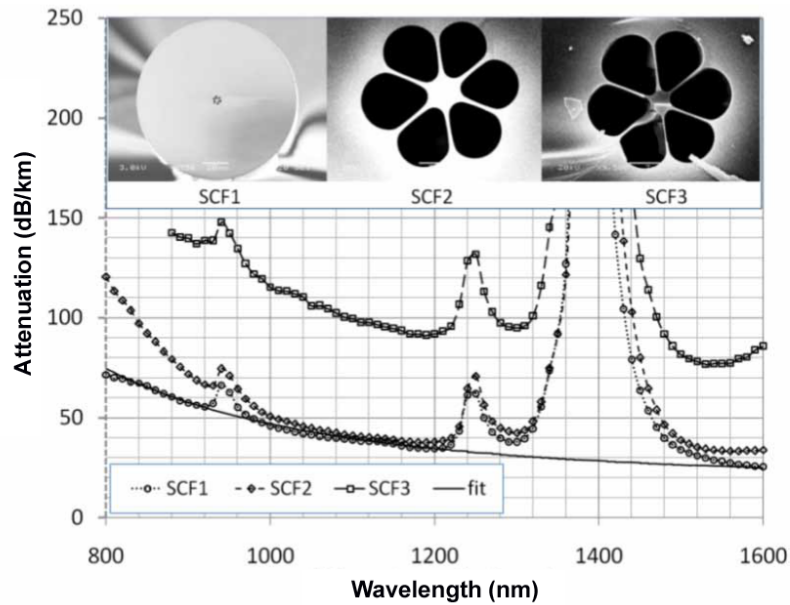


Figure 4.6: Measured loss for three suspended core fibers with details of their cross-sections [85].

## 4.2.2 Soft-glass microstructured fibers

As the technology has matured, novel glass materials have been utilized for microstructured fiber designs. Among the most exploited representatives chalcogenide MOFs and lead-silicate glass MOFs will be discussed as they provide extreme nonlinearities (in orders of $10^3$ and $10^4$ W$^{-1}$km$^{-1}$).

## Chalcogenide microstructured fibers

First report of a non-silica MOF came in the year 2000 by T.M.Monro et al. [86] with a gallium lanthanum sulphide (GLS) glass composition. GLS glass provided transparency till $5\mu$m with refractive index of 2.3~2.5. Later chalcogenide photonic crystal fibers (CHG-PCFs) with $As_2Se_3$ composition were presented [87] obtaining $\gamma$ of more than $2000W^{-1}km^{-1}$ (see Fig.4.7). Suspended core chalcogenide fibers (CHG-SCF) were simulteneously studied with great succes in effective area reduction and thus increased nonlinearity, also working with the $As_2Se_3$ composition. Highest achieved nonlinearity $\gamma$ of approximately $46000W^{-1}km^{-1}$ was presented [88]. Further tailoring of these CHG-SCF opened wide applications for wavelengths above $2\mu$m [89].
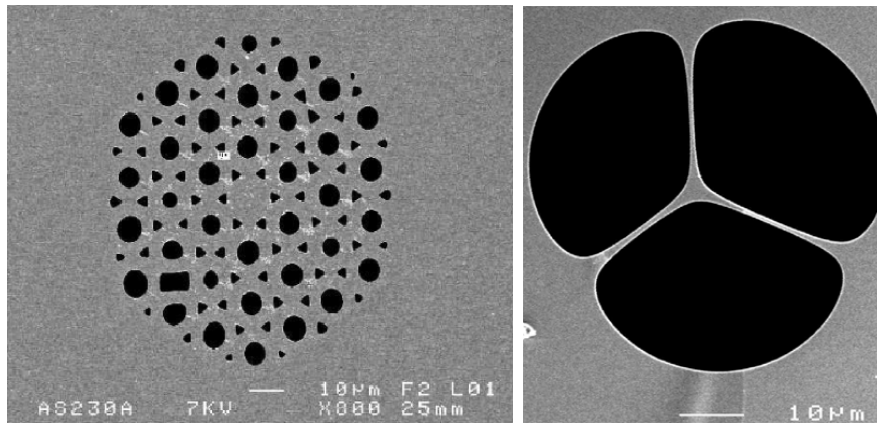


Figure 4.7: Cross section of $As_2Se_3$ CHG-PCF [87] (left) and $As_2Se_3$ CHG-SCF with $3.5\mu$m core diameter [89] (right).

## Lead-silicate microstructured fibers

Apart from chalcogenide glasses, heavy-metal oxide (HMO) glasses provide high refractive indices and thus also high nonlinear coeficients. HMO glasses have a relatively low melting temperature (under 1000°C) which makes fiber drawing more facile, but complicates fusion splicing to conventional SMFs. In [64] a broad study of various lead-silicate nonlinear fibers is presented, with discussion over refractive index profiles and microstructure types as depicted in Fig. 4.8. For this study a commercial Schott glass ($SiO_2PbO$, $PbO > 40$ mol. %) was employed.
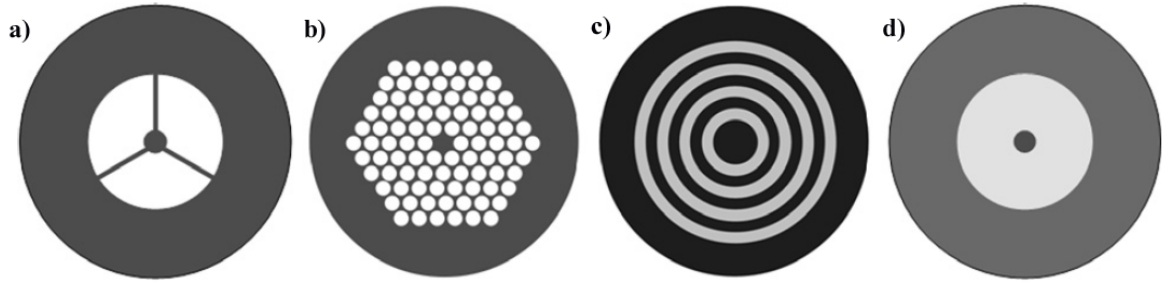
Figure 4.8: Cross sections of different lead-silicate fiber structures [64], a) SCF, b) 2D MOF, c) 1D MOF, d) W-profile (as for HNLF)

**Lead-bismuth-gallate microstructured fiber**

Microstructured lead-bismuth-gallium (in literature often denoted as PBG, plumbum-bismuth-gallium, but for this thesis to avoid term collision with photonic bandgap fibers denoted as LBG) fibers stand for a comparative candidate to conventional chalcogenide fibers, but provide considerably different dispersion profile. Nonlinearity of more than $1000\text{W}^{-1}\text{km}^{-1}$ was measured at 1064nm [37] for LBG PCF. Supercontinuum generation was presented on a 2cm and 8cm long LBG PCF respetively [90]. Cross sections of LBG PCF taken by scanning electron microscope (SEM) are presented in Fig. 4.9, with core diameter of $1.88\mu$m, hole diameter $\sim 2.15\mu$m and hole distance $\sim 2.30\mu$m. The microstructured area diameter was $\sim 30\mu$m and the whole fiber diamater was measured to be $75\mu$m. LBG-SCFs were developed for utilization in proposed OPS methodology, but due to ongoing technological process optimizations, they are not discussed further in the thesis.
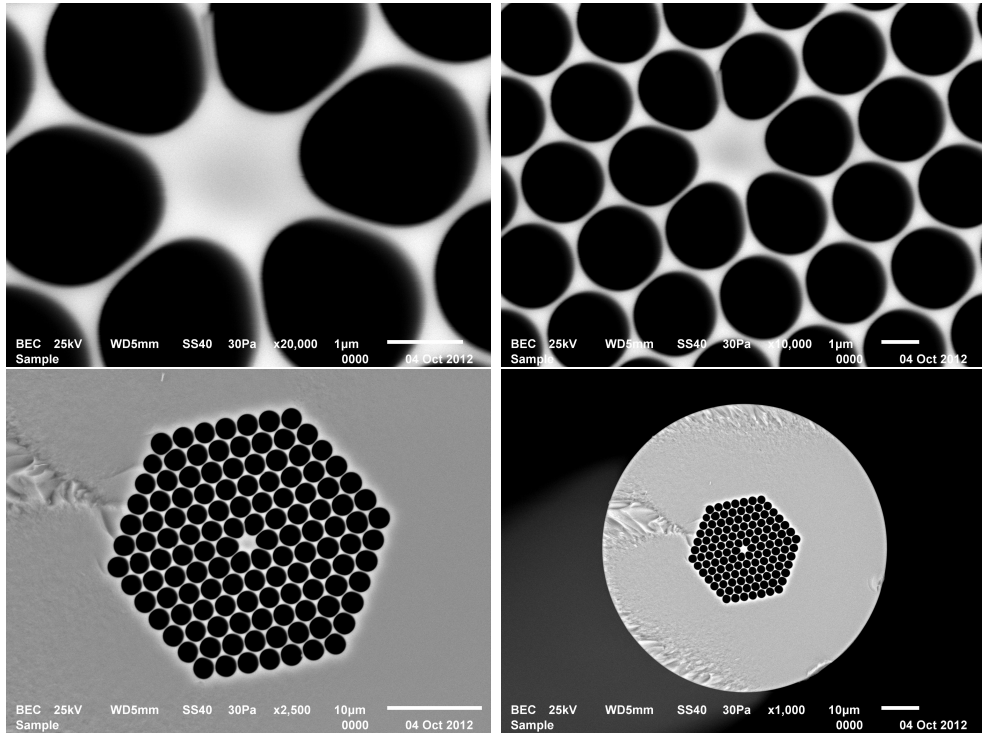
Figure 4.9: Cross sections of lead-bismuth-gallate MOF with details of core area, MOF structure and complete view of the fiber, taken by SEM.
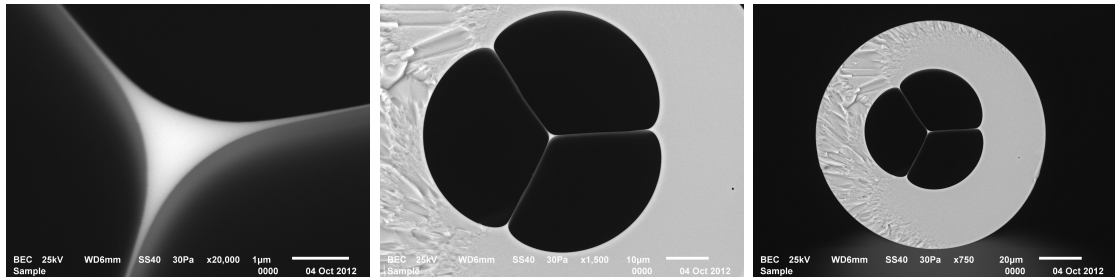


Figure 4.10: Cross sections of lead-bismuth-gallate SCF with details on core area, MOF structure and complete view of the fiber, taken by SEM.

In Fig. 4.10 SEM pictures of LBG SCF cross sections are presented. Core diameter was $1.09\mu$m, air-hole diameter was $\sim 29.3\mu$m with thin bridges of $\sim 0.08\mu$m between the airholes. The fiber diamater was $107\mu$m. Recent efforts were aimed at LBG SCF production with core diameter under $1\mu$m.

## 4.3 Fiber tapering

Further decrease of $A_{eff}$ can be achieved by fiber tapering. Fiber tapering represents a process, when the optical fiber is heated to its melting temperature and then stretched with precise tension, thus producing a so called fiber taper. The taper has two transition regions and a waist with diameter $d_{waist} < d_{fiber}$, whereas when waist diameter is tapered under one micron the so called nanowires or nanotapers are produced. Figure 4.11 illustrates optical wave propagation through a fiber taper, where significant energy compression is observed in the taper waist area.
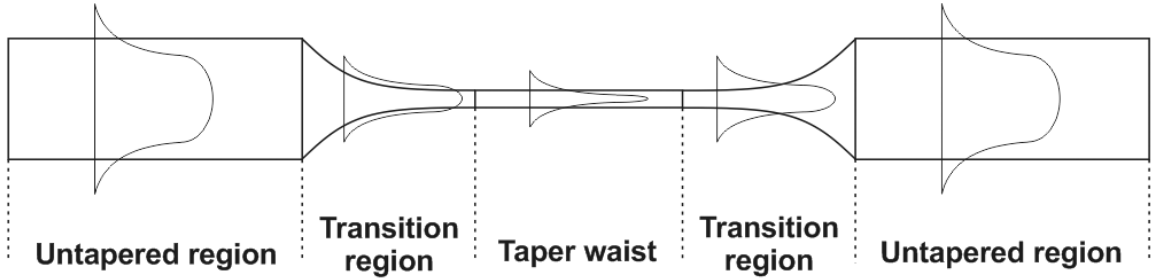


Figure 4.11: Fiber taper schematic and optical field evolution.

Tapering of silica fibers is a well known process for manufacturing couplers, beam expanders and wavelength selective components. Full theoretical description of fiber tapers was presented in 1992 [91] with a detailed study of propagating modes in different taper areas [92].

Recently fiber tapering extended from conventional fibers to microstructured and soft glass fibers. For these special applications the tapering process was modified and apart from heating over flame, $CO_2$ laser tapering has been utilized [93] or also ohmic heating has been employed [94].

## 4.4 Conclusion

This chapter provided a brief summary of state-of-art optical fibers for nonlinear switching. Various glass materials were discussed, with the emphasis on soft-glass as a candidate for achieving extreme nonlinearities over 1000 $W^{-1}km^{-1}$ suitable for switching processes. Microstructure designs were presented providing increased nonlinearity, where by combining soft-glass materials and microstructures even higher nonlinear coefficients can be obtained (more than 10000 $W^{-1}km^{-1}$). Finally fiber tapering was presented offering a comparable approach to microstructured fibers. Table 4.1 presents a summary of various state-of-art nonlinear fibers.

Table 4.1: Nonlinear fiber comparison - at 1550nm

| Fiber type | $n_2$ [m$^2$/W] | $\gamma$ [W$^{-1}$km$^{-1}$] | $A_{eff}$ [$\mu$m$^2$] | Ref. |
|---|---|---|---|---|
| Conventional silica | $2.6 \cdot 10^{-20}$ | 2 | 80 | |
| HNLF | $3.4 \cdot 10^{-20}$ | 30 | 8.5 | [66] |
| As$_2$Se$_3$ | $1.2 \cdot 10^{-17}$ | 1200 | 37.0 | [72] |
| Bismuth | $1.2 \cdot 10^{-18}$ | 1360 | 4.0 | [72] |
| Silica SCF | $2.6 \cdot 10^{-20}$ | 60 | 1.75 | [85] |
| As$_2$Se$_3$ PCF | $1.2 \cdot 10^{-17}$ | 2000 | 21.0 | [87] |
| As$_2$Se$_3$ SCF | $1.2 \cdot 10^{-17}$ | 46000 | 1.15 | [73] |
| Lead-silicate SCF* | $4.1 \cdot 10^{-19}$ | 1850 | - | [64] |
| Lead-silicate MOF* | $4.1 \cdot 10^{-19}$ | 270 | - | [64] |
| Silica taper* | $2.6 \cdot 10^{-20}$ | 67 | 1.36 | [95] |
| As$_2$Se$_3$ taper | $1.2 \cdot 10^{-17}$ | 2270 | 20.0 | [72] |
| As$_2$Se$_3$ nanotaper* | $1.2 \cdot 10^{-17}$ | 164000 | 0.26 | [95] |

\* - utilizing commercial SF6 Schott glass

\*\* - theoretical limits

# Chapter 5

# Thesis objectives

Main objectives of the dissertation thesis are to propose a novel switching methodology for optical packet switching based on nonlinear optics. An innovative approach to optical packet switching will be presented based on analysis of state-of-art materials and advancements in fiber technology. Switching method employing nonlinear phenomenon will be studied theoretically and analytically. As the topic spans over an extremely wide research area several decisions have to be made, to keep the thesis focused on solving its main aim.

**Major decisions:**

- Only one switching fabric (MEMS, monolithically integrated or fiber-based) will be discussed for optical packet switching.
- Only one labelling technique (WDM, OTDM, etc.) will be analyzed.
- Only one switching technique (Broadcast-and-select, space-switching, etc.) will be exploited.
- 1xN or NxN switching scheme will be employed.

First decision was the switching fabric selection. Employing MEMS for switching is speed-limited to the order of microseconds, therefore MEMS was discarded. The choice between monolithically integrated and fiber-based approach was decided by passive functionality of optical fibers and by substantial background in the technology of optical fibers preparation.

Labelling technique selection was carried out in favor of the WDM approach. The main reason is that WDM labelling does not require synchronization as the OTDM technique and the OCSS method is not as facile from the point of label generation as the WDM technique.

Third decision was to choose the switching technique. As the thesis is focused on nonlinear optics, wavelength routing was selected. Space-switching and broadcast-and-select switching methods were not considered.

Last decision was the choice between 1xN and NxN switching setup. As this thesis primarily develops the switching methodology and does not deal with engineering aspects

of the whole optical packet switch itself, 1xN setup was preffered.

**To summarize, for the purpose of this thesis the choice was made for 1xN fiber-based wavelength routing switching scheme with the WDM labelling technique.**

Based on the previous chapters the criteria for the new switching methodology have been then set as follows:

- Modulation format transparency
- Bitrate insensitivity
- Polarization insensitivity
- High-speed switching
- Switching efficiency
- Wavelength range
- Spectral efficiency

According to the above mentioned criteria and chosen methodology, following two chapters will be focused on the development of technological aspects of utilized optical fibers with enhanced nonlinearity and on the switching methodology. The most suitable approach will be analytically studied. A complete optical packet switch based on selected methodology will be constructed to enable wide range analyses.

**The main thesis focuses can be therefore stated as:**

- Technological development of novel nonlinearity enhanced optical fiber and their optimization for optical packet switching.
- Proposal and theoretical and experimental verification of the optical packet switching methodology.

# Chapter 6

# Nonlinear fiber technology development

## 6.1 Utilized enhanced nonlinearity fibers

First step to fulfill the thesis objectives was the technological development, characterization and optimization of enhanced nonlinearity fibers with appropriate parameters for optical packet switching. Two fibers were considered with HNLF as a reference. The following single-mode fibers were chosen:

- HNLF
- Chalcogenide $As_2Se_3$ fiber ($As_2Se_3$ fiber)
- Suspended core silica fiber with highly Ge-doped core (Ge-SCF)

### 6.1.1 Highly nonlinear silica fiber

A standard commercialy available HNLF was chosen as a representative of a conventional nonlinear fiber. HNLF utilized for the purpose of this thesis had the parameters given in Table 6.1. Fiber dimensions were similar to conventional silica single-mode SMF-28e fiber.

Table 6.1: HNLF parameters at 1550nm, manufactured by OFS

| | |
|---|---|
| Numerical aperture [-] | 0.16 |
| Effective mode area [$\mu m^2$] | 11.6 |
| Attenuation [dB/km] | 0.88 |
| Zero dispersion wavelength [nm] | 1559±4 |
| Dispersion [ps/nm/km] | -2.5 to 2.0 |
| Dispersion slope [ps/nm$^2$/km] | 0.019±0.004 |
| Nonlinear coefficient [W$^{-1}$km$^{-1}$] | 11.5 (11.35*) |

* measured by the FWM technique

discussed in section 6.2

Among the main advantages of the HNLF are ZDWL in close vicinity of 1550nm, almost flat dispersion profile in the C-band region and also silica glass material, which implies facile connections to conventional SMF-28e fibers.

## 6.1.2 Suspended core silica fiber with highly Ge-doped core

A suspended core silica fiber with highly Ge-doped core provided by IPHT, Jena, Germany was exploited for the purpose of this thesis. Cross-section of utilized Ge-SCF is presented in Fig. 6.1 with the core diameter of $6.6\mu$m.
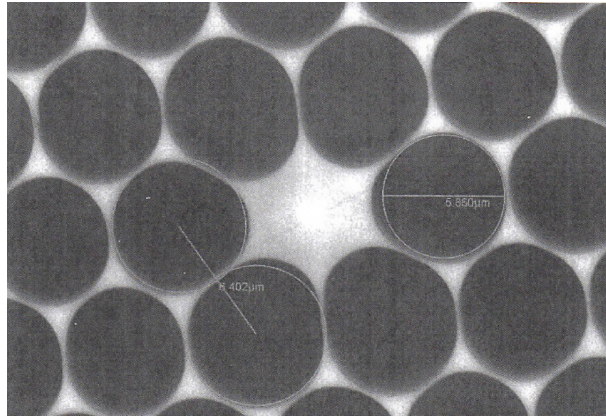


Figure 6.1: Cross-section of utilized Ge-SCF, manufactured at IPHT, Jena, Germany. Taken by SEM.

Table 6.2 summarizes Ge-SCF parameters for two types of the employed fiber. First sample 318b10 had a smaller Ge-doped area than sample 252b3, which resulted in lower mode confinement, also with the smaller core diameter. On the other hand larger Ge-doped area for sample 252b3 implied larger total dopant concentration, therefore also higher nonlinear response of sample 252b3. Lower attenuation of sample 252b3 enables utilization of longer component than for sample 318b10.

**Ge-SCFs connection to SMF-28e**

A splicing method has been developed for Ge-SCF connection to a conventional silica SMF-28e fiber. Almost negligible splice losses were obtained at 1550nm (<1 dB per splice). All these procedures were carried out in cooperation with SQS Fiber optics, Czech Republic, therefore exact technological processing steps cannot be mentioned in this thesis due to ongoing patent application.

Table 6.2: Ge-SCF parameters at 1550nm, given by manufacturer.

| | Sample 318b10 | Sample 252b3 |
|---|---|---|
| Ge-doped area diameter [$\mu$m] | 0.9 | 1.4 |
| Core diameter [$\mu$m] | 5.9 | 6.6 |
| Air-hole diameter [$\mu$m] | 5.9 | 5.8 |
| Air-hole distance [$\mu$m] | 6.4 | - |
| Bridge width [$\mu$m] | 0.5 | 0.7 |
| MOF area diameter [$\mu$m] | 66.6 | 61.5 |
| Fiber diameter [$\mu$m] | 139.9 | 127.0 |
| Coating diameter [$\mu$m] | 236.3 | 226.8 |
| Numerical aperture [-] | - | 0.45 |
| Mode field diameter [$\mu$m] | - | 3.3 |
| Attenuation [dB/m] | 0.070 | 0.043 |
| Dispersion [ps/nm/km] | 32.6 | - |
| Dispersion slope [ps/nm$^2$/km] | 0.141 | - |
| Nonlinear coefficient [W$^{-1}$km$^{-1}$] | 21.0 | - |

### 6.1.3 Chalcogenide As$_2$Se$_3$ fiber

Chalcogenide As$_2$Se$_3$ single-mode fiber was employed in this thesis. The fiber was prepared by the double-crucible technique developed at the Naval Research Laboratory (NRT) [68].

First sample with single-mode cut-off at ∼1500nm was utilized with dimensions of 6.3/172/310$\mu$m core/cladding/coating and numerical aperture NA ≈0.16. Due to drawing technique imperfections, core excentricity of more than 6$\mu$m was observed. This fact together with large refractive index contrast to conventional silica fiber caused extreme connection losses and even when operating with these losses, single-mode regime was not achieved, probably due to waveguiding defects. Mode-strippers were applied to eliminate modes propagating in the cladding, which proved as a succesfull approach, but the whole component losses were still over 20 dB.

Second sample with single-mode cut-off at approximately ∼1300nm has been employed in the latest measurements. Its main parameters are summarized in Table 6.3. Major difference between the second and the first sample lies in minimized core excentricity, leading to simplified coupling to conventional fibers. Also the fiber attenuation was significantly reduced by the improved drawing technique and the need for mode-strippers was eliminated. The importance of the reduced attenuation for switching purposes will be discussed in detail in the following subsection.

Table 6.3: $As_2Se_3$ fiber sample parameters at 1550nm

| | 1300nm cut-off sample |
|---|---|
| Core diameter [$\mu$m] | 5.8 |
| Fiber diameter [$\mu$m] | 172 |
| Coating diameter [$\mu$m] | 310 |
| Numerical aperture [-] | 0.16 |
| Attenuation [dB/m] | 0.58 |
| Dispersion [ps/nm/km] | -560 |

**Chalcogenides connection to SMF-28e**

The crucial part of $As_2Se_3$ fibers implementation lies in coupling of the propagated light from/to conventional silica SMF-28e fiber. $As_2Se_3$ fiber samples employed in this thesis provide refractive index of 2.8, which in contrast to $\sim$1.46 of silica causes connection loss of $\sim$20% at each boundary.

Methods utilizing free-space optics (FSO) to couple light from silica to chalcogenide fibers (mostly of smaller core diameter and of different NA) were avoided in this thesis. This approach is feasible for laboratory measurements only, but as a component in an optical packet switch, FSO is inappropriate due to the need of precise adjustment and due to the thermal/vibrational instability of the FSO configuration. Fusion splicing of $As_2Se_3$ to conventional silica is however not possible due to large difference in melting temperatures of both materials, where for silica the melting temperature is around 1600°C and for $As_2Se_3$ it is substantialy lower around 190°C.

Connectorization technology had to be developed as well. Major challenges with $As_2Se_3$ fibers lie in four times higher glass fragility than silica, in their toxicity and in their small bending radius, thus excluding some well-known technological procedures. In Fig. 6.2 facets of three damaged flat polished connectors from our development stage are presented, illustrating fragility of the chalcogenide fiber and need of precise technological process. Specific technological procedures were evaluated in cooperation with SQS Fiber optics, Czech Republic, where reduced connection losses were observed (<1dB per connection). This was achieved by employing antireflex coating decreasing the detrimental effect of the refractive index difference (<1% reflection in the C-band). Recently a technological process for chalcogenide connectorization was mastered at SQS Fiber optics, Czech Republic and is currently being patented.
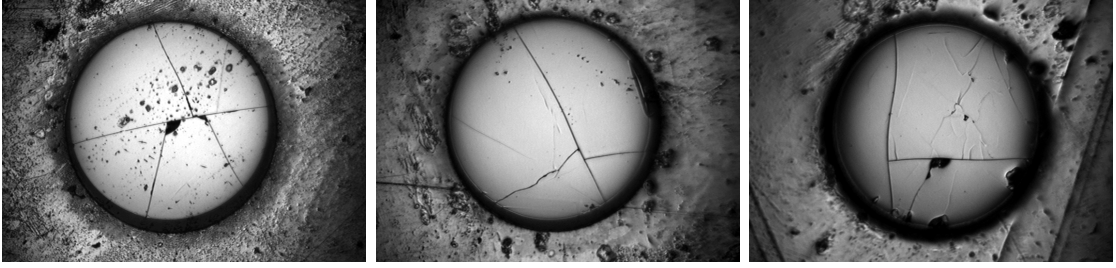
Figure 6.2: Facets of $As_2Se_3$ fiber samples damaged during the connectorization process.

A final component containing 26m $As_2Se_3$ fiber spool with standard silica SMF-28e fibers at output was developed. Insertion loss of 15.5 dB for the whole component was obtained. From this results one extremely important fact. We have developed a component with SMF-28e compatible outputs formed by $As_2Se_3$ fiber with attenuation lower than the value provided by manufacturer. In the following chapter a study of backreflected power was performed, which provided evidence of relatively significant reflection at the input $As_2Se_3$ connection, therefore we assume ∼1dB loss per connection. This leads to fiber attenuation of less than 0.6dB/m, which is the lowest loss for a $As_2Se_3$ single-mode fiber reported world-wide up to date (according to authors knowledge). It is then possible to develop $As_2Se_3$ components of ∼1m lengths with insertion loss <3dB, which is important for nonlinear processes.

## 6.2 Nonlinear coefficient estimation

To exactly measure nonlinear coefficient of evaluated fibers a method utilizing FWM [96] was employed. It considers two equal pump probe powers $P_0$ and equal FWM 1st order products of powers $P_1$. Measurement setup is depicted in Fig. 6.3. Two CW lasers served as pump signals, polarization controllers (PC1 and PC2) served for the purpose of polarization state matching. Pumps were then coupled (MUX) and propagated through a polarization isolator (PISO) and to suppress the effect of SBS, they were phase modulated (MOD) and amplified (AMP) in the range of 10 to 27dBm total power. Optical power was measured by a power meter before the fiber under test (FUT) and after the FWM process, where the generated idlers were filtered (DEMUX).

Nonlinear coefficient $\gamma$ was derived from equations [96]:

$$\triangle\varphi_{NL} = \gamma P_0 L_{eff}, \tag{6.1}$$

$$\frac{P_0}{P_1} = \frac{J_0^2(\varphi_{NL}/2) + J_1^2(\varphi_{NL}/2)}{J_1^2(\varphi_{NL}/2) + J_2^2(\varphi_{NL}/2)} \tag{6.2}$$

where $J_i$ represent the Bessel roots, $\varphi_{NL}$ stands for nonlinear phase shift and $L_{eff}$ is the effective length.
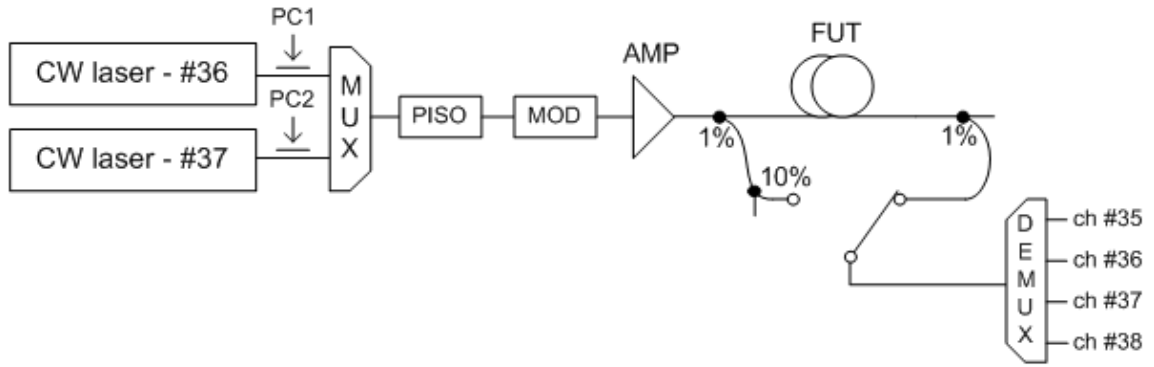
Figure 6.3: Nonlinear coefficient measurement setup.

First application of the measurement technique focused on the HNLF to verify the selected approach and to develop a processing tool for data evaluation. The manufacturer of utilized HNLF provided nonlinear coefficient value of 11.5 $\mathrm{W^{-1}km^{-1}}$. We have measured $\gamma$ of 11.35 $\mathrm{W^{-1}km^{-1}}$, thus verifying the method. Figure 6.4 illustrates one of the measured spectra for nonlinear coefficient estimation via the FWM method.
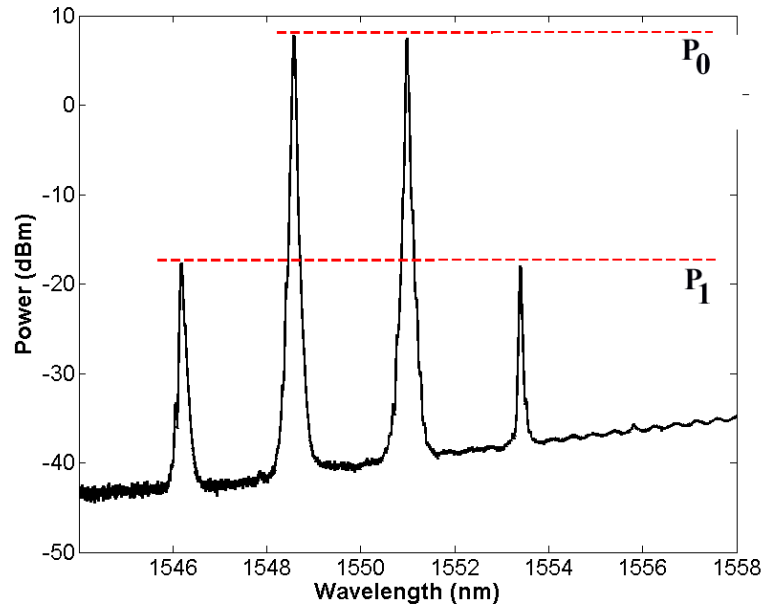


Figure 6.4: Measured FWM spectrum for nonlinear coefficient estimation.

For the $\mathrm{As_2Se_3}$ fiber $\gamma$ of 1300 $\mathrm{W^{-1}km^{-1}}$ was measured, confirming the results in papers related to chalcogenide fibers [72]. Ge-SCF was not measured by the FWM method and for further evaluations $\gamma$ of 21 $\mathrm{W^{-1}km^{-1}}$ (given by manufacturer) was considered for both type 318b10 and 252b3 (see Table 6.2), as type 252b3 had larger core, inducing lower mode confinement but on the other hand had larger Ge-doped area diameter. These two

facts counteract from the point of nonlinear coefficient and therefore the same value can be utilized for approximate solutions.

## 6.3   SPM measurements

For nonlinear response evaluation of chosen fibers the SPM effect was measured. Figure 6.5 depicts the SPM measurement setup. An u2t laser tuned to 1563nm and capable of generating pulses of 2ps in FWHM with a 10Gbps repetition rate served as a pump. Pulses were thereafter amplified in EDFA with a total output power of 10-20dBm, which means pulse peak powers ranging from 23-33dBm, if 5ps pulse is considered (pulse broadening in amplifier is taken into account). Excess amplifier noise was filtered by a spectrally-narrow filter (BF) and signal was then coupled into FUT. After propagating through FUT the signal was attenuated in two cascaded 90/10 couplers and measured by an optical spectral analyzer (OSA).
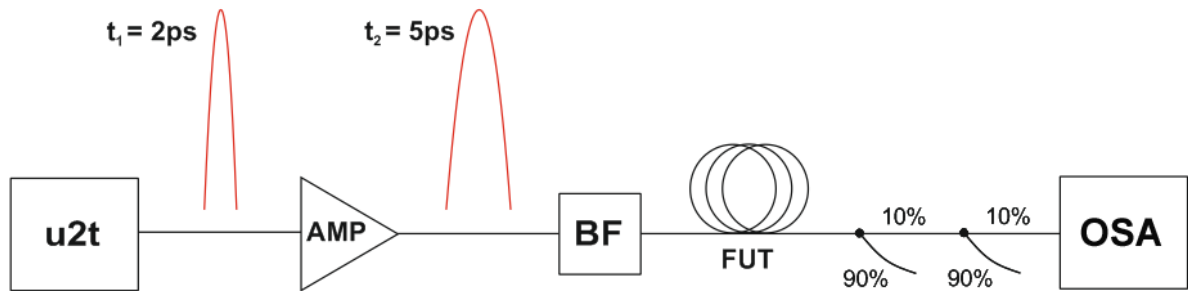


Figure 6.5: SPM measurement setup.

Pump peak powers were set in range of 3 to 13dBm. For Ge-SCF no spectral broadening was observed. $As_2Se_3$ showed broadening of only several nanometers (see Fig. 6.6). HNLF spectral broadening over 100nm depicted in Fig. 6.7 resulted from HNLF flat dispersion profile and normal dispersion at the wavelength of the u2t laser (tested HNLF had ZDWL at 1559nm).
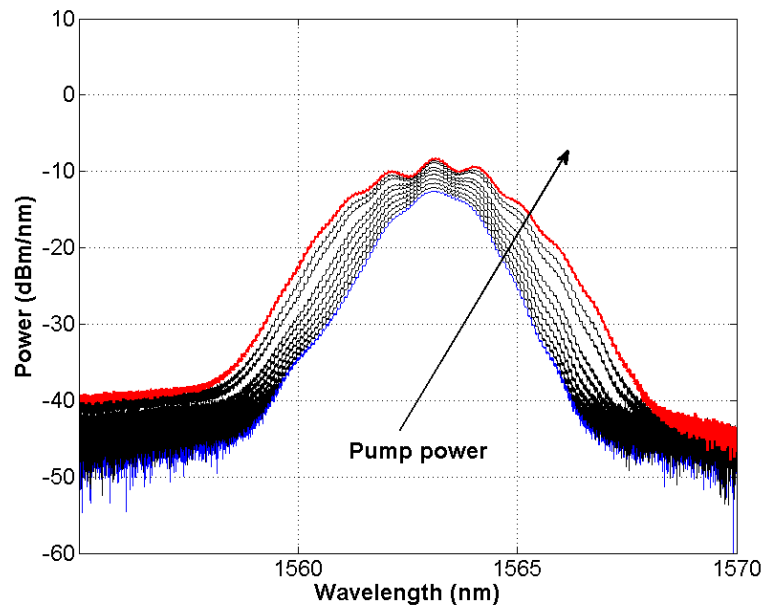
Figure 6.6: SPM spectral broadening in 26m As₂Se₃.
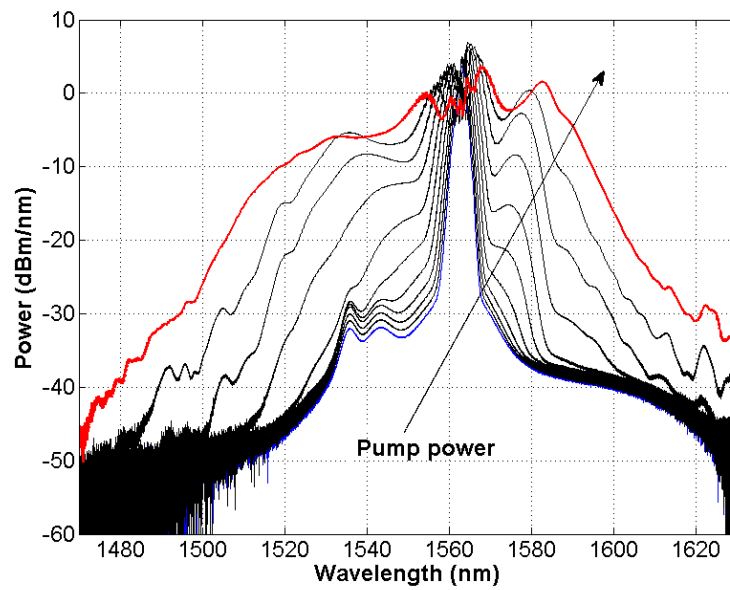


Figure 6.7: SPM spectral broadening in 500m HNLF.

## 6.4 Chalcogenides thermal tests

Thermal properties of chalcogenide glass fibers have been experimentally evaluated at NRT [97, 98, 99]. Arsenic-selenide fibers have proven to be thermally stable from +20 to +150°C in wavelength range of 2-5$\mu$m with maximum relative loss variation of 0.1dB/m [98]. Thermal study of microstructured chalcogenide fibers was performed for the purpose of multiple drawing process in [69] with the result of decreased losses of ~1dB/m in the region of 1.5 to 4$\mu$m.

The above mentioned references do not cover the whole temperature range required for the proposed switching methodology (-40 to +80°C) and were presented 10 years ago, whereas nowadays a perfected drawing technique is employed. Therefore more detailed parametrization was carried out. Furthermore, increased attenuation affects not only final component insetion loss but also nonlinear processes, e.g. conversion efficiency, when the generated idler can be attenuated. For the material study a multimode $As_2Se_3$ fibers with 172$\mu$m core and 330$\mu$m polymer cladding was utilized, where obtained results could be transferred to the $As_2Se_3$ single-mode fiber employed in the proposed optical packet switching methodology.

Measurement setup is depicted in Fig. 6.8. As a broadband light source a halogen lamp (HL) was utilized, providing 20W of output optical power within 350 to 2500nm. A 200$\mu$m polymer-clad silica (PCS) reference fiber was attached to the halogen lamp and at the sample output OSA was employed. Fibers under test (FUTs), all from the same fiber spool each of ~1m long, were placed in the isolated thermal chamber (ITC) with the possibility of setting temperature in the range of -70 to +180°C. FUT connectors were placed outside ITC, in order not to influence the measurement results (length of FUT in ITC was therefore less than 1m and was measured exactly for each separate measurement). Considering the fact that chalcogenide glasses are photosensitive and when exposed to irradiation of even relatively small optical powers, permanent material change can occur. This was suppressed by having the FUT in ITC blocked from external light. ITC throughput was sealed to eliminate any thermal losses or unwanted humidity in ITC during cooling tests. Temperature was detected in the vicinity of FUT by Comet thermometer (COMET) with -50 to +250°C temperature range (for temperatures below -50°C ITC internal thermometer was utilized). Reference room temperature was set to +20°C. Measured samples of FUT relative loss change were obtained for each 10°C step after reaching thermal equilibrium (approximately 15mins).
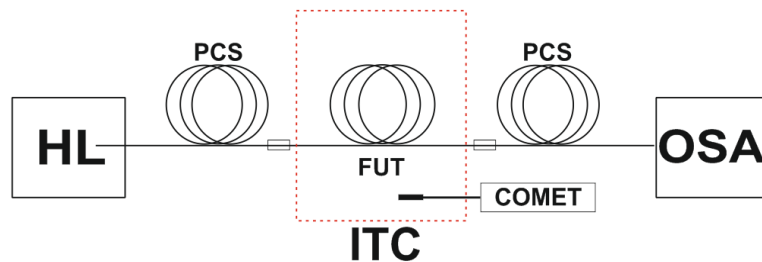


Figure 6.8: Measurement setup for thermal evaluation of $As_2Se_3$ fibers.
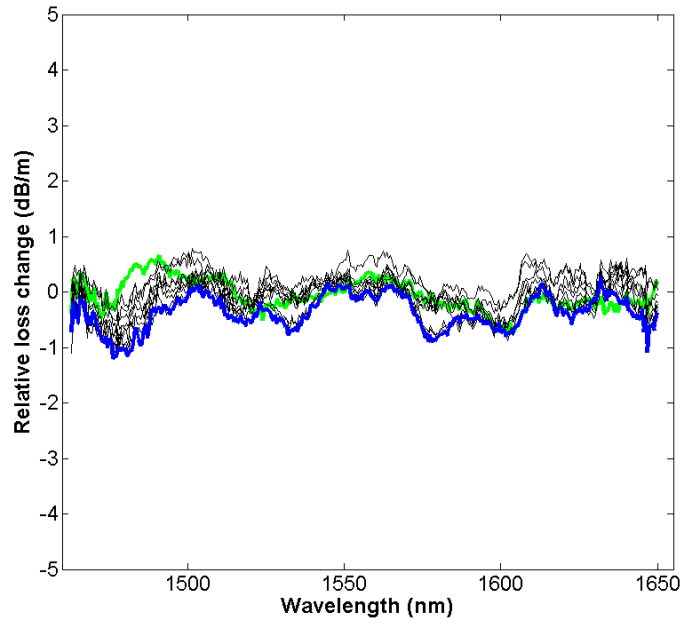
Figure 6.9: As$_2$Se$_3$ measured relative loss change for temperatures -70°C (green) to +20°C (blue).
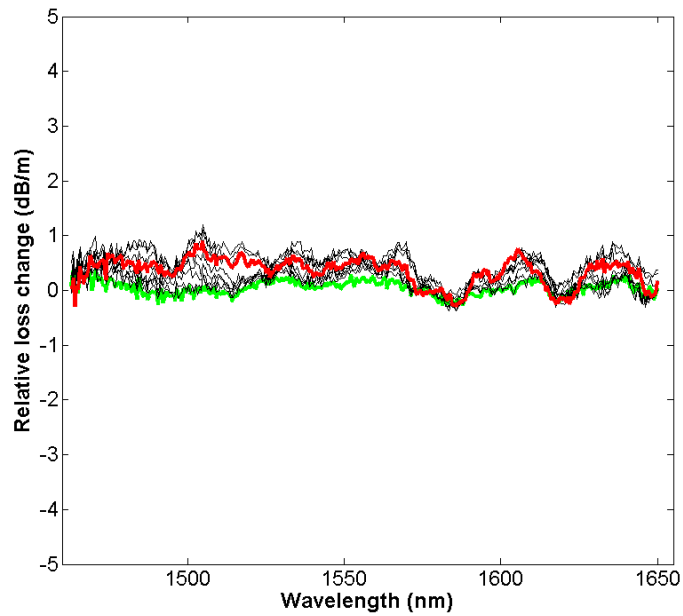


Figure 6.10: As$_2$Se$_3$ measured relative loss change for temperatures +20°C (green) to +110°C (red).

Obtained results for wavelengths 1460nm to 1650nm are presented in Fig. 6.9 for cooling measurements for temperatures from +20°C to -70°C and in Fig. 6.10 for heating

57

measurements for temperatures from $+20°$C to $+110°$C. Relative loss deviation from the reference value in the studied temperature range was under 1dB/m, which implies maximum $As_2Se_3$ single-mode fiber attenuation of $\sim$1.5dB/m. Calculated temperature dependence of the relative loss change in contrast to reference temperature was for heating $\partial(\triangle\alpha)/\partial T = 4\cdot10^{-3}$ dB/m/$°$C and for cooling $\partial(\triangle\alpha)/\partial T = 5\cdot10^{-3}$ dB/m/$°$C.

## 6.5 Arrayed-waveguide grating development

AWGs were developed at SQS Fiber optics, Czech Republic [100, 101] and were able to work under room temperature without any detuning. AWGs with 44 channels placed 100GHz apart on the ITU-grid were employed. For final application athermal-AWG (AAWG) were developed (for operation principle of AAWG see e.g. [102] ). They provided thermal stability in the range of -40 to $+80°$. Figure 6.11 depicts measured AWG spectrum with focus on one AWG period and in Fig. 6.12 with focus on AWG cyclicity. Functional samples for the AWG and AAWG were applied to provide legal protection of the technological procedures.
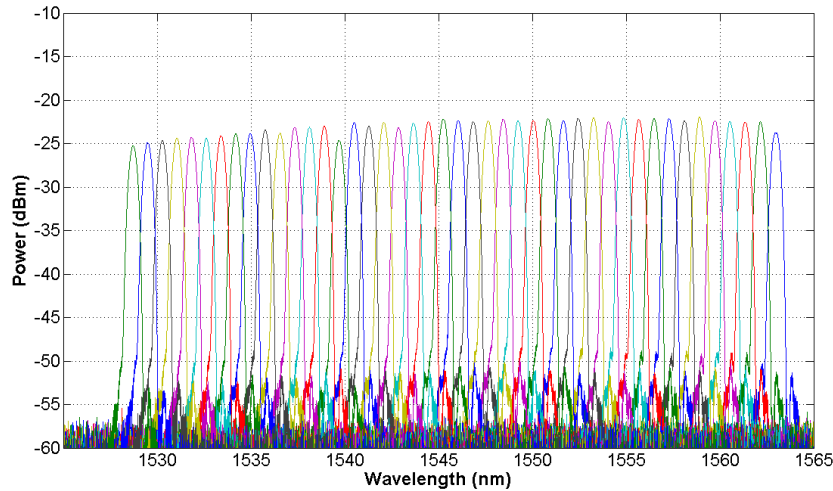


Figure 6.11: C-band spectrum of employed AWG by SQS Fiber optics, Czech Republic.

Measured spectra for AWG cyclicity have in practice equal power levels (insertion loss), but were limited in this measurement by the superluminiscent diode (SLED) emission spectrum. Cross-talks of AAWG were lower than -30dB with insertion loss of maximum 3.2dB.
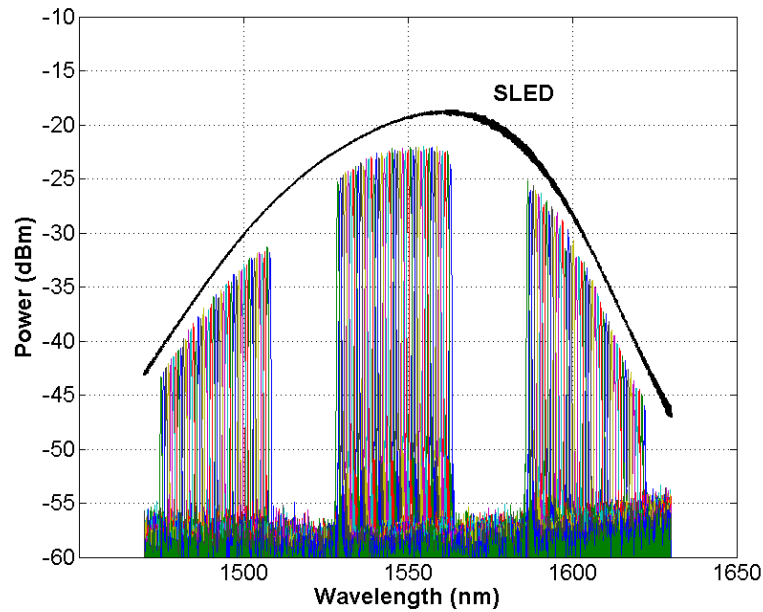
Figure 6.12: Cyclicity of employed AWG by SQS Fiber optics, Czech Republic, SLED - superluminescent light emmiting diode.

## 6.6 Conclusion

Three enhanced nonlinearity fibers were discussed. A commercially available HNLF was measured and its nonlinear coefficient of $11.35\text{W}^{-1}\text{km}^{-1}$ was verified by the FWM method, which is half the value of Ge-SCF nonlinear coefficient. $As_2Se_3$ fibers provided nonlinear coefficient of $\sim$1300 $\text{W}^{-1}\text{km}^{-1}$, but $As_2Se_3$ glass composition implied problematic connectioning to conventional fibers, therefore technology of both $As_2Se_3$ and also Ge-SCF connections to conventional silica fibers has been developed. Connectorization technology was mastered in SQS Fiber optics, Czech Republic and also permanent connections were prepared inducing losses of less than 1dB per connection. It has to be emphasized that presented technological advances and applied research have led to patent application (low-loss chalcogenide connection to silica fiber), several functional samples (AWG, AAWG) and pilot production (AAWG). SPM nonlinear response was measured for all utilized fibers with a significant spectral broadening of more than 100nm for HNLF. Thermal stability of chalcogenide $As_2Se_3$ was measured and thermal loss dependency was derived. Utilization from -70°C to more than +100°C in the C-band region with less than 1dB variation is possible based on measurement results.

# Chapter 7

# Proposal of the optical packet switching methodology

Though optical packet switched networks have not yet been employed in practice, some general OPS specifications may be set. Basic criteria were already summarized in the Thesis objectives (Chapter 5), such as polarization insensitivity, modulation format transparency, etc. There is also a standard set by the ITU-T [103] covering some OPS basic specifications. Other limitations and requirements can be deduced from opto-electronical counterparts, which are utilized in current networks. This chapter is focused on the switching methodology proposal. First development of a complete optical packet switch with focus on particular OPS segments is presented and then the switching methodology itself is discussed.

The chapter is divided into three sections. First section describes particular OPS segments development. Second section discusses the switching methodology itself with focus on various aspects of four-wave mixing and nonlinear fiber optimization. Last section then concludes the chapter with a summary of achieved results and proposal of the final OPS methodology.

## 7.1  Optical packet switch

First experimental setup of the hybrid OPS for testing of switching methods and nonlinear fibers is depicted in Fig. 7.1. Developed OPS consisted of four functional segments. First segment was composed of a payload generator, label generator and a multiplexer forming the optical packet. The generated optical packet was then propagated through a network segment and then the label was separated. Second segment was responsible for payload buffering. Third segment detected and processed the packet label and governed routing signal generation. Afterwards the buffered payload was multiplexed with the routing signal. In the fourth section propagation through the nonlinear fiber and new label attachment took place.
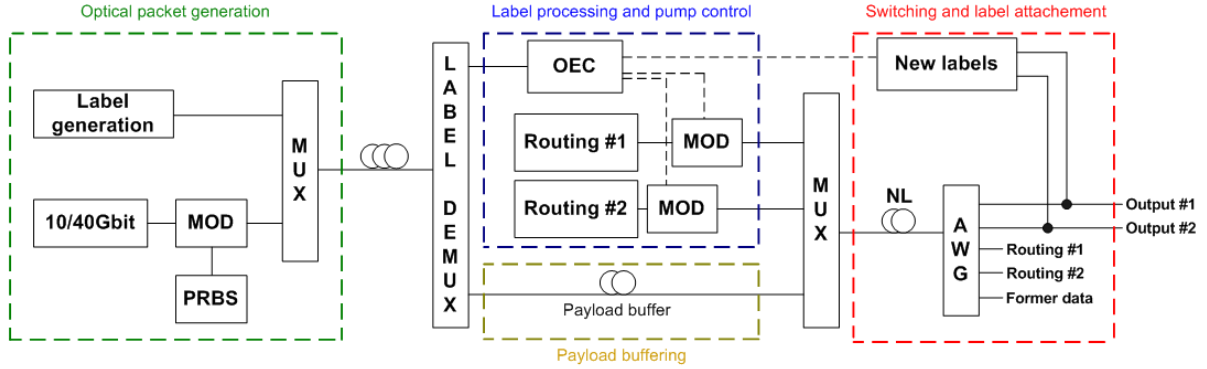
Figure 7.1: Proposed OPS setup, MOD - Mach-Zehnder modulator, MUX/DEMUX - multi/demultiplexer, PRBS - pseudo-random bit sequence, OEC - opto-electronic controller, NL - nonlinear fiber, AWG - arrayed-waveguide grating.

## 7.1.1 Optical packet generation

Data laser allocated on the 100GHz DWDM ITU-grid was externally modulated with a pseudo-random binary sequence (PRBS), thus forming the optical packet payload. In bit-error-rate (BER) measurements, the laser was replaced by a BER tester (BERT). For label generation two approaches were exploited, first approach employed small form-factor pluggable (SFP) modules placed on the CWDM grid, providing labels with slow modulation ($\sim$MHz) at wavelengths not coinciding with the data spectrum. Second approach considered CW label lasers allocated on the DWDM grid close to the data wavelengths.

The label generated by the SFP module carried 8 bits with a 100MHz modulation, which implied label length of 80ns. Two different bit sequences were utilized to distinguish output ports. In the next approach two CW labels at two separate wavelengths represented two output port requests. For payload and label coupling either a standard coupler, a wavelength multiplexer or AWG could be employed.

As the WDM out-band labelling was employed, the label could be separated from the data payload employing the same components as for payload and label coupling. With the two approaches considered, CW labels placed on the DWDM ITU-grid were separated by the AWG and SFP generated labels exploiting the CWDM grid were separated by a CWDM DEMUX. In-band labelling was taken into account only theoretically as it requires very narrow FBGs ($\sim$0.03nm) and therefore the development process is more complicated as their wavelengths must be precisely matched to the label wavelength, which results in decreased OPS scalability.

## 7.1.2 Opto-electronic control unit

For this thesis the hybrid opto-electronic approach for label processing was utilized. An opto-electronic controller (OEC) was developed for the purposes of optical label recognition, proccessing and routing signal generation. With the decision for hybrid OPS, demands on label processing time had to be dealt with, considering an optical packet of

100ns duration and 20ns guard time. The processing time limit was set to <10ns. Simplified setup of the developed OEC is presented in Fig. 7.2. At the input of the OEC a SFP module was utilized for direct label detection. As the SFP module had both reciever and transmitter, both label detection and new label generation were possible with one SFP. The detected signal was then fed into the FPGA for further processing. The processed signal was sent into a driver and further amplified in a fast three-stage operational amplifier with +/-12V swing capability. At last the signal passed through an attenuator (att) with reed relays that allowed tuning of insertion losses (up to 11 dB) for precise pulse amplitude adjustment. The attenuator was controlled by a delayed-start circuit to eliminate any possible damage by power spikes during power-up. OEC exhibited fast transient response (less than 4 ns) and high power output capability (more than 100 mA into 50 $\Omega$).
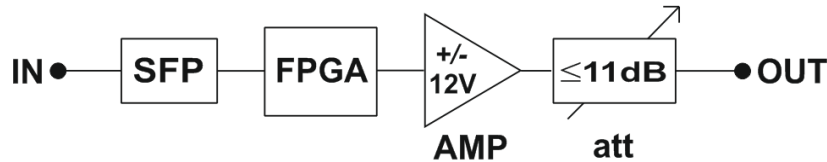


Figure 7.2: OEC configuration for label detection and processing.

The notable OEC advantages are attributed to the detection of low power optical pulses, 2R (re-shape and re-amplify) electronic regeneration and subsequent control of the routing signal laser diode. Thanks to its DC-coupling, optical data payload of arbitrary lengths could be switched. Major parameters of the developed OEC are summarized in Table 7.1.

Table 7.1: OEC parameters

| | |
|---|---|
| Rise time (fall time) | <5 ns |
| Peak-peak pulse amplitude | 112 mA/ 50$\Omega$ |
| Input sensitivity | < -21 dBm |
| Output amplitude tuning range | 0-22 dB |
| Wavelength range | C-band |
| Power consumption | <15 W |

For routing signal generation distributed feedback (DFB) Fitel Furukawa DWDM laser diodes with 10MHz line-width and internal cavity tuning were employed. Their operational wavelength sensitiveness to both temperature and injection current is a well-known phenomenon, but as they provide high output optical powers ($\sim$18dBm) in contrast to other commercial laser diodes, this disadvantage required solving. Figure 7.3 illustrates the measured temperature dependence of the utilized DFB diode. To obtain the highest possible optical power, maximal diode current was applied, which implied excess heating and thus precise temperature control was demanded.
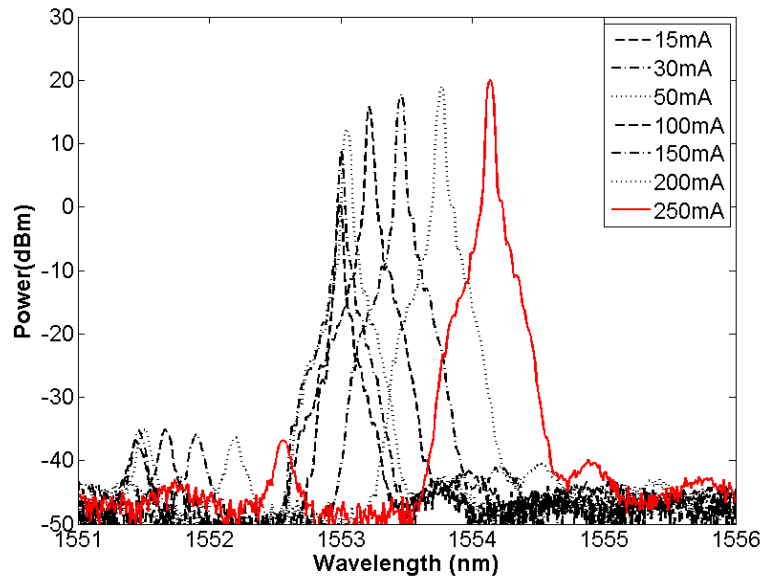
Figure 7.3: Wavelength dependence on injection current of the DFB Fitel Furukawa DWDM diode

To eliminate this temperature dependence external modulation was carried out via Mach-Zehnder amplitude modulators (MODs) controlled by OEC. These modulators, thanks to their nonlinear response to control current, provided switching speed of less than 3ns in contrast to the switching speed of the whole OEC. An eye-diagram of the generated routing signal after MOD is depicted in Fig. 7.4, providing 2.56ns rise time.
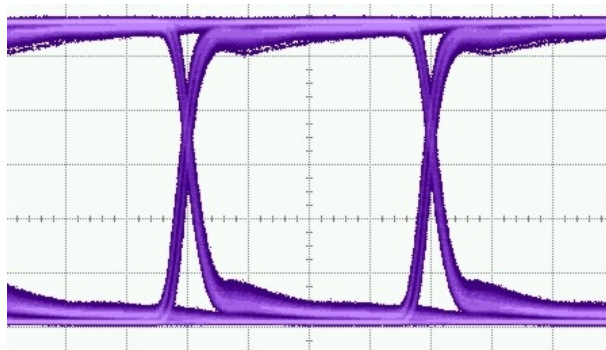


Figure 7.4: Eye-diagram of the routing signal at the MZ-MOD output, 17.54mW peak power, 3.16mW/div.

### 7.1.3 Payload buffering

While the packet label was being processed, it was necessary to delay the data payload. In the simplest approach a fixed fiber length buffer can be emloyed. According to measured maximum processing time the length of the buffer fiber was tailored. A buffer based on a recirculation loop was presented and published in our previous research [104]. This method was modified for the purpose of optical packet buffering as depicted in Fig. 7.5, where the significant part was formed by an "X" coupler with a 99/1 splitting ratio. Most of the input signal energy was therefore stored in the buffer. The recirculation loop can be further enhanced by employing direct amplification in an EDFA configuration with a bandpass filter (BF) to eliminate amplified spontanneous emission noise accumulation. This approach is suitable only for specific application, where only a single optical packet is stored, otherwise the next incoming packet will collide with the stored one.

### 7.1.4 New label attachement

Without a new label, switched data payload would be discarded at the next OPS in the network scheme. Therefore a new label had to be attached to the switched payload for further network propagation. Depending on label allocation and spectral efficiency a proper mechanism was chosen to allow simple new label generation and attachment. In proposed OPS setup the SFP module detected incoming label and after label processing also generated the new label. This label was synchronously with the routing signal fed into the proper output. Synchronization was achieved by FPGA, which simultaneously turned on the routing signal diode and sent the new label via the SFP transmittor.
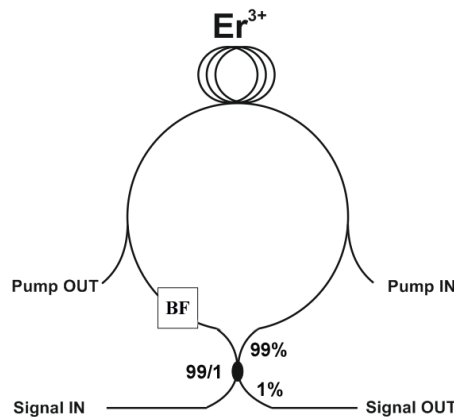


Figure 7.5: Modified resonator [104] for optical packet buffering.

## 7.2 Evaluation of the switching methodology

Based on the demands given in the Thesis objectives, advances in technology of nonlinear fibers discussed in Chapter 4 and the proposed OPS setup, the switching methodology

required to be developed to serve the desired purpose. This section is further divided into two subsections, where the first discusses optimization of employed specialty fibers and the second brings the switching methodology itself.

Numerous aspects were considered, evaluated and parametrized to achieve efficient optical packet switching, insensitive to states of polarization and with acceptable BER and OSNR values.

### 7.2.1 Demands

Modulation format insensitivity is closely related to bit rate and polarization insensitivities, e.g. when DP-QPSK is appllied, the signal is propagated in both polarization axes and is also phase modulated. Proposed methodology must be able to convert all or almost all modulation formats mentioned in Chapter 2. Attention is paid to selected formats utilized in current networks and recognized by the ITU-T - 10Gbps NRZ, 40Gbps DPSK and 100Gbps DP-QPSK. For the future data communications higher bitrates, higher levels of multiplexing are expected (m-QAM). 10Gbps NRZ was measured experimentally. DPSK, DP-QPSK and m-QAM were evaluated exploiting the same configuration within simulations.

Polarization insensitivity is crucial for efficient FWM, where high switching efficiency has to be ensured to eliminate the need for amplification, which adds ASE and thus lowers OSNR of the output data payload.

Fast switching time requirement depends on optical packet length and guard time between subsequent packets. Typical packet lengths are in the range of 100ns∼1us. For this thesis, packet length of 100ns is considered as it represents the most intriguing situation. Ultra-fast fundamental response of the optical fiber itself is in orders of femtoseconds, which is not significant for switching the whole packet, but for response of the nonlinear medium to subsequent optical pulses. Switching time under 5ns of the whole packet was already presented in the OEC development.

Conversion efficiency is the main factor of optical packet switching and is fundamentally dependent on optical fiber nonlinearity, optical fiber length and utilized optical power (pump peak power). These three parameters are first discussed from the point of enhanced nonlinearity fiber optimization and afterwards measurements are carried out. Wavelength range is evaluated and frequency plan is proposed for spectrally efficient OPS methodology.

## 7.2.2 Switching fabric optimization

Wavelength routing based on SOA, InP and PLZT were already discarded for their fundamental material speed limits for ultra-fast nonlinear switching. Another factor should be taken into consideration, which is active control of these fabrics, whereas nonlinear optical fibers included into the proposed OPS setup act passively only as a medium.

The optimization of the switching elements was carried out according to the following criteria: nonlinearity, component insertion loss, length and SBS limits. For this purpose three sample fibers were prepared, measured and evaluated to provide comparable parameters (for technological details see Chapter 6).

- 500m HNLF
- 100m Ge-SCF
- 26m $As_2Se_3$

### Nonlinearity

It is obvious that higher nonlinear refractive index $n_2$, i.e. nonlinear coefficient $\gamma$ results in more efficient nonlinear processes, but higher values of $n_2$ are in correlation with refractive index $n$, which implies higher refractive index contrast. When connecting the nonlinear fiber to conventional silica (which is sooner or later unavoidable in the OPS setup) connection losses are implied. Second factor which is interconnected with $n_2$ is material attenuation, which increases with higher $n_2$.

Nonlinear coefficient $\gamma$ depends apart from $n_2$ on $A_{eff}$ and $\lambda$. Wavelength for this thesis was considered fixed in vicinity of 1550nm (C-band), therefore only $A_{eff}$ can be minimized to increase nonlinearity. As discussed in Chapter 4, there are several approaches to achieve $A_{eff}$ decrease, with minimal values obtained by employing MOF or by fiber tapering. Both these methods again imply increased component attenuation.

Following table summarizes material losses and whole component measured losses for employed fibers (with connection to standard SMF-28e fiber).

Table 7.2: Nonlinearity, material attenuation and component insertion loss

| Fiber | $\alpha_{material}$ [dB/m] | $\alpha_{component}$ [dB] |
|---|---|---|
| 500m HNLF | $7 \cdot 10^{-4}$ | 0.55 |
| 26m $As_2Se_3$ | 0.58 | 15.50 |
| 100m Ge-SCF | 0.04 | 6.10 |

### Length optimization

In the OPS method evaluation only a CW routing signal (pump) was considered, thus only $L_{eff}$ and $L_{NL}$ were significant in experimental OPS optimization. But for a complete study, a pulsed pump was assumed, then fiber length becomes more crucial as by reducing fiber length it is possible to mitigate the effects of dispersion, when setting the dispersion length $L_D \gg L_{eff}$. Calculated $L_D$ and $L_{NL}$ for utilized nonlinear fibers are summarized

in Table 7.3. For $L_D$ two pulse FWHMs were considered, first a 100ps pulse (NRZ 10Gbps OOK, convetional 10Gbps transmissions) and second a 5ps pulse(generated by the u2t laser for SPM measurements). Average signal power was considered to be 20dBm, which implied pulse peak power of 23dBm for 100ps pulses and 33dBm for 5ps pulses. Wavelength was set at 1550nm.

Table 7.3: Effective, dispersion and nonlinear lengths $[m]$ of utilized fibers.

| Fiber | $L_{eff}$ | $L_{NL}$, 23dBm | $L_D$, 100ps | $L_{NL}$, 33dBm | $L_D$, 5ps |
|---|---|---|---|---|---|
| 500m HNLF | 475.0 | 441.0 | $1.0 \cdot 10^7$ | 44.0 | $2.6 \cdot 10^4$ |
| 26m As$_2$Se$_3$ | 7.5 | 3.8 | $1.3 \cdot 10^4$ | 0.38 | 32.0 |
| 100m Ge-SCF | 105.0 | 238.0 | $2.2 \cdot 10^5$ | 0.24 | 553.0 |

everal significant observations result from Table 7.3. First, all fibers fulfill $L_D \gg L_{eff}$ for 10Gbps signal with 100ps pulses, thus dispersion in this case can be neglected. For 5ps pulses $L_D$ is still longer than $L_{eff}$, but not as significantly ($L_D$ in case of As$_2$Se$_3$ is close to $L_{eff}$). Second observation says that for all fibers, when considering pulses with 33dBm peak powers, $L_{NL} \ll L_{eff}$, which leads to sufficient nonlinear phase-shift and efficient FWM. For pulses with peak powers of 23dBm sufficient nonlinear phase-shift is achieved only for As$_2$Se$_3$ and HNLF, where $L_{NL}$ was close to $L_{eff}$. The 23dBm peak pulse powers of 100ps pulses correspond to 20dBm CW pump, which results in higher power requirement for Ge-SCF, if sufficient nonlinear phase-shift is expected. Last observation of $L_{eff}$ brings the fact, that 26m long As$_2$Se$_3$ is not feasible for switching as only length of 7.5m is sufficient. Therefore it will be suitable to reduce the As$_2$Se$_3$ component length.

**SBS measurements**

Stimulated Brillouin scattering threshold is also affected by $L_{eff}$ as:

$$P_{th} = 21kA_{eff}/g_bL_{eff},$$ (7.1)

where it is important to solve this equation with different $g_b$ for different glass materials. It can be clearly observed that for lower $L_{eff}$ the Brillouin threshold is increased. Calculated thresholds for employed fibers are presented in Table 7.4.

Table 7.4: Calculated SBS thresholds for chosen fiber samples

| | $L_{eff}$ [m] | $A_{eff}$ [$\mu$m$^2$] | $g_b$ [m·W$^{-1}$] | $P_{th}$ [dBm] |
|---|---|---|---|---|
| 500m HNLF | 475.0 | 10.0 | $4.40 \cdot 10^{-11}$ | 13.0 |
| 26m As$_2$Se$_3$ | 7.5 | 58.0 | $6.75 \cdot 10^{-9}$ [105] | 16.8 |
| 100m Ge-SCF | 105.0 | 55.0 | $4.8 \cdot 10^{-11}$ | 26.6 |

Measurement setup for SBS evaluation is depicted in Fig. 7.6. A pump laser (PL) with 200kHz linewidth was fed into EDFA and afterwards useful bandwith was filtered (BF)

to reduce ASE noise. Then the signal was propagated through a 90/10 coupler, where the pump was coupled into the 90% branch and then propagated through the evaluated nonlinear fiber (FUT). At the 10% coupler branch the backreflected power was detected by a powermeter (PM) or an optical spectrum analyzer (OSA).
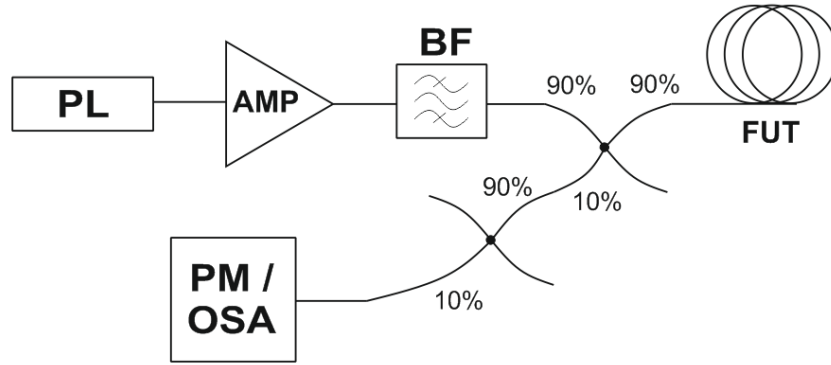


Figure 7.6: SBS measurement setup

Obtained SBS backscattered total power and peak power dependences on pump peak power for evaluated nonlinear fibers are presented in Fig. 7.7 and Fig. 7.8 respectively. The pump peak power was tuned from 6 to 16dBm. From previous calculations and measurement results for 500m long HNLF the SBS threshold was verified at 12dBm peak power, i.e. 15mW. For the $As_2Se_3$ fiber the SBS limit was observed at 16dBm, which corresponds with calculated theoretical value. Significant backreflected power was present for $As_2Se_3$ in the whole pump tuning range due to the large refractive index contrast at $As_2Se_3$/silica boundary. In contrast to the $As_2Se_3$ and HNLF, there was no observed SBS backscattered power for the Ge-SCF, but is expected to appear at 26dBm pump peak power.
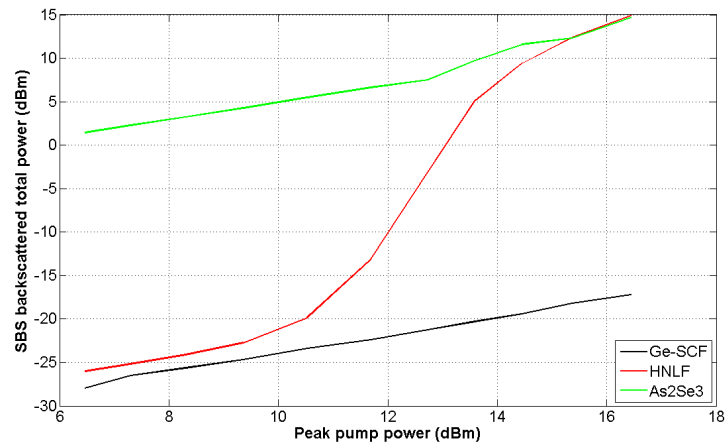


Figure 7.7: SBS backscattered total power in dependence on pump peak power.
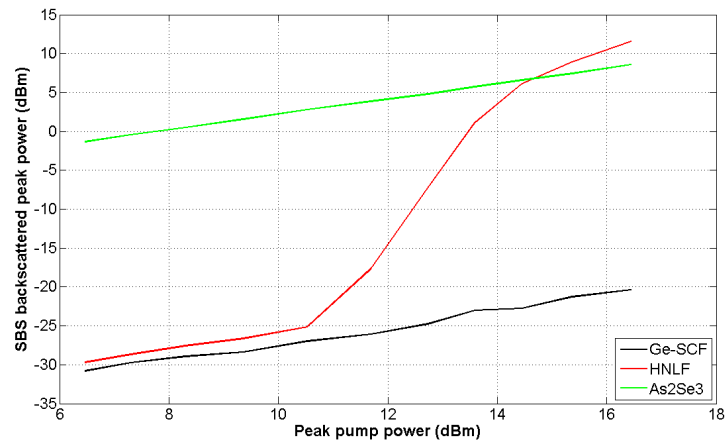
Figure 7.8: SBS backscattered peak power in dependence on pump peak power.

SBS backreflected spectra in dependence on pump peak power are illustrated in Fig. 7.9. The difference for As$_2$Se$_3$ in the SBS backreflected power curve for total and peak power can be understood from Fig. 7.9, where the SBS peak appears from pump peak power of 13dBm. As the peaks are equal at maximum pump peak powers in Fig. 7.9, no difference can be observed, but the total reflected power increases.
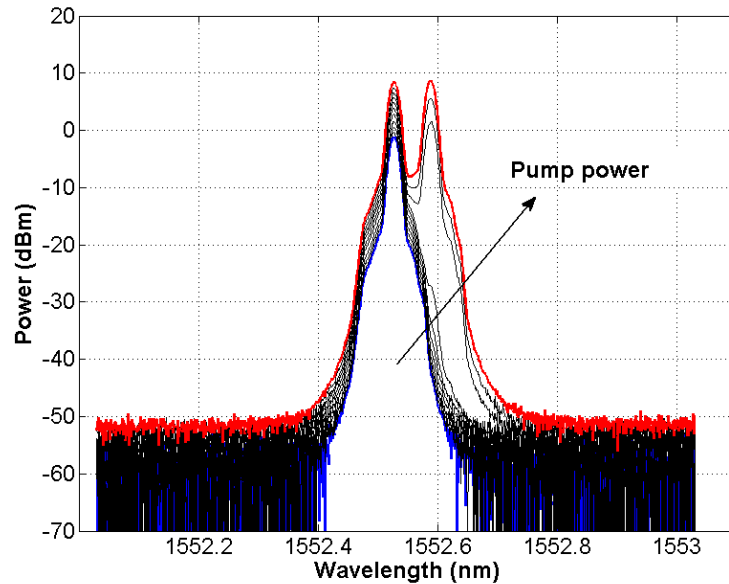


Figure 7.9: SBS backscattered spectra - 26m As$_2$Se$_3$, pump power from 6dBm (blue) to 16dBm (red).
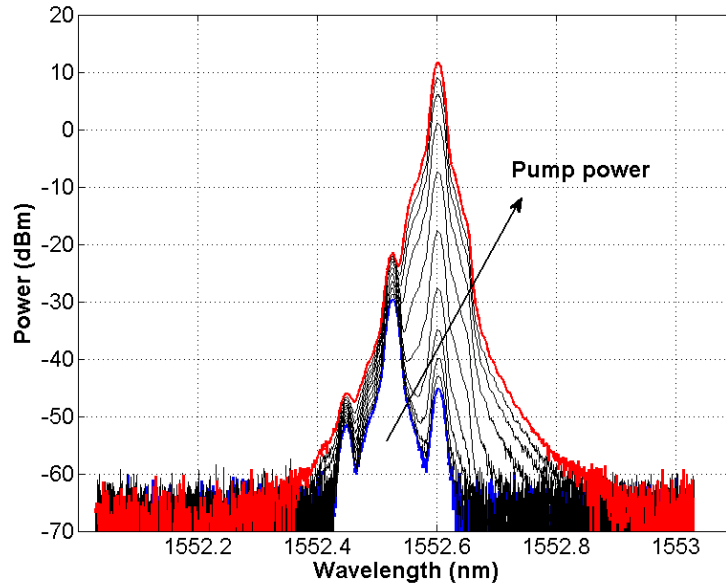
Figure 7.10: SBS backscattered spectra - 500m HNLF, pump power from 6dBm (blue) to 16dBm (red).

For verification of results presented in Fig. 7.7 and 7.8 spectral measurements of the SBS phenomenon are illustrated in Fig. 7.10, where a significant SBS frequency-shifted peak is observed from 12dBm pump peak power.

## 7.2.3 Wavelength conversion

In this section the FWM phenomenon for optical packet switching is discussed. First, frequency plan analysis for routing signals (pumps) and data payload allocation is carried out. Experimental measurements of conversion efficiencies for selected nonlinear fibers are presented. Polarization insensitive setup is proposed and measured in the last subsection and confronted with simulated results. Discussion of achieved OSNR values and eye-diagrams together with BER tests concludes the switching method section.

### Conversion efficiency

Wavelength conversion efficiency is independent of data payload power (Eq. 3.36), therefore only pump power plays the critical role. In this case it is limited by the SBS effect (HNLF at 13dBm, $As_2Se_3$ at 16dBm and Ge-SCF at 26dBm). Employed thin-film components (e.g. MUX, AWG) are power limited at 23dBm, which was significant only for Ge-SCF, as all other evaluated fibers had their SBS thresholds below the 23dBm value.

For HNLF and $As_2Se_3$ the phase-modulation technique mentioned in Chapter 3 to suppress SBS can be utilized to increase pump peak power, but if advanced modulation formats should be employed, phase-modulation of the pump severely decreases switched signal parameters, as is presented in detail in [106].

For initial comparison, all three evaluated nonlinear fibers were tested at +1 channel detuning from the pump (considering DWDM 100GHz ITU-grid). According to previous calculations and measurements the highest conversion efficiency was expected from HNLF, then from $As_2Se_3$ and the lowest conversion efficiency from Ge-SCF ($As_2Se_3$ provides highest $\gamma L$ coefficient from all utilized fibers, but due to the insertion loss of tested component, mediocre nonlinear response was expected).

In Fig. 7.11 Ge-SCF spectra after wavelength conversion are presented. The pump was tuned from 6 to 16dBm peak power, whereas the data signal was kept at the same level. When the pump signal was at 16dBm, Ge-SCF provided OSNR of generated idler under 10dB, which is below required values for optical communication. Almost no converted idler is present, therefore further employment in the OPS was not considered.
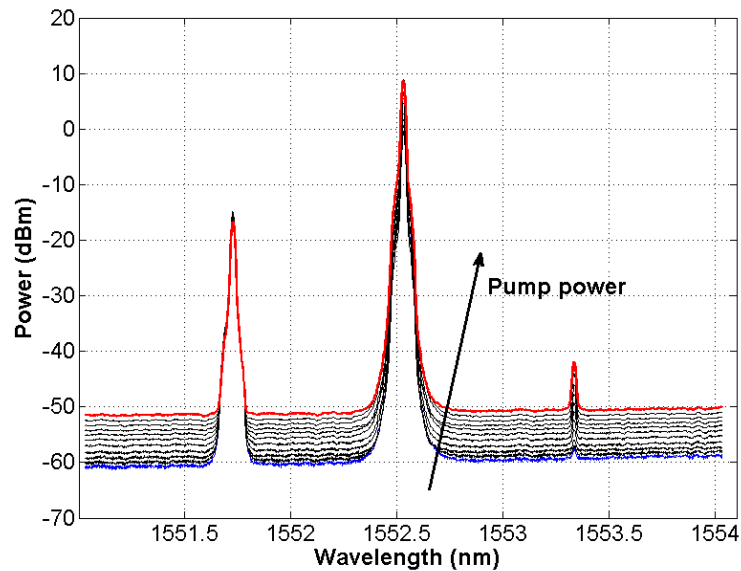


Figure 7.11: Four-wave mixing in 100m Ge-SCF, pump power from 6dBm (blue) to 16dBm (red).

HNLF measurements are presented in Fig. 7.12. with conversion efficiencies exceeding -20dB for pump peak powers over 12dBm. Achieved OSNR values also confirmed suitable results for the proposed OPS switching methodology. Starting from 9dBm peak powers, OSNR values exceeded 20dB (a detail study is presented together with BER tests for the final configuration).
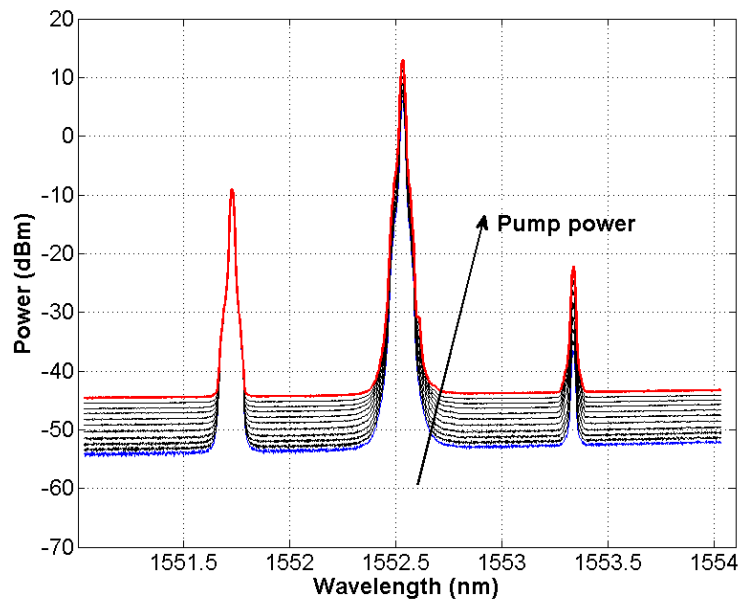
Figure 7.12: Four-wave mixing in 500m HNLF, pump power from 6dBm (blue) to 16dBm (red).
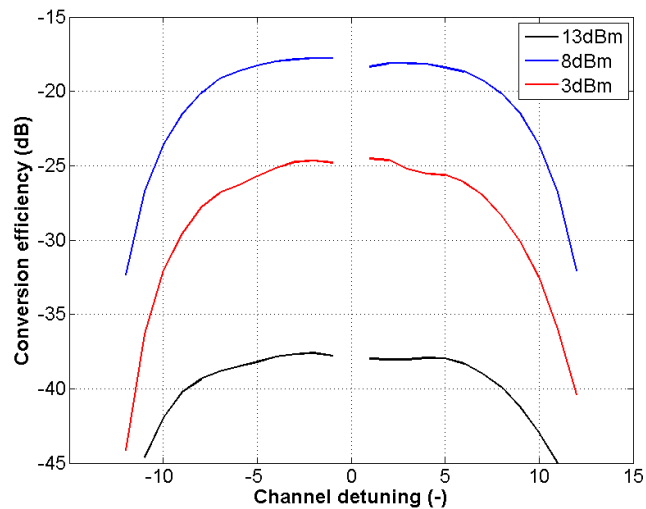


Figure 7.13: HNLF - conversion efficiency in dependence on channel detuning.

Whereas conversion efficiencies over -20dB were achieved for HNLF with one channel detuning, additional measurements were carried out to evaluate conversion efficiency within wider wavelength range. In Fig. 7.13 conversion efficiency in dependence on channel detuning is presented with pump allocation at 1552.52nm and with peak powers of 3dBm, 8dBm and 13dBm. As can be observed almost flat conversion efficiency profiles were achived for +/-8 channel detuning. The conversion efficiency increase between 8 and 13dBm pump was not as high as for 3 to 8dBm due to the onset of SBS.

As$_2$Se$_3$ fiber results are illustrated in Fig. 7.14. Chirped peaks appeared for the pump and the generated idler. They were initiated by the reflection of the pump signal on the As$_2$Se$_3$/silica boundary and induced SBS on the reflected pump (in practice there was a conventional SBS backscattered signal and another SBS backscattered signal caused by the reflected pump, which then propagated in the same direction as the pump, data and idler). Conversion efficiencies were under -40dB, where the major detrimental effect was implied by the component insertion loss. As was discussed before in switching fabric optimization, significant reduction of As$_2$Se$_3$ component is required.
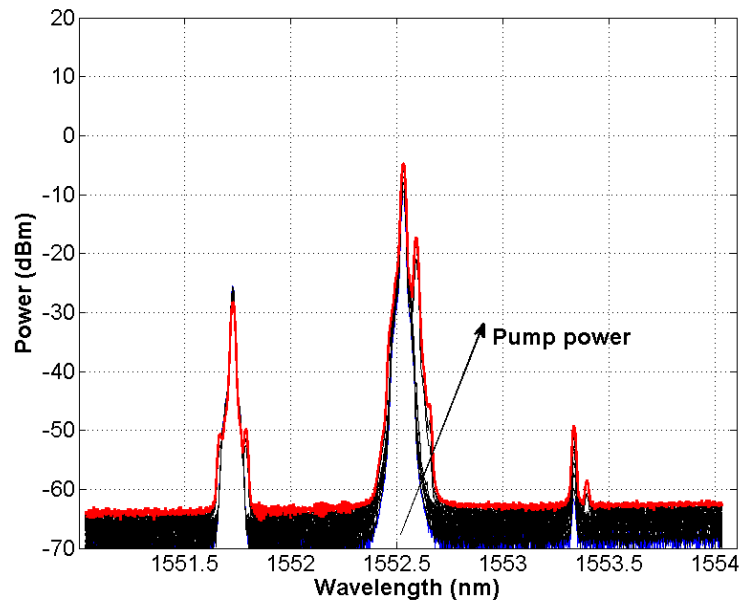


Figure 7.14: Four-wave mixing in 26m CHG, pump power from 6dBm (blue) to 16dBm (red).

**Frequency plan**

For OPS based on FWM it is significant to evaluate and decide for a spectrally efficient frequency plan. Based on the results from conversion efficiency measurement HNLF was considered for further application for optical packet switching and a sample frequency plan was based on experimental HNLF data. Attention was paid to facile routing signals and former data filtering, maximum conversion efficiency and frequency plan scalability. The final setup is illustrated in Fig. 7.15 with routing signals placed +3/+4 channels from the data payload. Generated idlers are then at +6/+8 channels from the former data signal.
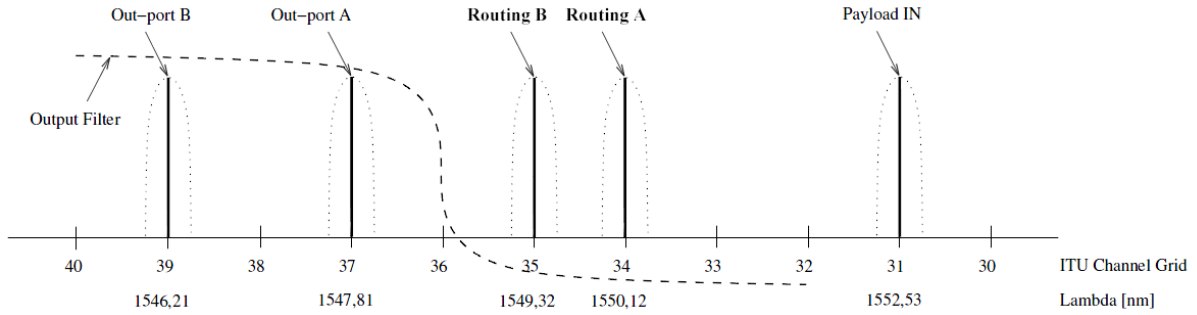
Figure 7.15: A sample frequency plan for FWM-based optical packet switching.

This setup enabled utilization of commercially available filters (without requirement for filtering adjacent channels). If more outputs are required, the setup can be expanded in a mirror-like fashion. Moreover routing signals can be placed e.g. at channels 32 and 36, thus resulting in generated idlers at 33 and 40 channel, but with significantly more complicated filtering or with high requirements on AWG adjacent channel isolation (in comparison to currently achieved 30dB isolation). In Fig. 7.16 measured spectra according to the frequency plan are presented.
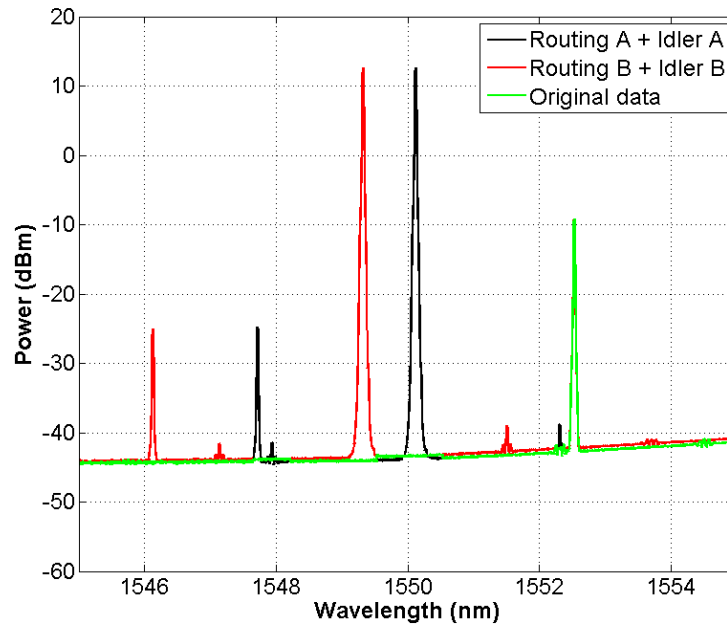


Figure 7.16: Final frequency plan for FWM-based optical packet switching - measured.

**Polarization insensitivity**

One of the crucial FWM phenomenon criteria apart from phase-matching condition is polarization sensitivity. The countermeasures were covered in detail in Chapter 3 and in demands placed on the final OPS functionality. For this thesis a setup incorporating a

circulator (CIRC) and PBS was selected. In Fig. 7.17a a setup of this configuration is depicted together with a polarization sensitive variant. Pump was as in previous measurements amplified, ASE from EDFA was filtered by a bandpass filter (BF #1) and then the pump was coupled with the signal. In a polarization sensitive variant (see Fig. 17b), both signals were co-propagated in the evaluated nonlinear fiber (FUT). In the polarization insensitive setup, the FUT was placed in a loop and PBS divided the signals into fast and slow axes. The only critical condition was to keep the pump polarization in 45° to the slow axis of PBS, so that the pump power was equaly divided into the clockwise and counter-clockwise directions. Then the pump and signal were filtered (via BF #2 and AWG) and only idler was detected at OSA.
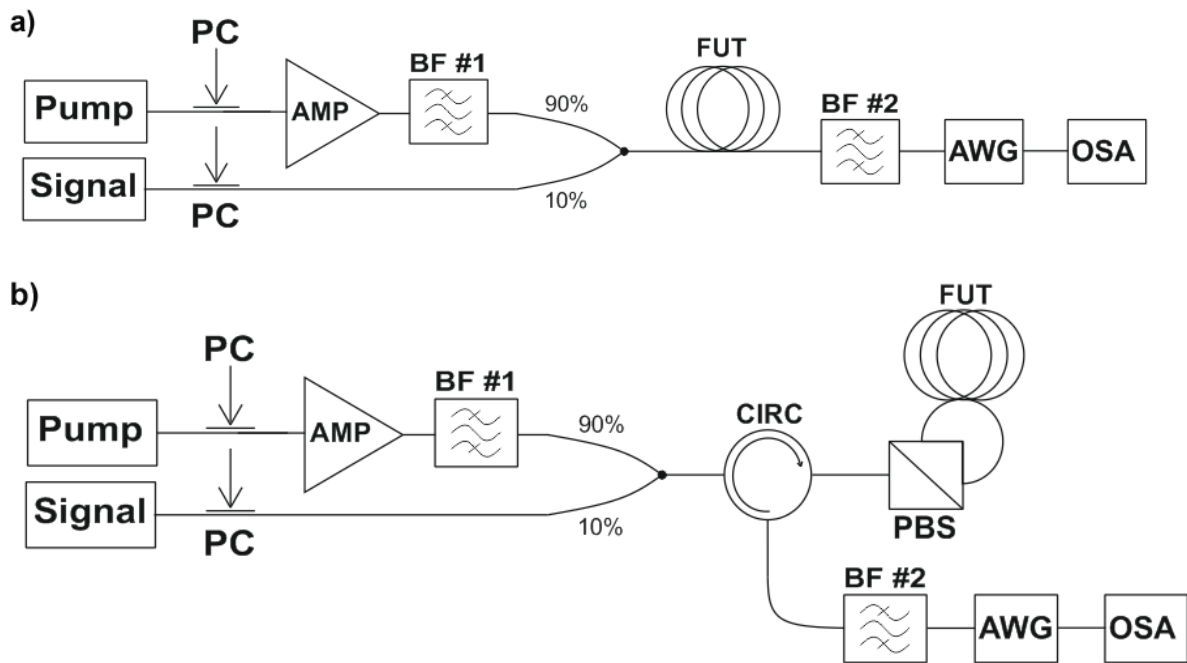


Figure 7.17: Polarization sensitive (a) and polarization insensitive (b) configuration for optical packet switching.

In the experimental measurement amplifier total gain was tuned from 10 to 20dBm, meaning approximately 4 to 14dBm pump peak powers. The inclusion of CIRC and PBS resulted in only 0.5dB insertion loss. Also by dividing the pump power, i.e. having two pumps with 3dB lower peak powers, the SBS threshold was increased, which can be observed in Fig. 7.18. Conversion efficiency difference between polarization sensitive (the best situation with co-polarized waves was considered) and insensitive variant at pump peak powers over 10dBm was around 3dB. Polarization state of the signal was then varied in a 90° range with maximal difference in conversion efficiency of +/-0.6dB. Tuning the pump polarization state from the optimal 45° by less then 10° resulted only in insignificant variations of the output idler power. When the state of polarization was varied in the polarization sensitive setup, the idler peak power values decreased rapidly according to the simulated results.
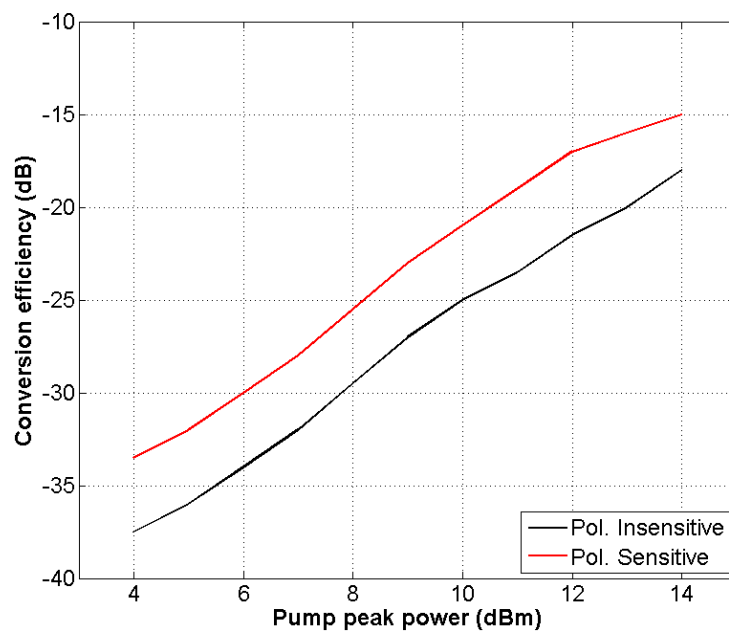
Figure 7.18: HNLF - polarization insensitive conversion efficiency

For comparison with measured characteristics a simulation model in Optiwave OptiSystem was evaluated, with identical configuration as in Fig. 7.17. Simulation results are presented in Fig. 7.19. For the polarization insensitive variant (blue) only small fluctuations of generated idler peak power are observed ($\sim$0.01dB). In case of the polarization sensitive setup (red), when the signal polarization state is tuned from $+0°$ to $+90°$ from the pump polarization state, almost 16 dB decrease in idler peak power level is present.
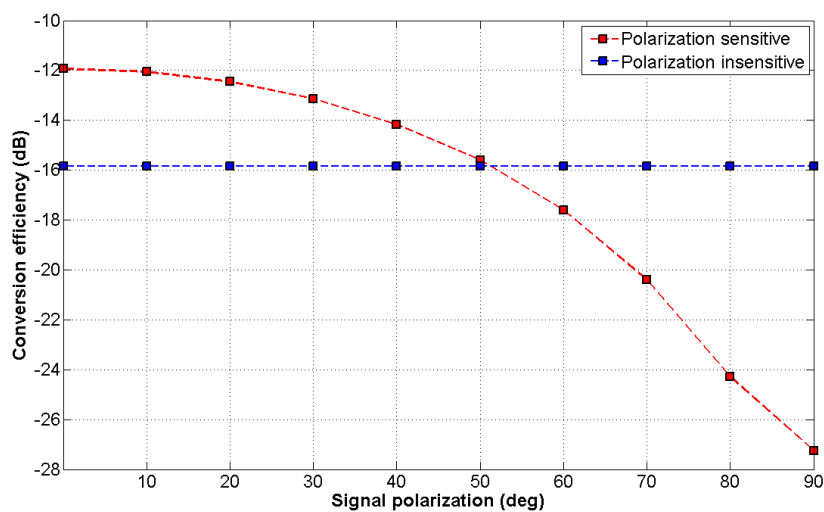


Figure 7.19: Simulated conversion efficiency in HNLF, pump polarization is tuned by $+0°$ to $+90°$ from the data signal.

**BER tests**

After the polarization insensitive OPS operation was achieved by employing the proposed methodology, BER tests were performed to verify data performance. A 10Gbps NRZ BERT was utilized as the data payload source in the same configuration as depicted in Fig. 7.17b for the polarization insensitive variant. As the pump source a DFB diode was utilized. Unfortunately no signal was detected at the BERT receiver when the pump peak power was tuned from 6dBm to 16dBm. The reason lay in too low data signal power after the wavelength conversion (around -30dBm, when considering -10dBm data signal before the HNLF). To counter this effect, EDFA was moved directly before the HNLF and instead of the 90/10 coupler a WDM-MUX was employed. Even with these changes, no signal was detected by the BERT receiver. It was necessary to further amplify the converted data signal by a power-booster (PB) and slightly change the filtering stage composition. The innovated polarization insensitive configuration is depicted in Fig. 7.20.
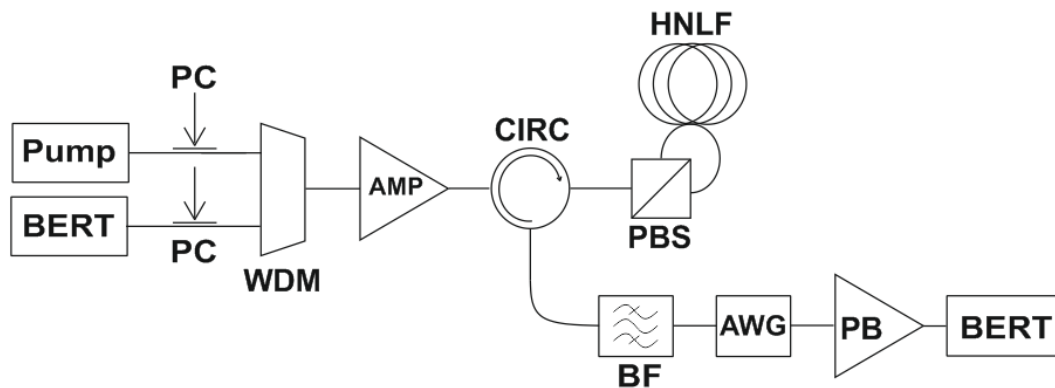


Figure 7.20: Innovated polarization insensitive setup for BER measurements.

Obtained results are illustrated in Fig. 7.21, where the dependence of total output EDFA power on BER is presented. The highest BER of $10^{-12}$ was achieved at 17dBm, whereas for 16 and 18dBm BER better then $10^{-10}$ was observed.
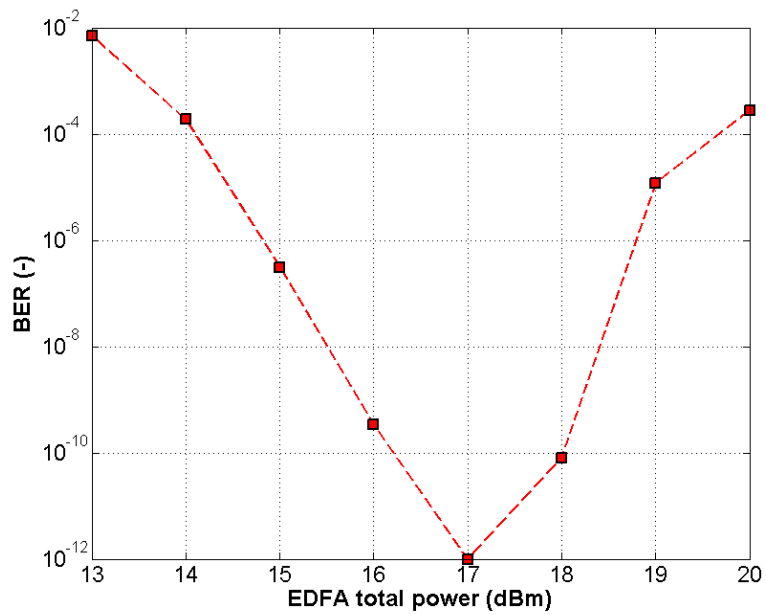
Figure 7.21: BER dependence on the EDFA total power.

Eye-diagram of the best BER is depicted in Fig. 7.22, with 8.23dB extinction ratio and a clear eye-opening. Measured in-band OSNR and extinction ratios for different EDFA total powers are presented in Fig. 7.23.
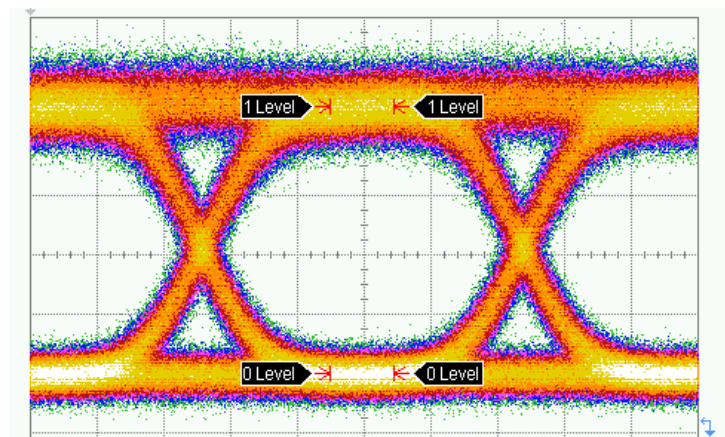


Figure 7.22: Eye-diagram of 10Gbps NRZ switched data signal, 8.23dB extinction ratio.
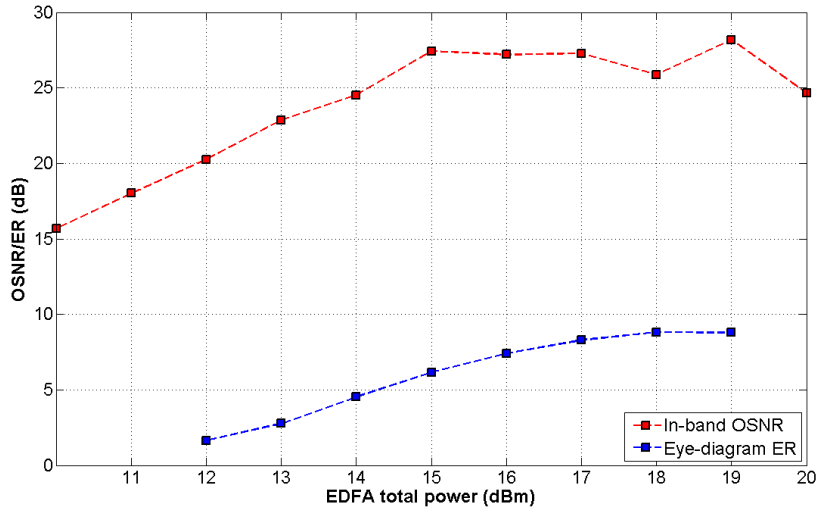
Figure 7.23: In-band idler OSNR and eye-diagram extinction ratios (ER) for different EDFA total powers.

**Modulation format transparency**

Advanced modulation formats are expected in future OPS applications. With achieving polarization insensitive wavelength conversion and utilization of the proposed frequency plan, the identical configuration was employed for simulations. Theory of FWM predicts modulation format transparency for PSK and QAM signal wavelength conversion. Analytical verification was performed in OptiSystem for one polarization state of 100Gbps DP-QPSK as presented in Fig. 7.24, where the constellation diagram of the switched signal showed only small distortion. The same quality of results was obtained for 4-QAM, where additional polarization control was required to conserve the switching performance. Therefore the proposed methodology and OPS configuration can be utilized for novel modulation formats.
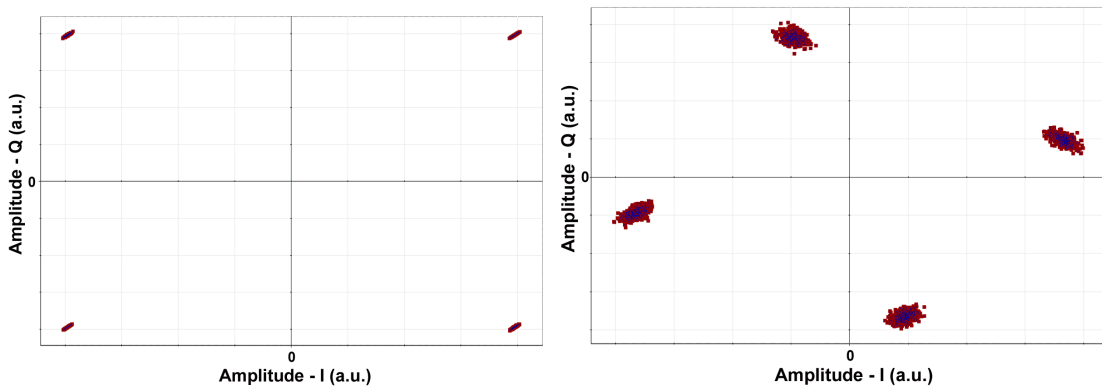


Figure 7.24: 100Gbps DP-QPSK constellation diagram before (left) and after (right) wavelength conversion.

# 7.3 Conclusion - Finalized OPS methodology

Based on previous analyses, optimizations, measurements and technological improvements a finalized OPS configuration is proposed (see Fig. 7.25). DFB diodes can be utilized as continuous-wave pumps (routing #1, #2 to #n), their polarization state has to be adjusted to 45° with respect to the PBS slow axis by a polarization controller (PC). Then they are modulated in a Mach-Zehnder modulator (MOD) controlled by OEC according to the label content. Routing signal and data payload are then multiplexed (WDM) and EDFA amplified (AMP). As the switching fabric HNLF was selected, which proved most suitable according to measurement results, and was included in a polarization insensitive fiber loop composed of a polarization beam splitter (PBS) and a circulator (CIRC). Generated idler is then filtered by a bandpass filter (BF) and AWG and afterwards amplified in a power-booster (PB). New label is generated by SFP and attached to the switched data payload. Table 7.5 then summarizes typical maximum insertion loss and thermal stability of some of the utilized components in the thesis. For $As_2Se_3$ fiber the value corresponds with the case of increased attenuation due to temperature changes.
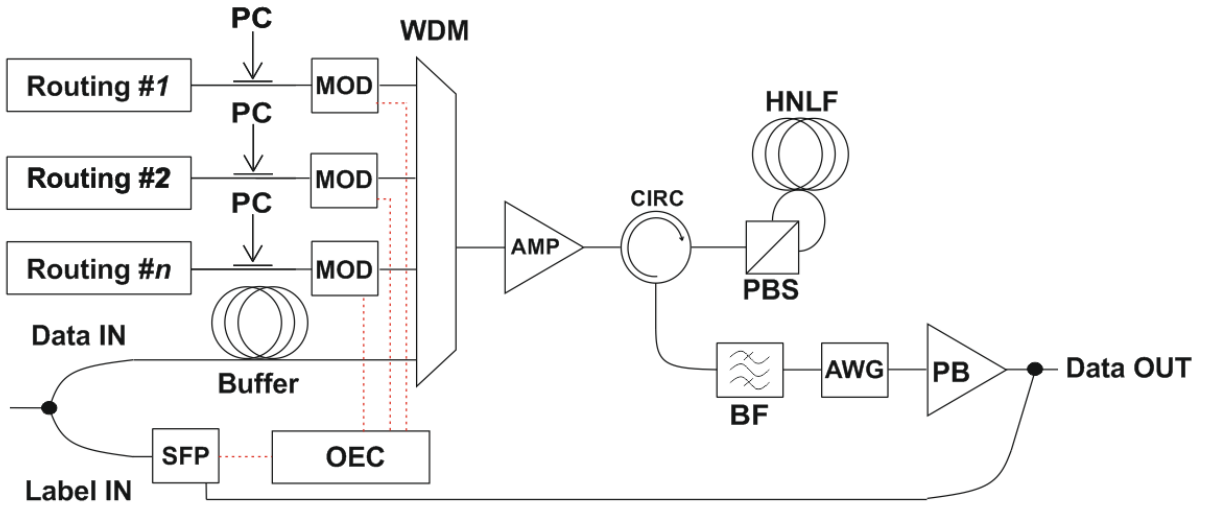


Figure 7.25: Final OPS configuration with $n$ routing signals, payload buffer and OEC modulator control.

Table 7.5: Component insertion loss and thermal stability.

| Component | Thermal stability (°) | Maximum insertion loss (dB) |
|---|---|---|
| MUX/DEMUX | -5 to +80 | 3.2 |
| DFB diode | +20 to +35 | - |
| AAWG | -5 to +70 | 2.8 |
| Modulator | 0 to +75 | 4.0 |
| Bandpass filter | 0 to +70 | 1.0 |
| HNLF | -40 to +80 | 0.9 dB/km |
| $As_2Se_3$ | -70 to +100 | 1.5 dB/m |

Length and nonlinearity of utilized nonlinear fibers were evaluated, with the emphasis on component insertion loss, SBS thresholds and required minimum length for the nonlinear phenomena to occur. According to these parameters HNLF provided the most suitable combination of low insertion loss (0.88dB) and $\gamma L$ coefficient of 5,67. As$_2$Se$_3$ provided higher $\gamma L$ coefficient of 33,8, but insertion loss of 15.5dB, which led to lower conversion efficiencies than for HNLF. SBS limits were lowest for HNLF (12dBm) and As$_2$Se$_3$ (16dBm). SRS threshold were not considered, as they require more than two orders higher optical powers than SBS thresholds.

The finalized methodology for optical packet switching was based on HNLF exploiting the FWM phenomenon. The switching methodology proved polarization insensitive, bitrate and modulation format transparent with ultra-fast nonlinear response provided by the optical fiber. A tailored frequency plan was proposed with almost 10 channel flat conversion efficiency of -15dB. Further enhancement will be possible by optimizing the As$_2$Se$_3$ fiber based on obtained measurement results.

# Chapter 8

# Thesis summary

The dissertation thesis was focused on optical packet switching based on nonlinear optics. To fulfill the aim of the thesis, an analysis of various OPS state-of-art aspects was carried out with the decision for a fiber-based optical packet switch. Consequently nonlinear optics with the focus on optical fibers was discussed. Theoretical background and basic principles of fiber-based switches were presented. Afterwards the state-of-art technological aspects of nonlinear fibers were summarized with the emphasis on various approaches of achieving higher nonlinear coefficient.

The two main thesis objectives were then selected. One with the aim of proposing a new switching methodology for optical packet switching and the other with the emphasis on technological aspects of nonlinear fibers and their preparation and optimization for the proposed methodology.

Advancements in technological aspects of nonlinear fibers were presented, where a conventional HNLF was employed to enable comparison with the other utilized enhanced nonlinearity fibers. A single-mode arsenic-selenide fiber with cut-off at 1300nm was connectorized and a component with 26m length was developed. Attenuation lower than 0.6dB/m was obtained with connection losses under 1dB, thus presenting enhancement of current state-of-art parameters. Ge-doped suspended-core fiber was evaluated as a representative of microstructured fibers, with nonlinear coefficient twice the HNLF. Splicing technology was developed and a 100m component was produced with approximately 6dB insertion loss. Chalcogenide tapering was also studied and a technological process was mastered, but utilizable samples were not prepared by the time of the thesis finalization. Chalcogenide $As_2Se_3$ and microstructured Ge-SCF technological connectorization processes were finalized and are currently being patented. Athermal AWGs are in pilot production.

Afterwards the development of the switching methodology was presented. First an opto-electronic controller was developed for label processing, achieving less than 5ns switching time. Routing signals were generated by DFB diodes, which proved to be thermally dependent, therefore they were externally modulated by Mach-Zehnder modulators controlled by OEC. New label generation was ensured by the SFP module and could be synchronously attached to the switched packet.

Conversion efficiencies were measured for all utilized fibers, where the best results

were obtained for HNLF. Conversion efficiency for the $As_2Se_3$ fiber was below -40dB due to high component insertion loss. Ge-SCF showed almost no nonlinear response, which was expected, as the nonlinear length was higher than the effective length, therefore it was discarded from the final OPS setup. $As_2Se_3$ fiber would require further optimization to provide better switching parameters than HNLF, mainly length reduction to decrease insertion loss. With length reduction of $As_2Se_3$ fiber the SBS treshold will increase, which gives $As_2Se_3$ an advantage over HNLF in future enhancement of the proposed optical packet switching methodology.

HNLF was employed for optical packet switching, with modulation format transparent switching, sixteen channels flat conversion efficiency profile and polarization insensitive operation in the final proposed switching methodology configuration. On the other hand SBS tresholds for HNLF were the lowest of all utilized fibers.

To conclude, a functional optical packet switch methodology was developed based on enhanced nonlinearity optical fiber. BER tests were performed for the polarization insensitive configuration with extinction ratio of more than 8dB for the best eye-diagrams. BER better than $10^{-10}$ was observed. Modulation format transparency for DPSK, DP-QPSK and QAM was verified in simulations with results indicating functionality of proposed switching methodology and OPS configuration. In-band OSNR measurements proved good signal resolution. Currently our proposed optical packet switching methodology is being applied as a utility model.

For future research, attention will be focused on $As_2Se_3$ and lead-silicate fibers. They will be considered both in conventional and microstructured design and will be optimized to provide better efficiencies than HNLF, while minimizing component insertion loss. Conversion efficiency of more than -10dB is desired.

# Bibliography

[1] Zhu, B.; Liu, X.; Chandrasekhar, S.; Taunay, T.F.; Fishteyn, M.; Yan, M.F.; Fini, J.M.; Monberg, E.M.; Dimarcello, F.V., "112-Tb/s (7160107Gb/s) space-division multiplexed DWDM transmission over a 76.8-km multicore fiber," Optical Communication (ECOC), 2011 37th European Conference and Exhibition on , vol., no., pp.1,3, 18-22 Sept. 2011.

[2] Seimetz, M.; Noelle, M.; Patzak, E., "Optical Systems With High-Order DPSK and Star QAM Modulation Based on Interferometric Direct Detection," Lightwave Technology, Journal of , vol.25, no.6, pp.1515,1530, June 2007.

[3] Gnauck, A.H.; Charlet, G.; Tran, P.; Winzer, P.J.; Doerr, C.R.; Centanni, J.C.; Burrows, E.C.; Kawanishi, T.; Sakamoto, T.; Higuma, K., "25.6-Tb/s WDM Transmission of Polarization-Multiplexed RZ-DQPSK Signals," Lightwave Technology, Journal of , vol.26, no.1, pp.79,84, Jan.1, 2008.

[4] Nakazawa, M.; Okamoto, S.; Omiya, T.; Kasai, K.; Yoshida, M., "256 QAM (64 Gbit/s) coherent optical transmission over 160 km with an optical bandwidth of 5.4 GHz," Optical Fiber Communication (OFC), collocated National Fiber Optic Engineers Conference, 2010 Conference on (OFC/NFOEC) , vol., no., pp.1,3, 21-25 March 2010.

[5] Takahashi H., Al Amin A., Jansen S., Morita I., and Tanaka H., "DWDM Transmission with 7.0-bit/s/Hz Spectral Efficiency Using 8x65.1-Gbit/s Coherent PDM-OFDM Signals," in Optical Fiber Communication Conference and National Fiber Optic Engineers Conference, OSA Technical Digest (CD) Optical Society of America, paper PDPB7, 2009.

[6] Lotz T., Liu X., Chandrasekhar S., Winzer P., Haunstein H., Randel S., Corteselli S., Zhu B., and Peckham D., "Coded PDM-OFDM Transmission With Shaped 256-Iterative-Polar-Modulation Achieving 11.15-b/s/Hz Intrachannel Spectral Efficiency and 800-km Reach," J. Lightwave Technol. 31, 538-545, 2013.

[7] Calabretta, N.; Hyun-Do Jung; Tangdiongga, E.; Dorren, H., "All-Optical Packet Switching and Label Rewriting for Data Packets Beyond 160 Gb/s," Photonics Journal, IEEE , vol.2, no.2, pp.113,129, April 2010.

[8] Nakazawa, M.; Hirooka, T.; Yoshida, M.; Kasai, K., "Ultrafast Coherent Optical Transmission," Selected Topics in Quantum Electronics, IEEE Journal of , vol.18, no.1, pp.363,376, Jan.-Feb. 2012.

[9] Ming-Fang Huang; Dayou Qian; Ip, E., "50.53-Gb/s PDM-1024QAM-OFDM transmission using pilot-based phase noise mitigation," OptoeElectronics and Communications Conference (OECC), 2011 16th , vol., no., pp.752,753, 4-8 July 2011.

[10] Tipsuwannakul, E.; Jianqiang Li; Karlsson, M.; Andrekson, P.A., "Performance Comparisons of DP-16QAM and Duobinary-Shaped DP-QPSK for Optical Systems With

4.1 Bit/s/Hz Spectral Efficiency," Lightwave Technology, Journal of , vol.30, no.14, pp.2307,2314, July15, 2012.

[11] Winzer, P.J., "Modulation and multiplexing in optical communications," Lasers and Electro-Optics, 2009 and 2009 Conference on Quantum electronics and Laser Science Conference. CLEO/QELS 2009. Conference on , vol., no., pp.1,2, 2-4 June 2009.

[12] Peric, Z.H.; Djordjevic, I.B.; Bogosavljevic, S.M.; Stefanovic, M.C., "Design of signal constellations for Gaussian channel by using iterative polar quantization," Electrotechnical Conference, 1998. MELECON 98., 9th Mediterranean , vol.2, no., pp.866,869 vol.2, 18-20 May 1998.

[13] Wei Wang; Rau, L.G.; Blumenthal, D.J., "160 Gb/s variable length packet/10 Gb/s-label all-optical label switching with wavelength conversion and unicast/multicast operation," Lightwave Technology, Journal of , vol.23, no.1, pp.211,218, Jan. 2005.

[14] Mack, J.P.; Nguyen, K.N.; Dummer, M.M.; Burmeister, E.F.; Poulsen, H.N.; Stamenic, B.; Kurczveil, G.; Bowers, J.E.; Coldren, L.A.; Blumenthal, D.J., "40 Gb/s buffered 2x2 optical packet switching using photonic integrated circuits," Lasers and Electro-Optics, 2009 and 2009 Conference on Quantum electronics and Laser Science Conference. CLEO/QELS 2009. Conference on , vol., no., pp.1,2, 2-4 June 2009.

[15] Chowdhury, A.; Jianjun Yu; Gee-Kung Chang, "Same Wavelength Packet Switching in Optical Label Switched Networks," Lightwave Technology, Journal of , vol.24, no.12, pp.4838,4849, Dec. 2006.

[16] Takagi, M.; Imaizumi, H.; Tanemura, T.; Iio, S.; Suehiro, M.; Nakano, Y.; Hiroyuki Morikawa, "200Gb/s Multi-Wavelength Optical Packet Switching with 2ns ultra-fast optical switch," OptoElectronics and Communications Conference, 2009. OECC 2009. 14th , vol., no., pp.1,2, 13-17 July 2009.

[17] Jun Luo; Dorren, H. J S; Calabretta, N., "Optical RF Tone In-Band Labeling for Large-Scale and Low-Latency Optical Packet Switches," Lightwave Technology, Journal of , vol.30, no.16, pp.2637,2645, Aug.15, 2012.

[18] Kovacs, G.; Puerto, G.; Banky, T.; Martinez, A.; Csornyei, M.; Manzanedo, M. D.; Pastor, D.; Ortega, B.; Berceli, T.; Capmany, J., "Subcarrier multiplexed optical label swapping networks," Optoelectronics, IET , vol.4, no.6, pp.235,246, December 2010.

[19] Dawei Wang; Tee-Hiang Cheng; Zhaowen Xu; Jianguo Liu; Yong-Kee Yeo; Yixin Wang, "A space-diversity optical labeling scheme with optical labels derived from ASE noise," Information, Communications and Signal Processing, 2009. ICICS 2009. 7th International Conference on , vol., no., pp.1,4, 8-10 Dec. 2009.

[20] Zhang Chongfu; Qiu Kun; Yawei, Wang; He Yin; Zhou Heng, "On experiment and analysis of MOOCS-based optical labels for optical packets switching," Broadband Network & Multimedia Technology, 2009. IC-BNMT '09. 2nd IEEE International Conference on , vol., no., pp.383,387, 18-20 Oct. 2009.

[21] Dorren, H.J.S.; Hill, M.T.; Liu, Y.; Calabretta, N.; Srivatsa, A.; Huijskens, F.M.; de Waardt, H.; Khoe, G-D, "Optical packet switching and buffering by using all-optical signal processing methods," Lightwave Technology, Journal of , vol.21, no.1, pp.2,12, Jan 2003.

[22] Negishi, K.; Uenohara, H., "Investigation of optical label recognition using optical serial-to-parallel converter with phase operation for DPSK signal," Opto-Electronics and Communications Conference (OECC), 2012 17th , vol., no., pp.913,914, 2-6 July 2012.

[23] Zhang C., Wang L., Perumal S., Qiu K., and Zhou H., "All-optical recognition method of double two-dimensional optical orthogonal codes-based labels using four-wave mixing," Opt. Express 19, 14937-14948, 2011.

[24] Okubo, K.; Kishikawa, H.; Goto, N.; Yanagiya, S., "Optical QPSK label recognition by time-space conversion using two-dimensional matched filtering," Opto-Electronics and Communications Conference (OECC), 2012 17th , vol., no., pp.313,314, 2-6 July 2012.

[25] Makimoto, Y.; Goto, N.; Yanagiya, S., "Improvement of contrast ratio for recognition of optical QPSK labels with waveguide circuits," Microopics Conference (MOC), 2011 17th , vol., no., pp.1,2, Oct. 30 2011-Nov. 2 2011.

[26] George N. Rouskas, Lisong Xu, "Optical Packet Switching." Emerging Optical Network Technologies: Architectures, Protocols and Performance, (Krishna Sivalingam and Suresh Subramaniam, Editors), pp. 111-127, Springer, 2004.

[27] Guillemot, C.; Renaud, M.; Gambini, Piero; Janz, C.; Andonovic, Ivan; Bauknecht, R.; Bostica, B.; Burzio, M.; Callegati, F.; Casoni, M.; Chiaroni, D.; Clerot, F.; Danielsen, S.L.; Dorgeuille, F.; Dupas, A.; Franzen, A.; Hansen, P.B.; Hunter, D.K.; Kloch, A.; Krahenbuhl, R.; Lavigne, B.; Le Corre, A.; Raffaelli, C.; Schilling, M.; Simon, J.-C.; Zucchelli, L., "Transparent optical packet switching: the European ACTS KEOPS project approach," Lightwave Technology, Journal of , vol.16, no.12, pp.2117,2134, Dec 1998.

[28] Calabretta, N.; Wang, W.; Ditewig, T.; Raz, O.; Agis, F.G.; de Waardt, S.Z.H.; Dorren, H.J.S., "Scalable Optical Packet Switches for Multiple Data Formats and Data Rates Packets," Photonics Technology Letters, IEEE , vol.22, no.7, pp.483,485, April1, 2010.

[29] Segawa T., Matsuo S., Kakitsuka T., Shibata Y., Sato T., and Takahashi R., "A monolithic wavelength-routing switch using double-ring-resonator-coupled tunable lasers with highly reflective mirrors," in Indium Phosphide and Related Materials (IPRM), 2010 International Conference on, pp. 1-4, 2010.

[30] Soganci, I.M.; Tanemura, T.; Williams, K.A.; Calabretta, N.; De Vries, Tjibbe; Smalbrugge, E.; Smit, M.K.; Dorren, H. J S; Nakano, Y., "Monolithically Integrated InP 1 16 Optical Switch With Wavelength-Insensitive Operation," Photonics Technology Letters, IEEE , vol.22, no.3, pp.143,145, Feb.1, 2010.

[31] Wada N.; Shinada, S.; Furukawa, H., "Modulation format free optical packet switching technology," in Transparent Optical Networks (ICTON), 2010 12th International Conference on, pp. 1-4, 2010.

[32] Neukermans A., and Ramaswami R., "MEMS technology for optical networking applications," Communications Magazine, IEEE, vol. 39, pp. 62-69, 2001.

[33] T. Tanemura; Al Amin, A.; Nakano, Y., "Multihop Field Trial of Optical Burst Switching Testbed With PLZT Optical Matrix Switch," Photonics Technology Letters, IEEE, vol. 21, pp. 42-44, 2009.

[34] Yamaguchi J.; Tomomi S.; Nobuhiro S.; Hiromu I.; Fusao S.; and Tsuyoshi Y., "High-yield Fabrication Methods for MEMS Tilt Mirror Array for Optical Switches," NTT Technical Review, vol. 5, 2007.

[35] Xiang Zhou; Jianjun Yu; Ming-Fang Huang; Yin Shao; Ting Wang; Magill, P.; Cvijetic, M.; Nelson, L.; Birk, M.; Guodong Zhang; Ten, S.; Matthew, H. B.; Mishra, S.K., "32Tb/s (320x114Gb/s) PDM-RZ-8QAM transmission over 580km of SMF-28 ultra-low-loss fiber," Optical Fiber Communication - incudes post deadline papers, 2009. OFC 2009. Conference on , vol., no., pp.1,3, 22-26 March 2009.

[36] Agrawal G.P., "Nonlinear fibre optics," Fourth Edition, Academic Press, 2007.

[37] Ducros, N.; Humbert, G.; Fevrier, S.; Buczynski, R.; Pysz, D.; Stepien, R., "Nonlinear spectral broadening in lead-bismuth-gallate glass photonic crystal fiber," Lasers and Electro-Optics, 2009 and 2009 Conference on Quantum electronics and Laser Science Conference. CLEO/QELS 2009. Conference on , vol., no., pp.1,2, 2-4 June 2009.

[38] Chen Xie; Ming-Lie Hu; Da-Peng Zhang; Cheng-Lin Gu; You-Jian Song; Lu Chai; Wang, Ching-Yue, "Generation of 25-fs High Energy Pulses by SPM-Induced Spectral Broadening in a Photonic Crystal Fiber Laser System," Photonics Technology Letters, IEEE , vol.24, no.7, pp.551,553, April1, 2012.

[39] Wei Wang; Rau, L.; Blumenthal, D.J., "All-optical label switching/swapping of 160 Gbps variable length packets and 10 Gbps labels using a WDM Raman enhanced-XPM fiber wavelength converter with unicast/multicast operation," Optical Fiber Communication Conference, 2004. OFC 2004 , vol.2, no., pp.3 pp. vol.2,, 23-27 Feb. 2004.

[40] Raman, C. V., "A new radiation". Indian J. Phys. 2: 387398, 1928.

[41] Chamorovskiy, A.; Golant, K.M.; Okhotnikov, O.G., "Hybrid fiber Raman-bismuth amplifier pumped by semiconductor disk laser operating at 1.3 m," Optical Communication (ECOC), 2011 37th European Conference and Exhibition on , vol., no., pp.1,3, 18-22 Sept. 2011.

[42] Castellani, C. E S; Kelleher, E. J R; Popa, D.; Sun, Z.; Hasan, T.; Ferrari, A.C.; Popov, S.V.; Taylor, J. R., "Nanotube-based passively mode-locked Ytterbium-pumped Raman laser," Lasers and Electro-Optics Europe (CLEO EUROPE/EQEC), 2011 Conference on and 12th European Quantum Electronics Conference , vol., no., pp.1,1, 22-26 May 2011.

[43] Torounidis T., "Fiber optic parametric amplifiers in single and multi wavelength applications," PhD thesis, Chalmers University of Technology, 2006.

[44] Mao, X. P.; Tkach, R.W.; Chraplyvy, A.R.; Jopson, R.M.; Derosier, R. M., "Stimulated Brillouin threshold dependence on fiber type and uniformity," Photonics Technology Letters, IEEE , vol.4, no.1, pp.66,69, Jan. 1992.

[45] Shiraki, K.; Ohashi, M.; Tateda, M., "SBS threshold of a fiber with a Brillouin frequency shift distribution," Lightwave Technology, Journal of , vol.14, no.1, pp.50,57, Jan 1996.

[46] Boggio, J.C.; Marconi, J.D.; Fragnito, H. L., "Experimental and numerical investigation of the SBS-threshold increase in an optical fiber by applying strain distributions," Lightwave Technology, Journal of , vol.23, no.11, pp.3808,3814, Nov. 2005.

[47] Rau, L.; Wei Wang; Poulsen, H.N.; Blumenthal, D.J., "160 Gb/s OTDM wavelength conversion using XPM in dispersion shifted fiber," Optical Fiber Communication Conference, 2004. OFC 2004 , vol.2, no., pp.3 pp. vol.2,, 23-27 Feb. 2004.

[48] Olsson, B.; Ohlen, P.; Rau, L.; Blumenthal, D.J., "A simple and robust 40-Gb/s wavelength converter using fiber cross-phase modulation and optical filtering," Photonics Technology Letters, IEEE , vol.12, no.7, pp.846,848, July 2000.

[49] Honzatko P., All-optical wavelength converter based on fiber cross-phase modulation and fiber Bragg grating, Optics Communications, Volume 283, Issue 9, Pages 1744-1749, 2010.

[50] Jianjun Yu; Jeppesen, P., "80-Gb/s wavelength conversion based on cross-phase modulation in high-nonlinearity dispersion-shifted fiber and optical filtering," Photonics Technology Letters, IEEE , vol.13, no.8, pp.833,835, 2001.

[51] Guoxiu Huang; Miyoshi, Y.; Maruta, A.; Yoshida, Y.; Kitayama, K., "All-Optical OOK to 16-QAM Modulation Format Conversion Employing Nonlinear Optical Loop Mirror," Lightwave Technology, Journal of , vol.30, no.9, pp.1342,1350, 2012.

[52] Kabakova I., Grobnic D., Mihailov S., Magi E., de Sterke C., and Eggleton B., "Bragg grating-based optical switching in a bismuth-oxide fiber with strong ?(3)-nonlinearity," Opt. Express 19, 5868-5873, 2011.

[53] Inoue, K.; Toba, H., "Wavelength conversion experiment using fiber four-wave mixing," Photonics Technology Letters, IEEE , vol.4, no.1, pp.69,72, Jan. 1992.

[54] Nowak, G.A.; Kao, Y.-H.; Xia, T.J.; Islam, M.N.; Nolan, D., "Low-power, high-efficiency wavelength conversion based on modulation instability in high nonlinearity optical fiber," Optical Fiber Communication Conference and Exhibit, 1998. OFC '98., Technical Digest , vol., no., pp.373,374, 22-27 Feb. 1998.

[55] Guanshi Qin; Xin Yan; Kito, C.; Meisong Liao; Suzuki, T.; Mori, A.; Ohishi, Y., "Highly nonlinear tellurite microstructured fibers for broadband wavelength conversion and flattened supercontinuum generation," Journal of Applied Physics , vol.107, no.4, pp.043108,043108-4, Feb 2010.

[56] Hasegawa, T.; Inoue, K.; Oda, K., "Polarization independent frequency conversion by fiber four-wave mixing with a polarization diversity technique," Photonics Technology Letters, IEEE , vol.5, no.8, pp.947,949, Aug. 1993.

[57] Tanemura, T.; Kikuchi, K., "Polarization-independent broad-band wavelength conversion using two-pump fiber optical parametric amplification without idler spectral broadening," Photonics Technology Letters, IEEE , vol.15, no.11, pp.1573,1575, Nov. 2003.

[58] Aso, O.; Shin-Ichi Arai; Yagi, T.; Tadakuma, M.; Suzuki, Y.; Namiki, S., "Broadband four-wave mixing generation in short optical fibres," Electronics Letters , vol.36, no.8, pp.709,711, 13 Apr 2000.

[59] Kwan Lau; Wang, S.H.; Lixin Xu; Lui, L.; Wai, P.K.A.; Lu, C.; Tam, H. -Y, "All-Optical Multicast Switch based on Raman-Assisted Four-Wave Mixing in Dispersion-shifted Fiber," Lasers and Electro-Optics - Pacific Rim, 2007. CLEO/Pacific Rim 2007. Conference on , vol., no., pp.1,2, 26-31 Aug. 2007.

[60] Yu, C.; Pan, Z.; Wang, Y.; Song, Y.; Gurkan, D.; Hauer, M.; Willner, A.; Starodubov, D., "Polarization-insensitive four-wave mixing wavelength conversion using a fiber Bragg grating and a Faraday rotator mirror," Optical Fiber Communications Conference, 2003. OFC 2003 , vol., no., pp.347,349 vol.1, 23-28 March 2003.

[61] Sakamoto, T.; Koji Seo; Taira, K.; Nam Su Moon; Kikuchi, K., "Polarization-insensitive all-optical time-division demultiplexing using a fiber four-wave mixer with a peak-holding optical phase-locked loop," Photonics Technology Letters, IEEE , vol.16, no.2, pp.563,565, Feb. 2004.

[62] Hao Hu; Mulvad, H.C.H.; Galili, M.; Palushani, E.; Jing Xu; Clausen, A.T.; Oxenlowe, L.K.; Jeppesen, P., "Polarization-Insensitive 640 Gb/s Demultiplexing Based on Four Wave Mixing in a Polarization-Maintaining Fibre Loop," Lightwave Technology, Journal of , vol.28, no.12, pp.1789,1795, June15, 2010.

[63] Chow, K.K.; Shu, C.; Chinlon Lin; Bjarklev, A., "Polarization-insensitive widely tunable wavelength converter based on four-wave mixing in a dispersion-flattened nonlinear photonic Crystal fiber," Photonics Technology Letters, IEEE , vol.17, no.3, pp.624,626, March 2005.

[64] Feng X., Poletti F., Camerlingo A., Parmigiani F., Petropoulos P., Horak P., Ponzo G. M., Petrovich M., Shi J., Wei H. Loh, and Richardson D. J., "Dispersion controlled highly nonlinear fibers for all-optical processing at telecoms wavelengths," Optical Fiber Technology, Volume 16, Issue 6, Pages 378-391, 2010.

[65] Onishi M., Okuno T., Kashiwada T., Ishikawa S., Akasaka N., and Nishimura M., "Highly Nonlinear Dispersion-Shifted Fibers and Their Application to Broadband Wavelength Converter," Optical Fiber Technology, Volume 4, Issue 2, Pages 204-214, 1998.

[66] Nakanishi T., Hirano M., Okuno T., and Onishi M., " Silica-Based Highly Nonlinear Fiber with g =30/W/km and Its FWM-Based Conversion Efficiency," in Optical Fiber Communication Conference and Exposition and The National Fiber Optic Engineers Conference, Technical Digest (CD) Optical Society of America, paper OTuH, 2006.

[67] Zakery, A. and Elliott, S. R., "Optical Nonlinearities in Chalcogenide Glasses and their Applications", Springer, 2010.

[68] Mossadegh R., Sanghera J. S., Schaafsma D., Cole B. J., Nguyen V. Q., Miklos R. E., and Aggarwal I. D., "Fabrication of Single-Mode Chalcogenide Optical Fiber," Journal of Lightwave Technology, Vol. 16, No. 2, 1998.

[69] Desevedavy F., Renversez G., Brilland L., Houizot P., Troles J., Coulombier Q., Smektala F., Traynor N., and Adam J.-L., "Small-core chalcogenide microstructured fibers for the infrared," Applied Optics, Vol. 47, No. 32, 2008.

[70] Alexey F. Kosolapov, Andrey D. Pryamikov, Alexander S. Biriukov, Vladimir S. Shiryaev, Maxim S. Astapovich, Gennady E. Snopatin, Victor G. Plotnichenko, Mikhail F. Churbanov, and Evgeny M. Dianov "Demonstration of CO2-laser power delivery through chalcogenide-glass fiber with negative-curvature hollow core," Optics Express,Vol. 19, No.25, pp. 25723-25728, 2011.

[71] Dekker S., Xiong C., Magi E., Judge A. C., Sanghera J. S., Shaw L. B., Aggarwal I. D., Moss D. J., and Eggleton B. J., "Broadband Low Power Super-continuum Generation in As2S3 Chalcogenide Glass Fiber Nanotapers," OSA/CLEO/QELS, 2010.

[72] Eggleton: "Applications of Highly-Nonlinear Chalcogenide Glass Devices Tailored for High-Speed All-Optical Signal Processing," TUGboat Vol. 9, No. 1, 2008.

[73] Le S. D., Nguyen D. M., Thual M., Bramerie L., Costa e Silva M., Lengle K., Gay M., Chartier T., Brilland L., Mechin D., Toupin P., Troles J., "Efficient Four-Wave Mixing in a Ultra-Highly Nonlinear Suspended-Core Chalcogenide Fiber," ECOC, 2011.

[74] Abedin K. S.: "Efficient Slow Light Generation Using Highly Nonlinear Non-Silica-Based Fibers," ICTON, 2007.

[75] J. S. Sanghera, L. B. Shaw, I. D. Aggarwal, "Applications of chalcogenide glass optical fibers," Comptes Rendus Chimie, Volume 5, Issue 12, Pages 873-883, 2002

[76] Dianov E. and Bufetov I., "Progress in Bismuth-Doped Silica-Based Fiber Lasers and Amplifiers," in Asia Communications and Photonics Conference, OSA Technical Digest (online) (Optical Society of America, paper ATh3A.2, 2012.

[77] You-Min Chang; Junsu Lee; Ju Han Lee, "Bismuth Nonlinear Optical Fiber for Photonic Ultrawideband Radio-Signal Processing," Selected Topics in Quantum Electronics, IEEE Journal of , vol.18, no.2, pp.891,898, March-April 2012.

[78] Hasegawa, T.; Nagashima, T.; Ohara, S.; Sugimoto, N., "High nonlinearity bismuth fibers and their applications," Optical Fiber Communication Conference, 2006 and the 2006 National Fiber Optic Engineers Conference. OFC 2006 , vol., no., pp.3 pp.,, 5-10 March 2006.

[79] Knight, J.C.; Birks, T.A.; Atkin, D.M.; Russell, P.S.-J., "Two-Dimensional Photonic Crystal Material in Fibre Form," Lasers and Electro-optics Europe, 1996. CLEO/Europe., Conference on , vol., no., pp.75,75, 8-13 Sept. 1996.

[80] P. Russell, "Photonic-Crystal Fibers," J. Lightwave Technol. 24, 4729-4749, 2006.

[81] Russell, P., "Recent advances in photonic crystal fibres," Transparent Optical Networks, 2003. Proceedings of 2003 5th International Conference on , vol.1, no., pp.8 vol.1,, 29 June-3 July 2003.

[82] Luan F., Knight J., Russell P., Campbell S., Xiao D., Reid D., Mangan B., Williams D., and Roberts P., "Femtosecond soliton pulse delivery at 800nm wavelength in hollow-core photonic bandgap fibers," Opt. Express 12, 835-840, 2004.

[83] Zhang R., Teipel J., and Giessen H., "Theoretical design of a liquid-core photonic crystal fiber for supercontinuum generation," Opt. Express 14, 6800-6812, 2006.

[84] Kaiser P., Marcatili E. A. J., and Miller S. E., "A New Optical Fiber," Bell. Syst. Tech. J., vol. 52, pp. 265?269, 1973.

[85] Dong L., Thomas B., and Fu L., "Highly nonlinear silica suspended core fibers," Opt. Express 16, 16423-16430, 2008.

[86] Monro, T.M.; West, Y.D.; Hewak, D.W.; Broderick, N.G.R.; Richardson, D.J., "Chalcogenide holey fibres," Electronics Letters , vol.36, no.24, pp.1998,2000, 2000.

[87] Fatome J., Fortier C., Nguyen T., Chartier T., Smektala F., Messaad K., Kibler B., Pitois S., Gadret G., Finot C., Troles J., Desevedavy F., Houizot P., Renversez G., Brilland L., and Traynor N., "Linear and Nonlinear Characterizations of Chalcogenide Photonic Crystal Fibers," J. Lightwave Technol. 27, 1707-1715, 2009.

[88] Le S., Nguyen D., Thual M., Bramerie L., Costa e Silva M., Lengle K., Gay M., Chartier T., Brilland L., Mechin D., Toupin P., and Troles J., "Efficient four-wave mixing in an ultra-highly nonlinear suspended-core chalcogenide As38Se62 fiber," Opt. Express 19, B653-B660, 2011.

[89] Renversez, G.; Duhant, M.; Renard, W.; Betourne, A.; Nguyen, T.; Canat, G.; Smektala, F.; Coulombier, Q.; Troles, J.; Brilland, L., "Nonlinear effects above 2 um in chalcogenide suspended core microstructured optical fibers: Modeling and experiments," Photonics Conference (PHO), 2011 IEEE , vol., no., pp.61,62, 9-13, Oct. 2011.

[90] Ducros, N.; Labruyere, A.; Fevrier, S.; Morin, F.; Druon, F.; Hanna, M.; Georges, P.; Buczynski, R.; Pysz, D.; Stepien, R., "Mid-infrared supercontinuum generation in lead-bismuth-gallium oxide glass photonic crystal fiber," Lasers and Electro-Optics (CLEO) and Quantum Electronics and Laser Science Conference (QELS), 2010 Conference on , vol., no., pp.1,2,16-21, May 2010.

[91] Birks, T.A.; Li, Y.W., "The shape of fiber tapers," Lightwave Technology, Journal of , vol.10, no.4, pp.432,438, Apr 1992.

[92] Fielding, A.J.; Edinger, Klaus; Davis, C.C., "Experimental observation of mode evolution in single-mode tapered optical fibers," Lightwave Technology, Journal of , vol.17, no.9, pp.1649,1656, Sep 1999.

[93] Chryssou C.E.; Theoretical analysis of tapering fused silica optical fibers using a carbon dioxide laser. Opt. Eng. 38(10):1645-1649, 1999.

[94] Schaafsma, D. T.; Moon, J. A.; Sanghera, J.S.; Aggarwal, I.D., "Fused taper infrared optical fiber couplers in chalcogenide glass," Lightwave Technology, Journal of , vol.15, no.12, pp.2242,2245, 1997.

[95] Magi E., Fu L., Nguyen H., Lamont M., Yeom D., and Eggleton B., "Enhanced Kerr nonlinearity in sub-wavelength diameter As2Se3 chalcogenide fiber tapers," Opt. Express 15, 10324-10329, 2007.

[96] Boskovic A., Chernikov S. V. and Taylor J. R., "Direct continuous-wave measurement of n2 in various types of telecommunication fiber at 1.55 ?m," Optics Letters 21(24), pp. 1966-1968, 1996.

[97] Nguyen V., Sanghera J., Kung F., Aggarwal I., and Lloyd I., "Effect of Temperature on the Absorption Loss of Chalcogenide Glass Fibers," Appl. Opt. 38, 3206-3213, 1999.

[98] Nguyen, V.Q.; Sanghera, J.S.; Pureza, P.C.; Aggarwal, I.D., "Effect of heating on the optical loss in the As-Se glass fiber," Lightwave Technology, Journal of , vol.21, no.1, pp.122,126, Jan 2003.

[99] Nguyen, V.Q.; Sanghera, J.S.; Kung, F.H.; Pureza, P.C.; Aggarwal, I.D., "Very large temperature-induced absorptive loss in high Te-containing chalcogenide fibers," Lightwave Technology, Journal of , vol.18, no.10, pp.1395,1401, Oct. 2000

[100] Komanec, M., Pisarik, M., Zvanovec, S.: Vlnove selektivni clen AWG. [Funkcni vzorek]. 2011.

[101] Pisarik, M., Komanec, M., Zvanovec, S.: Teplotne kompenzovany vlnove selektivni clen - AAWG. [Funkcni vzorek]. 2012.

[102] Hasegawa J. and Nara K., "Ultra-Low-Loss Athermal AWG Module with a Large Number of Channels," Furukawa Review, 2004.

[103] "Transmission Characteristic of Passive Optical Components," ed. Recommendation ITU-T Rec G. 671, 2009.

[104] Komanec, M., Honzatko, P., Zvanovec, S.: "Single-shot All-optical Sampling Oscilloscope using a Polarization-maintaining Resonator for Pulse Replication," Microwave and Optical Technology Letters., vol. 52, no. 11, p. 2452-2456, 2010.

[105] C. Florea, M. Bashkansky, Z. Dutton, J. Sanghera, P. Pureza, and I. Aggarwal, "Stimulated Brillouin scattering in single-mode As2S3 and As2Se3 chalcogenide fibers," Opt. Express 14, 12063-12070 (2006).

[106] Elschner, R.; Bunge, C. -A; Huttl, B.; i Coca, A.G.; Schmidt-Langhorst, C.; Ludwig, R.; Schubert, C.; Petermann, K., "Impact of Pump-Phase Modulation on FWM-Based Wavelength Conversion of D(Q)PSK Signals," Selected Topics in Quantum Electronics, IEEE Journal of , vol.14, no.3, pp.666,673, 2008.